POLITECNICO
MILANO 1863

Politecnico di Milano
Department of Electronics, Information, and Bioengineering
Doctoral Program In Information Technology

DYNAMIC SEDIMENT CONNECTIVITY MODELLING FOR STRATEGIC RIVER BASIN PLANNING

Doctoral Dissertation of:
Marco Tangi

Advisor:
Prof. Andrea Castelletti

Co-Advisor:
Prof. Simone Bizzi

Tutor:
Prof. Lorenzo Fagiano

The Chair of the Doctoral Program:
Prof. Barbara Pernici

2021 – XXXIV Cycle

"The thing the ecologically illiterate don't realize about an ecosystem,"
Kynes said, "Is that it's a system. A system!
A system maintains a certain fluid stability that can be destroyed by a misstep in just one niche. A system has order, a flowing from point to point.
If something dams that flow, order collapses.
The untrained might miss that collapse until it was too late.

That's why the highest function of ecology is the understanding of consequences."

Frank Herbert - Dune (1965)

Abstract

Rivers sediment (dis)connectivity is a distributed property of river networks, emerging from numerous sediment transport processes across the entire network and their interactions in time and space, and plays a profound influence on river health and human livelihood. However, anthropic activities have profoundly altered sediment transport in river systems: dam construction starves the channel and delta of material, while land-use change alters the characteristics and rate of sediment delivery. The resulting impacts range from delta shrinking and banks instability to ecosystem degradation in the river and on the connected floodplains. Nevertheless, the evaluation of sediment (dis)connectivity degradation by human activities is often performed at the local scale, ignoring the basin-wide implications on the network morphology and the cumulative effects of multiple alterations.

The research in this thesis focuses on developing network-scale sediment (dis)connectivity models for sediment processes characterization and anthropic alteration impact assessment. First, this work contributes the CASCADE toolbox for sediment transport modelling , which expands on the original CASCADE (CAtchment Sediment Connectivity and DElivery) model by partitioning sediment transport into distinct grain size classes and including fractional transport formulas. The new structure allows for a more extensive representation on the type and rate of sediment delivery throughout the network. The scarcity of input data for network hydro-morphology definition is compensated by using recently available large-scale datasets and performing extensive sensitivity analysis on the model parametrization. The toolbox is applied on the Vjosa river in Albania to quantify and characterize sediment transport and its influence on river forms stability in a data-scarce environment.

A second achievement is the development of D-CASCADE, a dynamic, network-scale sediment (dis)connectivity model. The framework traces sediment delivery and transport patterns across time and space, allowing for a more thorough representation of sediment (dis)connectivity. Add-ons components are integrated in the flexible model structure for detailed representation of channel morphodynamic response to sediment delivery alterations. We

tested the D-CASCADE model on the Bega river network, in Australia, to reconstruct historical morphological changes due to human activities across two centuries.

D-CASCADE represents an important tool for strategic and sustainable planning and management of multiple human infrastructures on river systems. In this research, we focused on water and sediment management in reservoirs, and demonstrated the potential of D-CASCADE to quantify the spatio-temporal effects of dam operations, both locally, e.g, reservoir storage losses due to sedimentation, and on the broader river sediment (dis)connectivity. The model network-scale scope allows for the representation of multiple reservoirs on the same system, and the evaluation of the changes in the cumulative effects on sediment transport given by different design and timing of reservoirs management strategies. These may include both standard operations like daily water release, and exceptional events like drawdown sediment flushing. The D-CASCADE model is tested on the 3S system, a tributary of the Mekong, to evaluate strategic water and sediment management in multi-dam schemes.

Finally, the new models presented are designed to be integrated into optimization-based frameworks for strategic reservoir management, to evaluate optimal trade-off between more traditional objectives like hydro-power production and irrigation demand, and the conservation of natural sediment (dis)connectivity.

Part of this research has appeared or are about to appear in the following journal publications:

- Tangi, M., Schmitt, R., Bizzi, S., Castelletti, A., 2019. The CASCADE toolbox for analyzing river sediment connectivity and management. Environmental Modelling & Software 119, 884 400–406. DOI:10.1016/j.envsoft.2019.07.008

- Bizzi, S., Tangi, M., Schmitt, R.J.P., Pitlick, J., Piégay, H. & Castelletti, A.F. (2021) Sediment transport at the network scale and its link to channel morphology in the braided Vjosa River system. Earth Surface Processes and Landforms, 46(14), 2946– 2962. DOI:10.1002/esp.5225

- Tangi, M., Bizzi, S., Fryirs, K., & Castelletti, A. (2022). A dynamic, network scale sediment (dis)connectivity model to reconstruct historical sediment transfer and river reach sediment budgets. Water Resources Research, 58. DOI: 10.1029/2021WR030784

- Tangi, M., Bizzi, S. and Castelletti, A. Strategic water and sediment management in reservoirs to reduce storage losses and protect network connectivity. (In preparation).

Sommario

Con il termine *(dis)connettività dei sedimenti* si indica una proprietà distribuita delle reti fluviali, risultante dalle interazioni spaziotemporali di molteplici processi di trasporto solido lungo tutto il bacino idrografico, che influenza profondamente la salute del sistema fluviale e il benessere delle popolazioni locali che da esso dipendono.

Le attività antropiche alterano i processi fluviali di trasporto di sedimenti: la costruzione di dighe, ad esempio, riduce l'apporto solido a canali e delta, mentre l'alterazione dell'uso del suolo modifica la tipologia e l'intensità dei contributi di materiali dai versanti. Queste modifiche portano a ampi impatti sul sistema fluviale, che possono includere restringimento dei delta, instabilità degli argini fluviali e deterioramento degli ecosistemi fluviali e delle adiacenti pianure alluvionali. Nonostante ciò, le analisi di impatto ambientale vengono solitamente svolte a scala locale, ignorando così le implicazioni a livello di bacino sulla connettività dei sedimenti e gli effetti cumulati di molteplici alterazioni su un singolo reticolo idrografico.

La ricerca illustrata nel presente lavoro di tesi è focalizzata sullo sviluppo di modelli che riproducano la (dis)connettività dei sedimenti a scala di bacino, caratterizzando i principali processi morfologici responsabili, e valutino gli impatti delle alterazioni antropiche.

Nella prima parte viene presentato ed illustrato il toolbox CASCADE, che permette la simulazione del trasporto di sedimenti sull'intero reticolo fluviale. Esso espande la struttura dell'originale modello CASCADE (CAtchment Sediment Connectivity And DElivery) includendo la rappresentazione differenziata del movimento di particelle di diverse grandezze attraverso l'uso di formule di trasporto solido frazionario. Questa nuova struttura permette di esplicitare la tipologia e la composizione dei materiali trasportati e depositati in ogni punto del sistema fluviale. La mancanza di dati di input distribuiti, raramente resi disponibili dalle campagne dati locali, è compensata dall'uso di database idromorfologici a larga scala e dall'impiego di analisi di sensitività sui parametri in ingresso al modello. Il toolbox è stato applicato sul fiume Vjosa, in Albania, con lo scopo di quantificare e caratterizzare il trasporto di sedimenti in un caso stu-

dio povero di dati e stabilire una relazione tra questi processi e la stabilità delle forme fluviali.

Un secondo contributo consiste nella presentazione di D-CASCADE, un modello per la simulazione dinamica della (dis)connettività dei sedimenti. D-CASCADE risulta capace di tracciare il trasporto di materiali sia nello spazio che nel tempo, garantendo una più completa rappresentazione dei processi morfologici. Componenti "add-on" sono stati integrati nella struttura flessibile del modello, garantendo così una rappresentazione più dettagliata della morfodinamica dei canali fluviali in risposta a cambiamenti nella disponibilità e nell' apporto di materiali solidi. D-CASCADE è stato testato sul fiume Bega, in Australia, per la ricostruzione di cambiamenti morfologici avvenuti lungo due secoli causati da attività umane nel bacino idrografico.

D-CASCADE rappresenta, inoltre, uno strumento innovativo per la pianificazione e la gestione strategica e sostenibile di molteplici infrastrutture antropiche su una singola rete fluviale.

In particolare, la ricerca qui presentata si concentra sulla regolazione del bilancio idrico e dei sedimenti nei bacini delle dighe, e dimostra l'ampio potenziale di D-CASCADE per la valutazione degli effetti, dislocati nello spazio e nel tempo, delle differenti strategie di gestione degli impianti, sia a livello locale, es. ad esempio attraverso il progressivo interramento dei bacini, sia sulla (dis)connettività dell'intero reticolo.

La prospettiva a larga scala permette di simulare la presenza di molteplici dighe su un singolo sistema fluviale, e di valutare gli effetti cumulati delle loro operazioni di gestione dei serbatoi sui processi morfologici; siano esse procedure standard come il rilascio giornaliero dall'impianto, o straordinarie come interventi di fluitazione a bacino vuoto per la rimozione del materiale depositato.

Il modello D-CASCADE è stato applicato al sistema 3S, un tributario del Mekong, per esplorare strategie sostenibili di gestione dell'acqua e dei sedimenti in molteplici dighe localizzate nello stesso sistema fluviale.

I nuovi modelli proposti sono stati sviluppati per essere integrati in processi di ottimizzazione della pianificazione e gestione di dighe, al fine di indentificare compromessi tra obiettivi tradizionali, come la produzione idroelettrica o la domanda irrigua e la protezione della naturale (dis)connettività dei sedimenti.

Parte della ricerca illustrata nel presente lavoro di tesi è stata pubblicata, o è in procinto di esserlo, sulle seguenti riviste scientifiche:

- Tangi, M., Schmitt, R., Bizzi, S., Castelletti, A., 2019. The CASCADE toolbox for analyzing river sediment connectivity and management. Environmental Modelling & Software 119, 884 400–406. DOI:10.1016/j.envsoft.2019.07.008

- Bizzi, S., Tangi, M., Schmitt, R.J.P., Pitlick, J., Piégay, H. & Castelletti, A.F. (2021) Sediment transport at the network scale and its link to channel morphology in the braided Vjosa River system. Earth Surface Processes and Landforms, 46(14), 2946– 2962. DOI:10.1002/esp.5225
- Tangi, M., Bizzi, S., Fryirs, K., & Castelletti, A. (2022). A dynamic, network scale sediment (dis)connectivity model to reconstruct historical sediment transfer and river reach sediment budgets. Water Resources Research, 58. DOI: 10.1029/2021WR030784
- Tangi, M., Bizzi, S. and Castelletti, A. Strategic water and sediment management in reservoirs to reduce storage losses and protect network connectivity. (In preparazione).

Acknowledgements

Many people have helped, supported and encouraged me during my Ph.D. studies, and I would like to express my sincere thanks to all of them.

First, my profound gratitude goes to my supervisor, prof. Andrea Castelletti, for allowing me to undertake my Ph.D. education, and guiding me in every subsequent step of the way with trust and appreciation. The teachings and opportunities he offered me were invaluable for growing as a person and as a researcher.

To prof. Simone Bizzi, my co-advisor, go my heartfelt thanks. For as long as I knew him, he has been an enthusiastic teacher, a thoughtful mentor, and a good friend. The passion he has for his job is truly inspiring.

This project would not have been possible without prof. Rafael Schmitt, who laid the foundations upon which my work was built and gave me his attentive and steady support throughout the years. His deep knowledge of the internal workings of the tools he developed was a tremendous asset for me to continue in his footsteps and experiment with new ideas.

My sincere appreciations go to prof. Guido Zolezzi and prof. Patrice Carbonneau, for taking the time to carefully review my thesis and providing valuable observations which raised interesting questions and significantly improved my research.

Special thanks go to the past and present members of the Environmental Intelligence Lab at Politecnico di Milano, which were a joy to work and interact with. You provided countless moments of levity, stimulating conversations, and precious support. I wish you all good fortune in all your future endeavors.

There are not enough words to express my love and appreciation for all the people outside the academic world I hold close to my heart, from my family to the people I have the pleasure to call friends. This thesis is yours too.

Contents

List of Figures

List of Tables

1

Introduction

1.1 River (Dis)connectivity in the Anthropocene

From the monumental meanders of the Amazon river to the humble alpine creek carving its way through the barren rocks, all rivers share the fundamental role of key connectors in the global hydrological and geochemical cycles. Water is collected across the watershed into the streams, from small tributaries to the largest channels, and carried across various landscapes to the sea, changing the morphology, landscape, and ecology of the areas it crosses. Carried along the bed or in suspension by the current, sediment of different sizes and compositions are delivered from many heterogeneous sources downstream to the floodplains, estuaries, and other oceanic or continental sinks where they deposit. Dissolved into the water or bounded to the sediment, nutrients are redistributed along the river's path, providing fundamental sustenance to riverine and coastal ecosystems, which contains a complex and interconnected ecological web composed of countless different species, all relying on the river for food, shelter, and transportation (Milliman and Meade, 1983; Syvitski et al., 2003; Vaughan et al., 2009; Abell et al., 2008).

Given the abundance of resources and services provided by fluvial landscapes, it's no surprise that river basins are regarded as cradles of civilization. From the first human settlements to the sprawling metropolis of today, human societies have risen and flourished along water courses (James, 2015), employing and exploiting the wide array of resources available for agricultural, industrial, cultural, and domestic use (Brismar, 2002). The Millennium Ecosystem Assessment (2005) classified these services into four broad domains, as listed in Table 1.1. River goods are continuously extracted or diverted from river

systems to be used for a variety of purposes, be it water for agricultural, domestic, and industrial uses, aquatic animals and plants for sustenance, wood and timber from vegetation(Horner et al., 2010) or sediment for construction (Kondolf, 1994). Riverine forests and floodplains also offer protection and mitigation from hydrological extremes. Moreover, river systems provide a reliable mean of transportation for goods and people and a reliable source of mechanical energy to be exploited. In this context, we can confidently state that rivers are key connectors of human civilization too.

Ecosystem Services	**Components**
Supporting	Nutrient cycling Soil formation Primary production from photosynthesis
Provisioning	Food Fresh water Wood and fiber Sediment for construction
Regulation	Climate regulation Flood regulation Disease regulation Riverbank Stabilization Water purification
Cultural	Aestetic Educational Recreational Spiritual

Table 1.1: *List of the ecosystem services provided by river systems and relative main components as reported from Millennium Ecosystem Assessment (2005)*

Many of the ecosystems services provided by river systems are deeply linked to the interplay between sediment and water transport (Gilvear et al., 2013). Hydraulic forces, influenced by geomorphic elements in channel and floodplains, shape the type and magnitude of solid material transport. Both these elements are in constrain co-evolution, resulting in a variety of different morphological structures like meanders, gullies, and knickpoints. These intertwined and dynamic processes involving water and solid material are commonly grouped under the term of hydro-geomorphology (Vogel, 2011).

Human influence on river systems

Human presence and river system disturbances have profoundly affected fluvial landscapes, dramatically altering their hydro-geomorphology and ecology. These alterations are a consequence, deliberate or not, of anthropic intervention intended to directly extract fluvial goods and services or regulate their availability to increase their utility for human activities. Under the first category, we find, for example, the deforestation of floodplains and riverine forests, sediment mining, and fishing activities. In contrast, the second category includes all fluvial infrastructures designed to divert, store, and generally control the availably of water for human use, like weirs, channels, and dams (Gallup et al., 1999).

The benefits guaranteed by these infrastructures are manifested in their widespread presence thought human history. Dams have been erected on rivers as early as the third millennia B.C., with traces of dams made of rock discovered on the Tigris, Euphrates, and Nile (Jansen, 2012). These projects were designed primarily for irrigation and water supply, to compensate for the wide heterogeneity in the natural water availability during the year, and for flood control and protection. In medieval Europe and China, the mechanical push of the water current, properly guided across weirs and mills, provided energy for milling, mining, and other intensive activities (Walter and Merritts, 2008). With the advent of electricity, dams started to be used for hydropower generation. As the first renewable energy source, hydropower played a pivotal role in the electrification and industrialization of human society starting in the 20^{th} century. During the second half of the 20^{th} century, starting from Europe and North America (World Commission on Dams, 2000), the number of dams skyrocketed all around the world. While the total number of dams existing nowadays is uncertain, Vörösmarty et al. (2003) estimated dams above 15 m to be more than 45000 worldwide. Lehner et al. (2011) stated that including smaller dams, around 46% of major rivers worldwide are dammed. Due to the reservoir's storage capacity, combined with the general predictability of the hydrological circle, hydropower generation is flexible and reliable, capable of covering both peaks and base energy demands, which is a unique property among renewable energy sources. As a relatively clean source whose power generation is not dependent on primary energy sources like fossil fuels, hydropower is considered a prime instrument for fostering sustainable development, as promoted by the U.N. Sustainable Development Goals (SDGs) (United Nations, 2019), as well as reducing dependency in developing countries (Chow et al., 2003) to fuel and energy imports. Given all these reasons, it's comprehensible that future projections show an ongoing boom in dam construction, which, if completed in its entirety, would increase the fraction of major dammed rivers to 72% (Zarfl et al., 2015).

Despite their clear advantages, human infrastructures in river systems often creates negative environmental externalities (Rosenberg et al., 1997; Brismar, 2002; Vörösmarty et al., 2003; Syvitski and Milliman, 2007). These can be broadly categorized into two distinct groups. Local externalities affect the area surrounding the dam and reservoir and range from the social aspects of expropriating and relocating local population and flooding settlements to the environmental damages of eradicating fluvial ecosystems within the impoundments Brismar (2002). Decomposition of submerged biomass typically releases a non-negligible amount of greenhouse gases (Almeida et al., 2019; Demarty and Bastien, 2011; Varis et al., 2012) while the impoundments may pose geophysical hazards (Liu et al., 2004). Evaporation and percolation from reservoirs may be responsible for considerable water losses, too (Sivapragasam et al., 2009). The drop in hydrodynamic forces in the current entering the reservoir also decreases the capacity of the current to transport sediment Kondolf (1994). Within the reservoir and, in particular, near the upstream end, sediment deposits may form deltas which may enhance flood risks and damage upstream infrastructures (Stevens, 2000). Moreover, the continuous trapping of sediment within the impoundments lowers the total storage capacity of the reservoir, decreasing efficiency and increasing maintenance costs of hydroelectric equipment. While often not considered while planning, economic losses due to lost impoundments may reach 30% of annual costs Palmieri et al. (2001). Globally, annual storage losses due to sedimentation are estimated to exceed the additional installed storage capacity (World Commission on Dams, 2000). Once decommissioned, reservoirs affected by heavy sedimentation may leave the former reservoir area covered with sediments whose removal may be too expensive, rendering the reservoir site unavailable for future generations Palmieri et al. (2001); Wisser et al. (2013).

Beyond local impacts, dams are by design a source of disconnectivity in the river system, as they physically break the continuity of the river network, and by doing so disrupt the natural hydro-geomorphic and biotic processes which are founded on this continuity (Rosenberg et al., 1997). The diversion and storage of water change its physical and chemical features, and released water could damage the river's ability to dilute pollutants and purify water near the reservoir and destroy animal populations sensible to changes in the water conditions (World Commission on Dams, 2000). Moreover, dam release is determined by its operating rule, which often differs from the natural hydrological regime of the river. Consequently, alterations in the frequency and magnitude of flows may have repercussions on the biotic and abiotic processes downstream. Reduction in flood pulse intensity may promote vegetation overgrowth, which increase disconnectivity between channel and banks and floodplains (Richter et al., 1996; Magilligan and Nislow, 2005). Aquatic fauna may be disoriented

by the disruption of the natural food timing and duration, and time cues for spawning (Næsje et al., 1995). Sediment connectivity is also deeply affected by dams. Sediment trapping reduces not only the quantity of sediment delivered downstream, but since coarser particles more readily deposit within the impoundment, it also alters the composition of the sediment released. In turn, this may have a lasting impact on the morphology and ecology of the river, further enhanced by changes in the hydrological cycle and flood frequency due to the dam operational strategy (Larinier, 2001). Water released from the dam possesses the energy to move sediment but has little or no material to carry. As a consequence, this so-called "hungry water" (Kondolf, 1994) erodes the river bed, causing scouring, incision, and channel degradation, increasing collapse hazard for building and infrastructures situated close to the river (Bizzi et al., 2015; Wyżga et al., 2016), and changing and degrading fish habitats and spawning grounds, damaging local fish populations and the communities that rely on them (Ligon et al., 1995; Kondolf, 2000; Larinier, 2001). The incision also increases the disconnectivity between rivers and floodplains, as incised channels are less prone to overbanking. Reduction in the frequency and intensity of floods brought by dam operations and channel incision may also reduce nutrient delivery to the floodplains and foster vegetation growth near the banks, further increasing floodplain disconnectivity. This, in turn, may decrease fish access to floodplains spawning grounds, drain groundwater resources, reduce soil fertility and lower the damping effects of the floodplain during extreme events (Sholtes and Doyle, 2011). At the river mouth, the lack of sediment supply decreases delta resilience, amplifying the risks of delta shrinking and coastal degradation posed by sea-level rise and coastal erosion (Vörösmarty et al., 2003; Syvitski et al., 2009; Yang et al., 2011).

Besides dams, most anthropic activities on rivers or their by-products can potentially alter the river's natural (dis)connectivity. Land-use change such as deforestation or urbanization may alter soil water retention and increase water, nutrient and chemical delivery to the river, as well as change the type and magnitude of sediment material delivered to the river or destabilize banks and hillsides, leading to further erosion (Boix-Fayos et al., 2008; Shrestha et al., 2021). Sediment mining alters the morphology of the river, changing channel shape gradient and mobilizing material to citerinaldi2005sediment,preciso2012land. Global climate change threatens to alter the natural hydrological cycle and all the hydromorphological processes related to it.

River (dis)connectivity impacts mitigation

To mitigate the negative effects brought by anthropic infrastructure and activities on river systems, a large variety of different interventions have been tested and implemented on a variety of rivers all over the globe. The aim of these

initiatives, which ranges greatly in scale and duration, is often to reconstruct ot at least partially restore the natural hydrological, biological and morphology (dis)connectivity of the fluvial systems.

Fragmentation in aquatic species habitats and blocking of migration pathways have often very tangible effects on local fishing communities and their economy (Hortle, 2009; Liermann et al., 2012). Fish by-passes are used all around the world to allow migratory aquatic species to cross artificial barriers. These are available in a variety of forms, ranging from poll-and-weirs passes used mostly on small infrastructures to fish elevators in larger dams (Larinier, 2000).

Permanent alterations of natural hydrological cycles are frequent observed in regulated rivers. Mitigations, for example in case of multiple dams systems on a single river network, may consist in changing the combined reservoirs release strategy to better mirror the natural hydrological seasonal cycles. "Environmental flow" is used as an indicator to evaluate the water demand, in terms of quantity, quality and timing, necessary to sustain fluvial and coastal ecosystems. Implementation of environmental flow conservation techniques are nowadays used worldwide in resulted systems (Acreman et al., 2014), although the approaches used to characterize this indicator in each river system are often situational and associated with large uncertainties (Dyson et al., 2003).

Alteration in sediment (dis)connectivity may have long-lasting and profound impacts on river systems. Strategies for maintaining or reconstructing natural sediment transport and delivery patters includes a very broad range of techniques with different objectives, areas of intervention, spatial and temporal frequencies and costs. As Kondolf et al. (2014a) defined in his seminar paper, sediment management techniques in regulated basin falls into three broad categories: 1) reducing sediment inflow, 2) prevention sedimentation within reservoir and 3) removing stored sediment.

Strategies which minimize sediment intake by reducing material delivery to the reservoir includes all techniques for reducing catchment sediment yield upstream the dam, e.g. soil erosion control via reforestation or changes in agricultural practices within the catchment. In-channel check-dams and sediment traps decreases sediment yield by reducing channel gradient and therefore transport capacity for bed material and debris flows (Takahara and Matsumura, 2008; Mizuyama, 2008), or by directly trapping incoming sediment yields (Kantoush and Sumi, 2010).

Approaches for sediment routing around and through the reservoirs aim to impede the incoming sediment flux from depositing in the reservoir. As the majority of sediment delivery happens during high discharge episodes, these techniques are usually performed during these events. They include structural intervention which must be include during reservoir construction, and

therefore designed beforehand, like sediment bypasses which collects and deliver downstream sediment-rich flood water and off-channel reservoir to be filled only with "clear" water. Alternately, management techniques like drawdowns sluicing aim to increase hydraulic forces within the reservoir by discharging high flows during sediment-laden flood events, to allow flood water to be transported through the basin with minimum sedimentation (Annandale, 2013). Sluicing is most effective in narrow reservoir with high discharge capacity, like the Three Gorges Dam (Zhou, 2007) but has proven somewhat effective in other case studies (Lee and Foster, 2013).

Removal of settled sediment includes all approaches aimed at reducing the volume of sediment already trapped and stored within the reservoir. Some of these techniques requires the use of heavy equipment and are often very costly: mechanical dredging removes solid material via scrapers, dump trucks, and other heavy equipment after the complete draw down of the reservoir, while dredging uses hydraulic suction machinery on barges to remove non-cohesive material (Stevens, 2000; Palmieri et al., 2003).

Other approaches exploit the hydraulic forces of the water current to scour the reservoir bed and re-mobilise material. Drawdown flushing is one of these techniques, and involves the total emptying of the dam basin through specifically designed low-level gates, to generate river-like flow conditions in the reservoir. If the water discharge is sufficient to induce movement in the deposited sediment, flushing should results in scouring of the sediment deposit, especially if performed during high flow seasons (Stevens, 2000; Kondolf et al., 2014a). However, there are limitations in the effectiveness of drawdown flushing. Flushing is most effective when performed in small, narrow reservoirs, or on rivers with strong seasonal flows. The drawdown process may be too difficult or expensive to be performed regularly for large dams, or the scouring effect of flushing may be too narrow for wide reservoirs. Kondolf et al. (2014a) assessed that the ratio of reservoir storage to mean annual flow should not exceed 4%, because of the difficulties in the drawdown procedures. Flushing may be ineffective in removing sufficient volumes of the coarser fraction of the deposited material. Moreover, release of sediment-rich water from these operations may damage downstream ecosystems, especially if performed during typically non-flood seasons, e.g. by destroying in fish spawning ground or increasing turbidity (Kondolf, 2000; Larinier, 2001). Despite all this, flushing is considered one of the most effective sediment management techniques, and has been performed successfully in numerous reservoirs around the globe (Stroffek et al., 1996; Atkinson, 1996; White, 2001; Palmieri et al., 2003). Alternatively, pressure flushing aim to remove sediment from reservoirs by inducing strong hydraulic forces without previous drawdown, by opening bottom gates and creating a flushing "cone" near the outlet. While less expensive, this technique typi-

cally affects material near the intake, and is therefore less effective as a sediment removal tool (Stevens, 2000; Annandale, 2013).

The frequency and duration of drawdown flushings present interesting tradeoff between effective sediment removal and power production losses both during the operation and due to the loss of the entirety of the stored water. Frequent flushings are considered preferable both for the removal of material from the reservoir, by consistently reducing storage losses while avoiding the creation of a cohesive, tough-to-break layer of material on the reservoir floor, and for the conservation of downstream ecosystems, by producing seasonal sediment delivery episodes which mimic natural morphological conditions. On the other hand, the cost of frequent flushing may be too high to bear, especially in large dams where drawdown is more costly (Kondolf et al., 2014a). The presence of multiple dams on the same river network introduces a new layer of complexity, as flushing initiatives must be coordinated to avoid unplanned consequences. For example, in the case of two dams in series on a river, sediment mobilized from drawdown flushing of the upstream dam may be delivered to the downstream reservoir, depositing in its basin and reducing its capacity. A real life example of this is the Genissiat Dam on the Rhône river, which periodically receives high sediment loads from the flushing operations of the upstream Verbois Dams and therefore must adopt sediment flushing techniques itself to avoid excessive sedimentation (Thareau et al., 2006).

River (dis)connectivity alterations assessment

Predicting and quantifying impacts brought by the alteration of the river's natural catchment-scale (dis)connectivity has often proved a daunting task. Negative externalities are commonly underestimated while planning human infrastructures and interventions on rivers Ansar et al. (2014), and impact assessments do not account for the interconnected nature of river systems, where impacts of various origins often extend beyond the vicinity of their local area of origin to broad Spatio-temporal scales (Rosenberg et al., 1997; Grill et al., 2015). To exacerbate the problem, large fluvial systems may present multiple infrastructures and alterations along their course, e.g., multi-dam schemes along the same river network. These works may be planned with years to the decade between each other and managed independently, like in the case of different stakeholders involved or in transboundary rivers. Consequently, while the benefits to anthropic alterations are easier to quantify, estimating negative impacts is often subject to uncertainty and speculations due to the sheer variety and Spatio-temporal scales involved in impact assessment. For example, otherwise identical dams may have drastically different impacts on the river system based on their locations, the hydromorphological and ecological property of the river system, the management strategy employed, and the presence

and legacy of other anthropic interventions or infrastructures on the river network (Andrews, 1991; Jager et al., 2015; Naiman et al., 2000). For the same reasons, adopting conservation strategies and river restoration initiatives may yield positive outcomes or no significant results and even be detrimental if the connective nature of river systems is not accounted for during planning.

To tackle this problem in its entirety would require the adoption of network-scale integrated modelling frameworks of the multiple domains of fluvial ecosystems (i.e., hydrology, ecology, morphology) to identify and estimates alterations over large temporal and spatial scale and considering the cumulative impacts of multiple alterations on the same river network (Richter et al., 2010; Kondolf et al., 2014b). These frameworks should then be included in integrated water resources management (IWRM) and planning approaches. Then, multi-objective analyses (M.A.) within these frameworks quantify and compare trade-offs between the environmental impacts of a proposed project or management strategy and the performances of said development plans for other objectives, be they economic, social, cultural or political (Mendoza and Martins, 2006; Zheng et al., 2009; Castelletti et al., 2008, 2014; Giuliani et al., 2014; Bizzi et al., 2012). However, integrated frameworks of this scale are often hardly feasible due to the sheer complexity of the processes involved, the resources requirement for the large-scale monitoring and data collection, and the numerous uncertainties correlated with modelling complex processes and quantifying future impacts. Thus, most hydromorphological and environmental risk-assessment models focus primarily on reproducing more-contained and more manageable processes, e.g., the estimation of dam impact on fish migration (Paulsen and Wernstedt, 1995; Kuby et al., 2005; Zheng et al., 2009; Ziv et al., 2012), or adopt broad indicators to supply simplified indexes of alterations, e.g., a topologic index (length of disconnected river network) to evaluate river fragmentation (Opperman et al., 2017).

Modelling hydromorphological processes presents a broad set of challenges due to their sheer complexity and lack of monitoring, calibration, and validation data. However, in recent years we can find examples of large-scale hydromorphological models Gilbert and Wilcox (2020); Czuba (2018); Pfeiffer et al. (2020), which in some cases are included in multi-objective analysis frameworks for integrated water resource management (Bizzi et al., 2015; Schmitt et al., 2018a; Wild et al., 2018). It is the scope of the next section to analyze the reasons behind the appearance of these models and explore advantages, limitations, and future potentials for large-scale hydromorphological and sediment transport modeling frameworks.

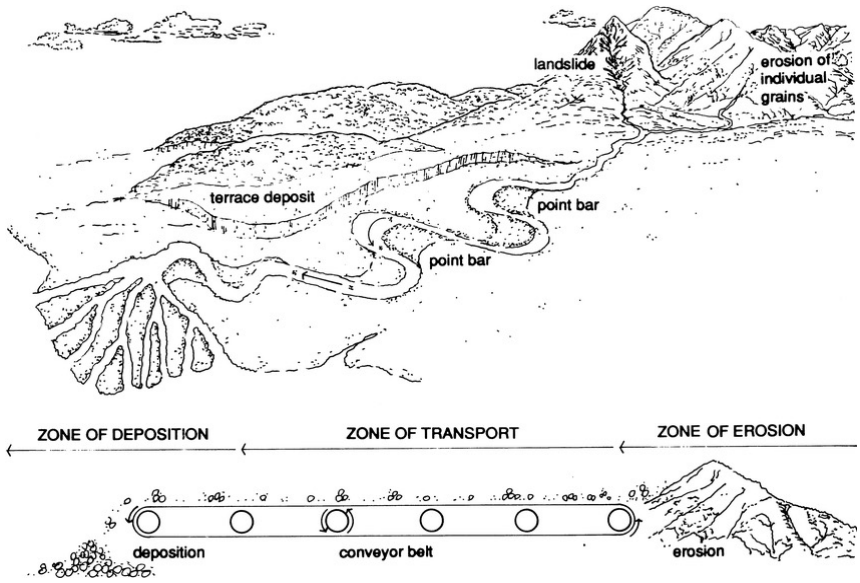

Figure 1.1: *Representation of network-scale sediment transport and delivery as a "jerky conveyor belt", which mobilized material from the zone of erosion, through the zone of transit and eventually to the zone of deposition. Figure from Kondolf (1997).*

1.2 The sediment delivery problem

In 1983, Professor D.E. Walling coined the term *"the sediment delivery problem"* to indicate the limited knowledge of the underlying hydromorphological processes responsible for sediment supply, transport, and storage. In his seminar paper (Walling, 1983), he called for researchers to examine the internal dynamics governing sediment transport and the pathways and timeframes which regulate them. This section introduces the fundamental processes controlling sediment delivery both in the watershed and the river network; and the different and complex interactions that control river hydromorphology.

To use Ferguson (1981)'s analogy, we can visualize river systems as *"jerky conveyor belts"* (Figure 1.1), i.e., a series of pathways where materials are transported heterogeneously through the catchment. On this "belt", we can distinguish three different zones: respectively erosion, transport and deposition. Instinctively, we would equate these zones to the river catchment's upper, middle and lower areas. While this is broadly true from a watershed perspective, this classification is not always correct at smaller scales, as differences in lithology, geology, topology, and ecology may contribute to classifying an area into one of these categories regardless of its position in the catchment (Fryirs, 2013). Dynamic changes within the area, determined by alterations in hydromorphology,

ecology and human activities, may also lead to periodical or permanent shifts in the classification (Fryirs and Brierley, 1999).

Sediments of different materials and sizes are delivered to the stream from the zone of erosion. These areas may be located on the hillslopes or in-channel: in the first case, sediment formation is controlled by weathering and erosion, while delivery to the river may be due to continuous, diffusive processes like rainfall or singular events like rockfalls or landslides; in the second, hydraulic forces within the stream are responsible for mobilizing sediment on the river bed or in the banks (Mueller et al., 2005). The sediment yield due to weathering, and by extension the frequency and intensity of singular erosion events, varies significantly across all scales: between climatic zones (Syvitski et al., 2003; Meybeck and Vörösmarty, 2005) and large watersheds (Andrews, 1991), among close catchments and within the same catchment (Fryirs and Brierley, 2001; Mueller and Pitlick, 2013), or even between single hillslopes and erosion events (Sklar et al., 2017). The driving factors behind sediment creation and delivery are numerous and again vary across scales. On continental scales, plate tectonics and basin relief greatly influence sediment yield (Syvitski et al., 2003). On the catchment scale, lithology, morphology, and difference in local climate and topology are key factors behind variations in sediment production (Andrews, 1991; Nicholas et al., 1995; Syvitski and Milliman, 2007; Andrews and Antweiler, 2012; Mueller and Pitlick, 2013). It is at this scale, moreover, that human influences becomes more relevant (Fryirs and Brierley, 2001; Lu et al., 2004; Shrestha et al., 2021). Within the same river catchment, sediment delivery to the river is influenced in varying degrees by discrepancies in local lithology, vegetation cover and density, elevation, channel morphology, and the presence of elements of disconnectivity like floodplains, swamps, and human infrastructures (Fryirs and Brierley, 1999; Sklar et al., 2017).

The combination of all the processes listed above results in sediment delivery which may differ significantly in both magnitude and composition (material and grain size) across continents, catchments, sub-catchments, and hillslopes. Within zones of transport, the availability and properties of sediments play an essential role in determining the fluvial transport rate (Wilcock and Crowe, 2003). These, together with the channel morphological properties features, e.g., gradient, wet width, and presence of logs and in-channel vegetation, determine the threshold of particle motion, i.e., the minimum energy exercised by the hydrodynamic forces to mobilize grain of a particular size (Engelund and Hansen, 1967; Lamb et al., 2008; Wilcock, 1998). Interaction among sediment of different grains size may also influence this threshold (Wilcock and Crowe, 2003). Once mobilized, sediments are transported at different velocities and with different types of motion: coarse material like cobbles, pebbles, and gravel are typically transported as bed-load, rolling, sliding, and hopping along the river bed

(Meyer-Peter and Müller, 1948; Parker and Klingeman, 1982). Finer grains are either transported in suspension (e.g., silt and clay), or mixed transport (e.g., sand) (Engelund and Hansen, 1967; Wilcock and Crowe, 2003). Again, hydrodynamic forces may influence the type of motion observed in grain particles. The amount of energy available in a reach for the transport of sediment of a particular grain glass is defined as the reach *transport capacity* (Engelund and Hansen, 1967; Molinas and Wu, 2000; Wilcock and Crowe, 2003). As long as the availability of sediment prone to transport exceeds the transport capacity, the river reach is defined as*" transport-limited"*, i.e., the transport capacity is the factor limiting sediment mobilization. On the other hand, when the transport capacity is not satisfied due to unavailability of material, the reach is identified as *"supply-limited"* Whipple and Tucker (2002). Of course, as transport capacity is specific to a sediment class, the same river reach can fall into either category according to the grain type considered. Sediment transport is not limited to the longitudinal scale (i.e., upstream to downstream) but also lateral (i.e.channel to banks and floodplains) and vertical (i.e., different water layers and between water and channel bed).

In most catchments, sediment remains in storage longer than in transport (Otto et al., 2009). Typically, sediment delivery in rivers is a sporadic and episodic process, and often the majority of transport occurs during high flow events (Tabarestani and Zarrati, 2015). At any point, if hydrodynamic forces drop below the threshold of particle motion due to a decrease in discharge or changes in channel morphological features, material may be put in storage in deposit zones. These can be broadly divided into two categories: sediment stores or sinks(Fryirs, 2013). Sediment stores are transient, short-lived, and frequently subject to reworking. Channel features such as banks and benches fall into this category, and according to the type and volume of material deposited, they may form and vanish rapidly, even in the span of two consecutive flood events (Fryirs and Brierley, 2001). Sinks areas are more permanent and less connected to the channel; sediment exchange between sinks and river may be constrained to exceptional flood events. This category includes slopes, floodplains, and terraces (Fryirs and Brierley, 2001). The location, type, and frequency of reworking of deposit zones are thus key drivers of sediment transport in the network. Often, the creation of a deposit zone is attributable to the presence of buffers, barriers, and blankets, which are structures, both natural and anthropic, that impede sediment transport, like swamps, alluvial fans, dams, and wooden debris (Fryirs, 2013). The final sediment sinks are found at the network outlet: estuaries and deltas, which are often consituted by the coarsest fraction delivered from upstream (Syvitski et al., 2009; Nittrouer and Viparelli, 2014).

All these processes interested in the formation, maintenance, and removal of the different zones of erosion, transport and deposition on the *"jerky conveyor*

belt" contribute to creating complex patterns of sediment supply and transport at river network scale, which are often unique to each fluvial system Bracken et al. (2015); Parsons et al. (2015). Therefore, anthropic alterations on river systems may disrupt these patterns at different points, times, and rates, resulting in impacts whose magnitude, timing, and location depends not only on the type of disturbance but also on the hydromorphological processes specific to the river system.

This complex web of dynamic and intertwined sediment transfer processes in river systems has been given the name of sediment (dis)connectivity (Poole, 2002; Heckmann and Schwanghart, 2013; Fryirs, 2013; Parsons et al., 2015; Bracken et al., 2015; Poeppl et al., 2020). At the local scale, connectivity can be defined as the water-mediated transfer of sediment (longitudinal, lateral, or vertical) between two different compartments in the river network Fryirs (2013). If we expand this definition to the catchment scale, we can characterize sediment (dis)connectivity as the connected transfer (or the lack thereof) between sediment sources and sinks over different temporal and spatial scales. In this way, we can conceptualize catchment sediment transfer as a combination of individual processes connecting different parts of the river network. This modelization is at the base of new numerical models, which started appearing in recent times to tackle the problem of describing and quantifying sediment transport and evaluate human impacts on connectivity on the scale of the entire river network (Czuba and Foufoula-Georgiou, 2014; Schmitt, 2016; Wild et al., 2021).

1.3 State of the art of sediment modelling

Modelling sediment transport and (dis)connectivity at a scale relevant for integration in basin-wide integrated multi-objective water resources frameworks has always posed significant research challenges. On the one hand, traditional morphodynamic models simulates hydromorphological processes in 1D-2D or 3D with high accuracy on a scale of single river reach, reproducing relevant morphological events like bar and banks dynamics and even response to local anthropic pressure (Merritt et al., 2003; Briere et al., 2011). However, their extensive computational time and data requirement, especially for the definition of the hydromorphological boundary condition of the river stretch analysed, limits their usefulness to small and well studied catchments and river segments. On the other hand, large-scale, grid-based hydrological models like SWAT, coupled with empirical soil loss equations, e.g USLE (Wischmeier and Smith, 1978) and RUSLE (Renard, 1997), allows for the estimation of sediment inputs and suspended sediment transport (Betrie et al., 2011; Ranzi et al., 2012). At larger scales, however, these models' computational effort hinder their viability, as it limits the possibility for extensive sensitivity analysis and parameters estima-

tion necessary for research at such scale and level of uncertainty.

One of the biggest limitation in the development of sediment connectivity models was the scarcity of field data, which, even when available, didn't have both the temporal and spatial scale necessary for the initialization and validation of dynamic basin-scale modelling efforts. However, in recent years, advances in remote sensing and image processing technologies have lead to an increase availability of large scale hydromorphological datasets, which allow to characterize river network properties at large scale with unparalleled accuracy. The frequent and automated data collection routines of these technology meant data are available for longer timeframes, and could therefore register dynamic hydromorphological changes over time (Van Der Knijff et al., 2010; Schmitt et al., 2014; Roux et al., 2015; Demarchi et al., 2017; Bizzi et al., 2019; Fryirs et al., 2019). These new resources spurred the development of new, more conceptual and numerical models of sediment connectivity and routing. These models lacked the accuracy of local-scale, physic-based morphodynamic models, traded in favour of a more flexible, typically one-dimensional structure which could cover wider spatio-temporal scales and guarantee lower computational times. Most importantly, the new frameworks could characterize and quantify network-scale sediment routing patterns and highlight (dis)connectivity pathways across the network (Benda and Dunne, 1997a,b; Wilkinson et al., 2006; Mueller et al., 2016; Lammers and Bledsoe, 2018; Beveridge et al., 2020; Khan et al., 2021).

Ferguson et al. (2015) proposed a 1-D multigrain modelling structure for a long section of the Colorado river to reconstruct the movement of a sediment pulse, which used empirical transport equation together with an optimization routine to derive patters of morphological response to disturbances in a data-scarce environment.

Czuba and Foufoula-Georgiou (2014) developed a dynamic framework which tracked the spatial and temporal sediment delivery patters on the Minnesota river basin. This model represented sediment transfer as the movement of multiple sediment *parcels*, each carrying a fixed mass of material and tracked as they moved downstream according to empirical sediment transport equations. The framework was expanded in Czuba (2018) with a fractional sediment transport formula which could account for mixed-size sediment transport. This framework has been applied to delineate sediment delivery patterns (Czuba and Foufoula-Georgiou, 2014, 2015), the network response to sediment pulses(Gran and Czuba, 2017), and the effects of post-wildfire sediment delivery (Murphy et al., 2019). However, this approach lacked both a proper sediment mass balances for each reach, and a proper tracing of the sediment sources. Therefore, this approach could not be used to derive information on where sediment from a certain source was deposited.

(Wild and Loucks, 2012b) introduced a daily, basin-scale river basin simulation screening tool for sediment transport and management in controlled river systems. His approach focuses on defining strategy of sediment management for series of dams on river systems Wild et al. (2016, 2019, 2021), and thus is not applied for the characterization of network sediment connectivity patterns.

(Gilbert and Wilcox, 2020) developed SeRFE, a spatially distributed sediment transport model which explicitly include representation of floodplain sediment exchange with river channels, and applied to reconstruct floodplain erosion after wildfire events in two watersheds in California. However, the model did not represent channel geometry changes caused by sediment deposition and erosion, and focused on simulating only short timeframes.

The frameworks presented here are some of the few available tools that try to tackle the challenge of reconstructing sediment (dis)connectivity patterns at the network scale. The complexity of this task alone means that applications of these models to provide indicators of connectivity impact assessment for sustainable water resources management are still in their infancy. Few attempts have been tried to integrate large-scale sediment connectivity models in decision-making frameworks. Some of the most successful of these endeavors have been conducted with the CASCADE model (CAtchment Sediment Connectivity And DElivery) (Schmitt, 2017), a basin-scale numerical sediment transport model designed to simulate network sediment (dis)connectivity in data-scarce environments and provide an exploratory tool to quantify sediment transport alterations due to anthropic disturbances.

1.4 The CASCADE model

CASCADE forms the structural basis of the work presented in this thesis. This section explores the structure and functioning of the CASCADE model and its limitation and potential for further development.

CASCADE employs a graph-based routing scheme, which has proven an effective tool to describe spatial patterns of connectivity in landscapes (Cheung et al., 2015; **?**) and fluvial systems (Czuba and Foufoula-Georgiou, 2015; Lammers and Bledsoe, 2018; Beveridge et al., 2020). The network is partitioned into different *reaches*, or *edges*, separated by *nodes* located at the edges. The nodes sited at the beginning of each river branch are defined as *source nodes*, and the reaches in the network that has an upstream node a source node as *source reaches*. Each reach is defined as a section of the river network with homogeneous hydromorphological features. Network partitioning may be uniform, with reaches of similar length, or feature-based, where rivers are segmented according to discontinuities in morphological or hydrological properties. Each reach is defined by a single set of hydromorphological features, e.g., discharge,

channel gradient, width, and roughness, and given a unique identification. Typically, the river network is extracted from Digital Elevation Models (DEMs) using software for topological analysis (Schwanghart and Scherler, 2014).

In CASCADE, the sediment delivery is described through the combination of individual transport processes called *"cascades"*, each one defined by its source: a single reach in the network. At its source, the cascade is characterized by a value of sediment flow and specific grain size. By proceeding through the reaches downstream the source, cascades can deposit part of its sediment load until either it depletes completely or it reaches the basin outlet. No new material con be added to an already existing cascade.

Figure 1.2 visually describes the fundamental concepts of the CASCADE approach. As they move downstream, multiple cascades may transit in the same reach. In this case, the sum of the sediment fluxes of the cascades passing through the reach indicates the total sediment flux. The delivery of sediment through a reach is controlled by the reach transport capacity, which is measured using standard sediment transport formulas which determine the total energy available for transportation from the network features (Engelund and Hansen, 1967; Yang, 1984; Wong and Parker, 2006). If the total combined flow carried by the cascade exceeds the transport capacity, part of the sediment flow deposits in the reach. The flow deposited for each cascade varies according to the total flux carried and the grain class. As transport capacity provides a singular value of maximum sediment flow, different scenarios of competition are defined to determine the deposit for each cascade (Schmitt et al., 2016). The total sediment flux carried by the cascade, now equal to the reach transport capacity, is then delivered to the downstream reach, where the process is repeated anew.

The resulting intertwined patterns of cascade movement provide numerous information on the morphological and connectivity properties of the network. At a reach scale, CASCADE produces information about the magnitude, provenance, and type of transported and deposited sediments. At a basin scale, the model helps to identify sediment (dis)connectivity patterns in the network and characterize the morphological role of each reach in the network.

CASCADE is a static model, providing information on the instantaneous sediment transport and connectivity for a specific water flow regiment. The estimation of annual sediment transport is thus performed by repeating CASCADE's runs with different water flow scenarios, covering both average and extreme hydrological conditions. The simulations outputs and then aggregated considering the yearly frequency of each scenario to obtain the annual sediment budget.

By appropriately changing reach features to reflect the introduction of anthropic disturbances, e.g., changing the morphological characteristic of reaches falling flooded by the reservoir of a planned dam, and comparing the resulting

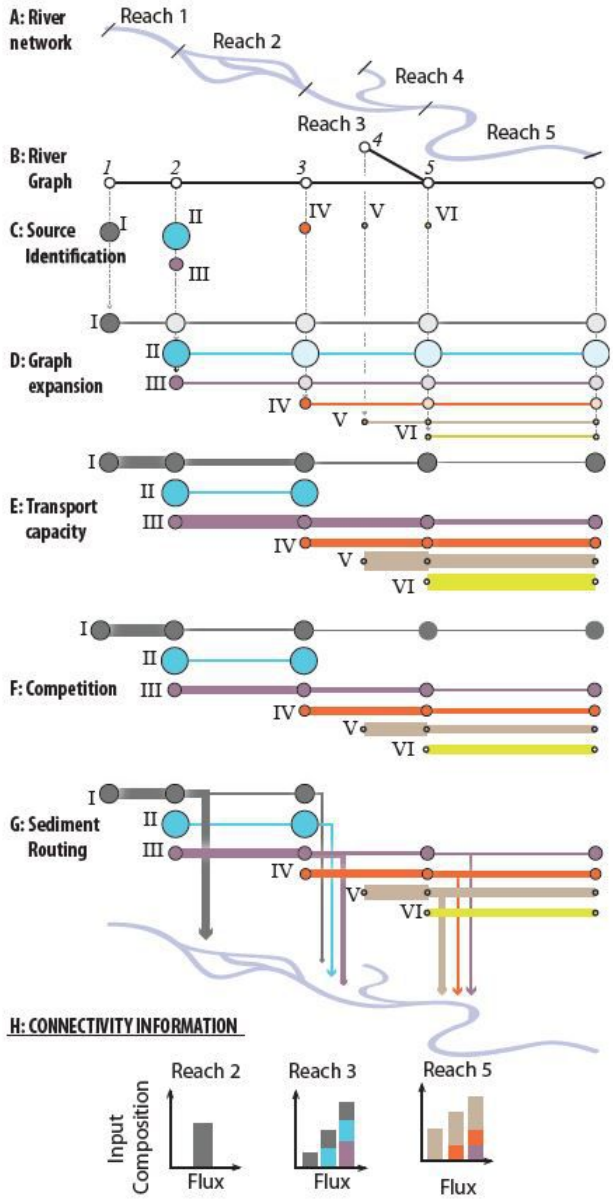

Figure 1.2: *Graphical representation of CASCADE framework. A: river network subdivision in reaches. B: graph representation of the river network by nodes and edges. C: sediment sources identification. D: graph expansion in the possible connected nodes. E: representation of the transport capacity for each grain size and for each reach, indicated by the line width. F: competition corrected transport capacity. G: routing of sediment cascades. H: informations about the sediment flux, provenance, sorting and connectivity are provided to each reach by the multiple cascades crossing it (Figure and caption adapted from Schmitt (2016)).*

CASCADE outputs with the baseline scenario, the model can derive distributed indicators on the cumulative alterations of sediment delivery and transport brought by said disturbances. The flexible and data parsimonious structure of the model allows for stochastic modelling of sediment fluxes to account for uncertainties and data-scarcity (Schmitt et al., 2018b), or for inclusion in integrated multi-objective water resource management and planning framework, to evaluate trade-offs between sediment connectivity conservation and energy production for the development of multi-dam schemes (Schmitt et al., 2018a, 2019).

However, the CASCADE model presents limitations in its structure, which limits its viability. First of all, attributing to each cascade a single grain size glass is a somewhat limiting modelling strategy, as, even in the span of a single reach, localized sediment sources may deliver to the stream material of very different sizes. Moreover, using total transport capacity formulas forces the model to adopt competition strategies to determine priority in deposition among cascades located in the same reach, which may be difficult to justify and validate.

Moreover, CASCADE is by its nature a static model, describing instantaneous sediment connectivity in a particular hydrological scenario or a combination of static scenarios extracted from hydrological records. Therefore, it cannot account for the temporal dynamics among sediment cascades and the timing in the delivery of cascades caused by different sediment transport velocities. Furthermore, it cannot explore the consequences of reach hydromorphological features evolution brought by dynamic disturbances to the sediment (dis)connectivity, ascribable to both natural and anthropic causes. Hence, CASCADE cannot evaluate the consequences on the hydromorphology of heterogeneous drivers of change that differentiate in timing, location, intensity, and duration at both the reach and network scales. The model's static framework cannot process the effects across years and decades of multiple disturbances displaced in time and space, e.g., basin-scale land-use change and infrastructure implementation on the timescale of years and decades. Furthermore, while CASCADE has been successfully tested in strategic dam portfolios planning scenarios, it lacks the tools to provide indicators of sediment (dis)connectivity alterations brought by the cumulative and intertwined effects of multiple reservoirs' operational strategies. Expanding the modelling framework to include a dynamic representation of sediment transport processes is thus a necessary step to increase the flexibility and relevancy of the model for applications in decision-making contexts.

1.5 Thesis motivation and objectives

Building on the aforementioned research challenges and opportunities in basin-scale (dis)connectivity modelling and integration in water resource management, this research contributes a set of novel modelling tools and techniques designed to simulate network pattens of sediment transport and delivery with greater accuracy and including representation of hydromorphological processes missing in state-of-the-art modelling frameworks. The foundation of these techniques remains the original CASCADE model, which is modified, sometimes substantially, to develop basin-scale sediment transport models in the pursuit of two different objectives:

1. *Morphological assessment and network (dis)connectivity analysis*. Sediment connectivity models for this objective are developed as analytical tools to estimate network morphodynamic properties, e.g., sediment load and type and their sensitivity to hydromorphological changes. The CASCADE model is adapted to analyze and disaggregate the effects of multiple, dynamic, and distributed drivers of change on network sediment (dis)connectivity patterns. Specific formulas and components are integrated into the framework to evaluate or even simulate morphological changes in the reaches brought by sediment transport and delivery.

2. *Sustainable water resources planning and management*. This task focuses on incorporating tools in the new frameworks to evaluate the river system's geomorphological response to multiple human disturbances. These include multiple alterations displaced in time and space across the network, e.g., cumulative dam operational strategies, progressive land-use change, channelization, sediment mining, and others. In these contexts, the models are designed to provide network-scale sediment delivery and transport alterations indicators to explore and compare competing and contrasting development and management plans.

In the work presented, these two broad objectives translate in a series of focused tasks, which pursuit in greater detail specific aspects of the objectives:

- integration of multi-class sediment delivery and fractional transport capacity computation in the CASCADE framework;
- development of a open source toolbox which includes the base multi-class CASCADE model, completed with different customization options and interactive output visualization tools;
- generation of distributed hydromorphological information in data-scarce environment, using optimization tools and global sensitivity analysis; the

model outputs are then integrated into traditional morphological analysis tool to evaluate channel resilience to fluvial form shifts.

- development of a new dynamic modelling framework for network-scale sediment transport and reach sediment budget and deposition. The new model traces and deconstructs Spatio-temporal routing pathways at the basin level and simulates the combined effects of sediment delivery from multiple heterogeneous sources displaced in time, location, and type and magnitude of sediment carried;
- integration in the new dynamic framework of add-ons components to reproduce dynamic changes in river morphological features, e.g., channel width and gradient, brought by variations in sediment delivery, deposition, and entraining;
- inclusion and simulation of the effects of multiple reservoirs on river networks. This analysis is not limited to reservoir siting. Instead, it includes the representation of dynamic variations in water and sediment storage in the reservoir, the simulation of the network-scale hydrological and morphological effects of different operational strategies, and the integration of sediment management techniques like drawdown flushing.

The development of the two sediment transport models represents the major novelty presented in this thesis. Both expand the range of river and catchment sediment (dis)connectivity processes represented in large-scale, data parsimonious modelling efforts and showcase promising potential as exploratory tools to quantify distributed indicators of morphological alterations brought by anthropic disturbances on river systems. These indicators can then be integrated into optimization-based, multi-objectives decision frameworks for exploring trade-offs between sediment (dis)connectivity conservation and other objectives among competing river resources management strategies, following the procedure seen in Schmitt et al. (2018a, 2019).

1.6 Thesis outline

Figure 1.3 illustrates the five main components of this thesis, along with their main objectives and accomplishments. Each one of the thesis chapters is dedicated to one of these components.

Chapter 2 Chapter 2 presents the CASCADE toolbox, a Matlab-based toolbox for large scale sediment modelling which expands on the original CASCADE model by including a multi-class representation of cascades and fractional sediment transport capacity formulas which provides a more complete

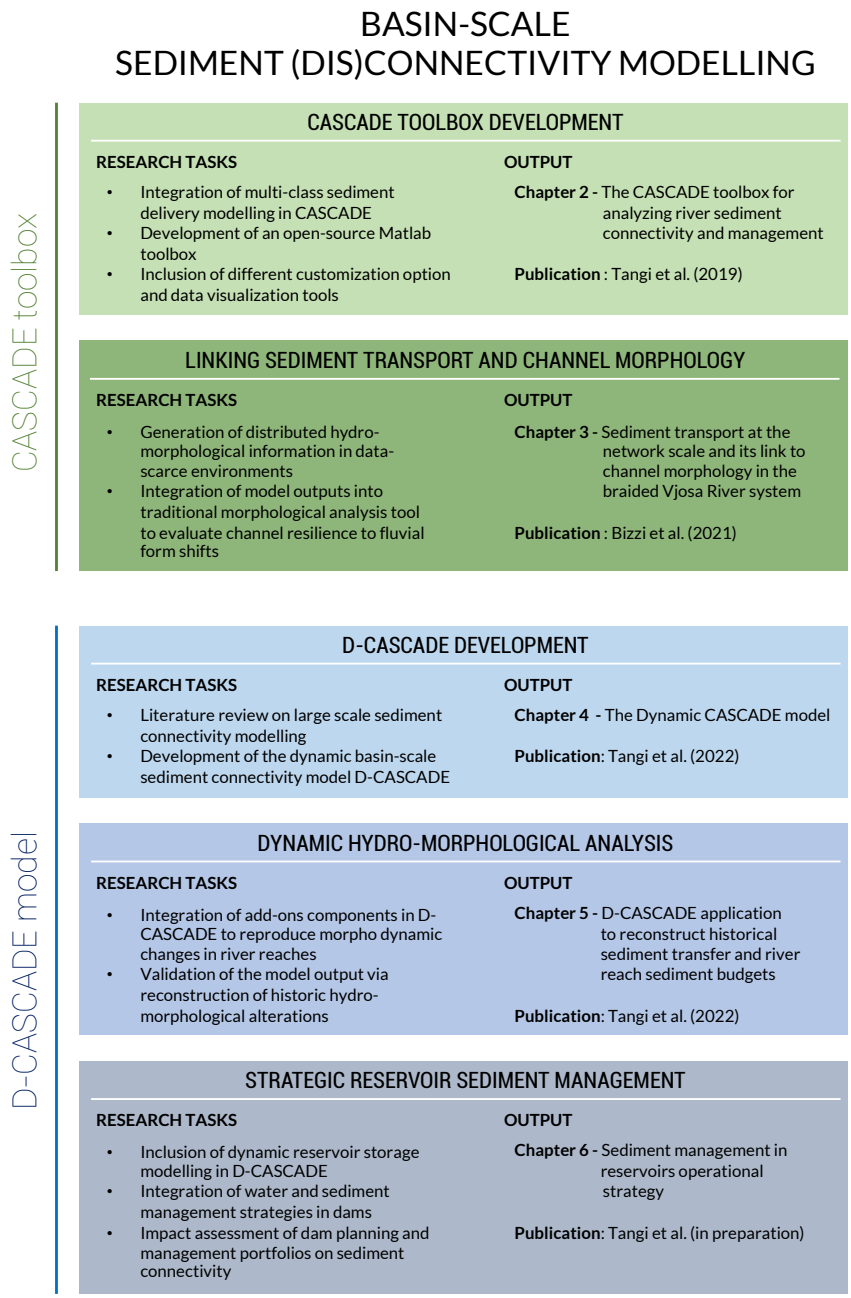

Figure 1.3: *Overview of the main research tasks accomplished in this thesis, and their relative outputs.*

representation of the sediment deliver process. The toolbox is designed to be flexible, data parsimonious and computationally efficient, with multiple customization options and output visualization tools to tailor the model to the specifics of the research objectives and case studies.

The content of this chapter is adapted from Tangi et al. (2019) and focuses on Objective 1.

Chapter 3 Chapter 3, details the application of the multi-class CASCADE model described in chapter2 to the Vjosa river network, in Albania, one of the last unimpaired braided fluvial system in Europe, with the dual purpose of gaining distributed informations on surface grain size distribution and bedload transport, and estimating braided reach resilience to shifts toward single-channel fluvial forms.

The content of this chapter is adapted from Bizzi et al. (2021) and focuses on Objective 1.

Chapter 4 Chapter 4 introduces the dynamic CASCADE model, or D-CASCADE, a dynamic, network scale sediment connectivity and transfer model. The framework introduces a discrete, daily time representation of sediment delivery, entraining and deposition. Cascades are routed thought the network according to sediment velocity estimates by empiric hydromorphological equations. Changes in reach features like bed deposit stratigraphy, channel gradient and width are also modelled via specific add-ons components. The dynamic and intertwined representation of these processes allows for simulations of various morphological events, such as bed armouring and scourging, bank erosion, variations in reach GSDs, discontinuous or pulse delivery of material from flood events and punctual sources, and others.

The content of this chapter is partially adapted from Tangi et al. (2022) and explores aspects of Objective 1 and 2.

Chapter 5 Chapter 5 introduces the Bega river network case study, in NSW, Australia, and showcases how D-CASCADE can be used to reconstruct the historical effects of distributed anthropic drivers of change on the network (dis)connectivity, offering an unique network-scale perspective on hydromorphological dynamics and what happens when they are disrupted by multiple, distributed and time-varying disturbances. The abundance of knowledge on the Bega river system morphological history, and the availability of large hydromorphological dataset makes the Bega river network an ideal case study for testing and validating the D-CASCADE model.

The content of this chapter is adapted from Tangi et al. (2022) and pursuits Objective 1.

Chapter 6 In Chapter 6, the D-CASCADE model is applied on the 3S river system, a tributary of the Mekong, to evaluate basin-scale sediment transport and evaluate the effects of reservoir water and sediment management strategies on network connectivity. Specific components are added to integrate reservoir impoundment into the network, represent dynamic variations of water and sediment storage and simulate dam release strategies and their effects on downstream reaches hydromorphology. Network sediment yield is estimated for competing dam development scenarios, and with different frequency and timing of drawdown flushing.

The content of this chapter is adapted from Tangi et al, "Sediment connectivity conservation in the Mekong via strategic reservoirs water and sediment management." (in preparation) and focuses on Objective 2.

Chapter 7 Chapter 7 summarizes the main achievements and results of the previous chapters, highlights limitations in the modelling and theoretical approaches and showcases the potential for further developments in the field of river sediment (dis)connectivity modelling and its integration in water resource planning and management.

2

The CASCADE toolbox for analyzing river sediment connectivity and management

Sediment connectivity in rivers directly links to most fluvial processes and ecosystem services. Modelling network-scale sediment connectivity and its response to anthropic alterations, such as dams or land-use changes, is key to better understanding river processes and to inform river basin management. This chapter described a Matlab toolbox for network-scale sediment connectivity based on an implementation of the CASCADE (CAtchment Sediment Connectivity And DElivery) model. CASCADE combines concepts of graph theory with empirical sediment transport formulas to quantify sediment transfers between many connected sediment sources and sinks in a river network. Improved numerical efficiency compared to common hydrodynamic models enables application to large river networks, stochastic simulations of sediment connectivity, and screening impacts of many infrastructure portfolios. Input data requirements are flexible and basic functionality is available with globally available datasets to ensure applicability to poorly monitored basins. The toolbox offers options for customization and interactive output visualization tools.

This chapter is developed based on: Tangi, M., Schmitt, R., Bizzi, S., Castelletti, A., 2019. The CASCADE toolbox for analyzing river sediment connectivity and management. Environmental Modelling & Software 119, 884 400–406. DOI:10.1016/j.envsoft.2019.07.008.

2.1 Introduction

River sediment connectivity describes the transfer of sediment between many connected sources and sinks in a river network. Sediment connectivity plays a crucial role in river management and conservation as it drives processes forming the physical shape (morphology) of river channels, which controls, for example, the provision of habitat or the stability of river bed and banks. Connectivity is an emergent property of river networks, as it includes not only spatial relations between sediment sources and sinks, but also process rates and timing of sediment transfers (Fryirs et al., 2007; Bracken et al., 2015; Heckmann et al., 2018; Wohl et al., 2019). These process rates vary across the many sediment sources in a river network as a function of supply rates, supplied grain sizes, and the transport capacity of the river network. The transport capacity is, in turn, a function of the hydromorphologic properties of the network, i.e., river gradient, width, and discharge, and of the river grain size and the resulting grain size distribution of transported sediment. These factors make sediment connectivity of significantly higher complexity than the mere topological connectivity of a river network. Supply and transport processes driving sediment connectivity have been greatly altered in many rivers by anthropic disturbances (Clément and Piégay, 2003; Surian and Rinaldi, 2003; Simon and Rinaldi, 2006; Poeppl et al., 2017; Gregory, 2019). Land use change, such as deforestation and mining, increases rates and types of sediment supply. Reservoirs typically trap parts of the incoming sediment and reduce sediment supply to the downstream network (Kondolf et al., 2014b). Changing discharge magnitude and pattern, e.g., because of hydroclimatic changes or hydropower operations, alters the conveyance capacity of river channels (Bizzi et al., 2015). Together, these competing or compounding drivers cumulatively impact sediment connectivity and lead to major shifts in river processes on local and whole-network scales (Fryirs and Brierley, 2001; Syvitski et al., 2009; Kondolf et al., 2014b; Dufour et al., 2015). Network scale models for sediment transport are hence a prerequisite to analyze human impacts and develop river basins plans with less impacts on sediment transport and related ecosystems services.

Currently, there is a gap in the ability to model sediment connectivity at the network scale. Morphodynamic models for engineering and research applications allow modeling river morphologic processes in 1D, 2D and 3D with high accuracy. However, their computational demand and their data needs make them generally limited to specific well monitored river sections , or, even in case of simplified model formulations, to river segments where well defined boundary conditions of sediment supply and hydromorphology can be defined (Briere et al., 2011; Lammers and Bledsoe, 2018). Even where data and computer power are available, such models do not take into account the connected nature of sediment transfers, where a single river segment is influenced by sediment supply

and transport processes in the entire upstream river network (Merritt et al., 2003; Fryirs et al., 2007).

Recently, numerical models of network-scale sediment connectivity have emerged (Betrie et al., 2011; Ranzi et al., 2012; Czuba and Foufoula-Georgiou, 2014, 2015; Schmitt, 2016; Coulthard and Van De Wiel, 2017; Czuba et al., 2017; Czuba, 2018), a development which was largely enabled by network-scale derivation of relevant data from remote sensing (Schmitt et al., 2014; Demarchi et al., 2017; Bizzi et al., 2019). CASCADE (CAtchment Sediment Connectivity And DElivery) (Schmitt et al., 2016) belongs to this group of models designed to merge the representation of relevant complexity in network sediment transport with simplifications required to make their application practical for large river networks and river basin management tasks (Schmitt et al., 2018a,b).

In this chapter, we present the implementation of CASCADE as an open-source MATLAB toolbox. The toolbox simulates sediment fluxes and their provenances for any reach in a network, and allows to integrate disturbances, such as dams and barriers, and natural and man-made local sediment supply features such as debris flows flow, alluvial fans, or mines. The toolbox comes with an interactive user interface supporting visual analytics of model outputs and allows to explore and quantify how anthropic and natural sediment connectivity alterations affect basin-scale sediment fluxes from the reach to the network scale.

2.2 CASCADE model

Fig 2.1 details the three steps to simulate sediment connectivity in a river network using the CASCADE model. In a nutshell, CASCADE first extracts the river network and assigns hydromorphologic parameters to each reach (Figure 2.1a). Second, additional features area added to the network. Such features can be sediment sources, defined in terms of sediment supply rates and supplied grain size distribution (according to the Wentworth classification (Wentworth, 1922) as well as dams and other disturbances (Figure 2.1b). Third, connectivity for each sediment class from each source is calculated by applying either of four empirical sediment transport formulas at the network scale. The outputs can be interpreted in several ways, allowing to track the fate of sediment from a specific source, as well as determining the sediment flux and origins from many sediment sources from the perspective of a downstream reach (Figure 2.1 c).

2.2.1 Network extraction and hydromorphological characterization

As input, the model needs a representation of the river network (Figure 2.1 a) as a directed graph consisting of nodes and reaches. In the network, each

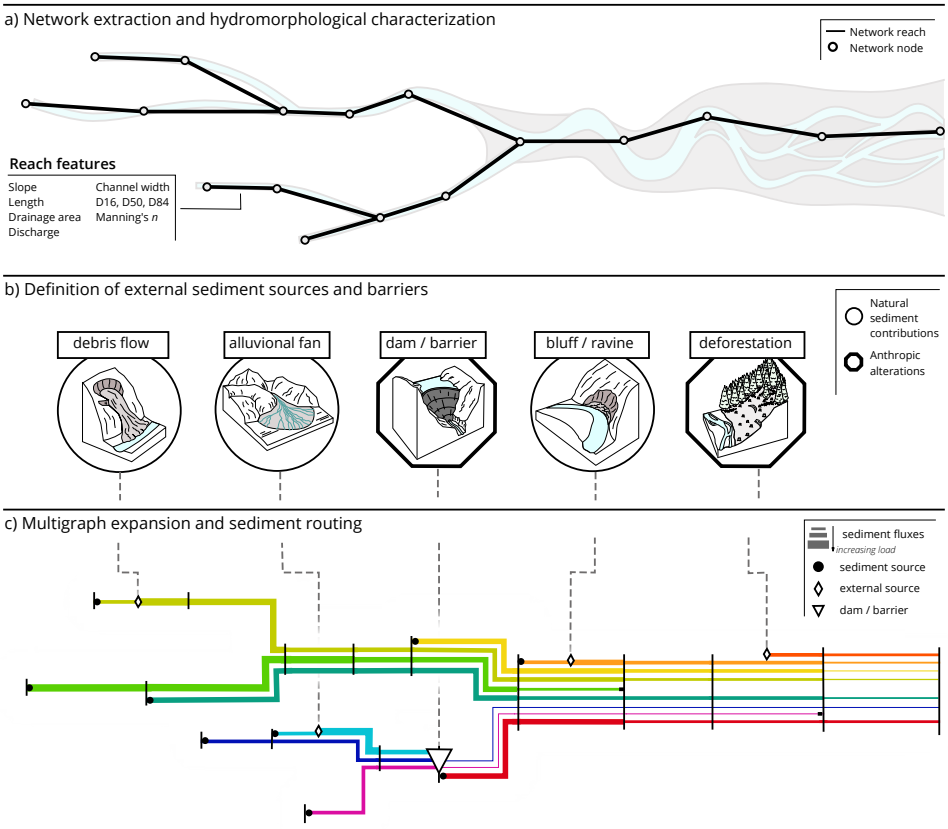

Figure 2.1: *Representation of the CASCADE framework. Fig a) shows the extraction of the river network and the characterization of the features for each network reach (reported in Table 2.1). Fig b) represents some examples of external sediment sources that can be included in the model. Fig c) visualizes the sediment routing process. Each line represents a sediment cascade, i.e., the transport process conveying sediment from a specific source through the downstream river network.*

Data source	Parameter	Description
Extracted from DEM	Slope [m/m]	Derived from the upstream and downstream node elevation of a reach.
	Length [m]	Desired length of individual reaches. Set by the user, derived from the network topology (see Table 2.2), and/or according to user supplied break points.
	Ad [Km^2]	Drainage area at the downstream node of a reach derived from the DEM.
User defined	Q [m^3/s]	Discharge for a chosen discharge scenario. Obtained from interpolation of gauging station datasets (Schmitt et al., 2016) or spatially distributed hydrological models (Schmitt et al., 2018b) .
	Active channel width [m]	Width of the channel section for a given discharge scenario. Obtained from satellite imagery(Schmitt et al., 2014; Schmitt, 2016; Schmitt et al., 2018b), field studies, or global data.
	D16, D50, D84 [m]	Grainsize distribution parameters of sediment on the surface of the river bed. Interpolated from available point sediment samples, expert-based assessments, or based on hypothesis regarding river sediment transport regimes.
	Manning's n	Manning's roughness coefficient for the bed material in the channel. Obtained from filed data or estimated from literature.

Table 2.1: *Key input parameters and the possible sources for deriving parameters values on network scales.*

reach connects two nodes and represents a part of the river network with homogeneous geomorphic and hydraulic features. The reach is the core modelling unit in CASCADE, as sediment transport rates are calculated based on reach-averaged values of geomorphic and hydraulic features. The reach definition can be automatized based on homogenous user-defined maximum length, network topology (Heckmann et al., 2015) or by user-supplied break points. The latter can be used, for example, to segment the network according to a geomorphic analysis.

The CASCADE toolbox includes all the functionalities to extract and preprocess a river network, run the CASCADE model and visualize and analyse results. The toolbox relies on Topotoolbox (Schwanghart and Scherler, 2014) for river network extraction from a Digital Elevation Model (DEM). Each reach is assigned a set of hydromorphologic attributes related to sediment transport (see Table 2.1). Some of these attributes, such as channel slope, length and drainage area, are derived from the DEM. The remaining attributes, such as discharge and active channel width, require external data sources, from modeling, surveys, field data or a mixture of those. Finally, grainsize distribution (GSD) in the bed surface (D16, D50, D84) and Manning's roughness coefficient need to be provided for each reach. This data is rarely available on network scale and can be initialized using interpolation from scattered field observations or based on hypothesis about regime calculations (Ferguson et al., 2015). CASCADE models the instantaneous sediment transport fluxes in Kg/s in each reach for a single discharge value, e.g., the mean annual discharge. Sediment transport during different discharge conditions can be represented through individual model runs.

The hydrologic and geomorphic attributes are used to compute the transport capacity of each reach, i.e. the amount of energy available in a reach for the transport of sediment of a specific size. Four alternative sediment transport formula are implemented in CASCADE: Wilcock and Crowe (2003), Engelund and Hansen (1967), Yang (1973), Wong and Parker (2006).

While Wilcock and Crowe (2003) is a fractional transport capacity formula, i.e. it returns transport fluxes for each grain size class, the other formulas provides only a single value of transport capacity often based on the D50 of the GSD given as input. Thus the toolbox provides two different partitioning methods for obtaining fractional transport rates, based on Molinas and Wu (2000). The Bed Material Fraction (BMF) approach computes the total transport capacity for each grain size class independently using the desired formula, assuming uniform sediment size and thus equating the D50 in the formula to the mean grain class diameter. Fractional transport capacity is then obtained by combining total transport rates for each class with grain class frequency in the sediment mixture. This approach is common in numerical models (Molinas and Yang, 1986; Rahuel et al., 1989; , US), however, it does not consider particle in-

teractions and shielding effects, and it's sensible to the number and frequency of the class sizes used (Hsu and Holly Jr, 1992). The Transport Capacity Fraction (TCF) approach, instead, first measures the total transport capacity using the chosen formula for the median grain size of the sediment mixture (D50), then it obtains fractional transport rates by breaking it into multiple fraction, one for each grain class, based on a transport capacity distribution function. In the toolbox, we implement a distribution function proposed by Molinas and Wu (2000).

2.2.2 External sediment sources and barriers

The CASCADE toolbox can account for user-defined sediment sources from the hillslopes or river banks (in Figure 2.1 b) and dams and barriers that retain sediment (triangle in Figure 2.1 b). Sediment sources are defined according to their supply rate and the grain size distribution of supplied sediment. Dams and barriers can be modeled using simple representation of reservoir hydraulics (Schmitt et al., 2018a), empirical formulas (Kondolf et al., 2014b), or from observed trapping rates.

2.2.3 Multigraph expansion and sediment routing

After the network extraction, the definition of reach attributes, the addition of external sediment sources and the calculation of the transport capacity CASCADE can use these data to simulate sediment connectivity. To do so, CASCADE uses principles of graph theory to describe the spatial relation between sediment sources and sinks in the river network (Heckmann et al., 2015). Sediment transport in the river network is described as a combination of "cascades", each representing the sediment transport from a specific sediment source through the downstream network. Each cascade originates from a source in the network (black dots in Figure 2.1 c) and its path toward the outlet node of the network is defined by the network topology. As a cascade traverses multiple downstream reaches, it might deposit part of the original sediment load, if the transport capacity of a reach exceeds the sediment flux. A cascade is terminated as soon as it deposited the entire sediment supply or reaches the outlet. A river reach can be traversed by many cascades (each from a specific source and hence with a specific sediment flux and grain size distribution). The original river graph, in which each edge represented a river reach, is hence expanded into a multi-graph, in which each multi-edge resents a sediment cascade in a specific river reach (Schmitt et al., 2016).

Compared to previous CASCADE applications (Schmitt et al., 2016, 2018b), sediment supply in this toolbox is defined not by a single grain size, but by sediment distribution. This is useful to more realistically represents sediment sup-

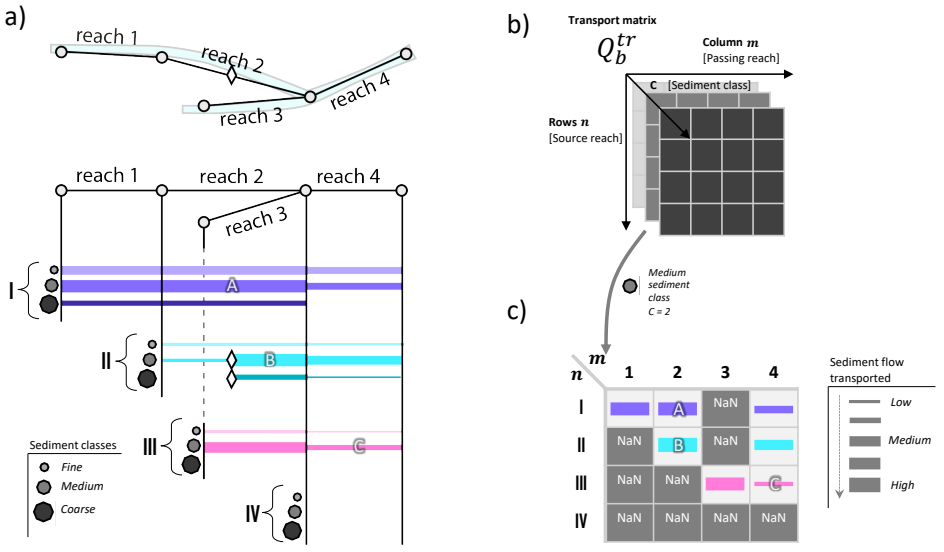

Figure 2.2: *Visualization of multiple cascades and the model output structure. Panel a visualizes how cascades (identified with roman numerals) are partitioned into sub-cascades carrying sediment of one of the a-priori defined sediment classes (three in this example), this panel is a cutout from Figure 2.1 c. Panel b visualizes the structure of the data-structure of outputs, which is as a three-dimensional matrix of dimensions n x m x c (in this case 4 x 4 x 3). The content of the matrix can be analysed in different dimensions. Panel c shows the analysis of sediment flux for a specific grainsize (c=2) for all edges. Cell C, for example, contains the sediment flux for sediment class 2 originating from source III in reach 4.*

ply to river channel. This requires that each cascade is expanded to represent the transport of multiple grain size classes, (Figure 2.2 a). By default, the toolbox uses 18 grain size classes. In each reach the model calculates sediment transport for mxccascades, where m is the number of upstream sources and c is the user-defined number of grainsize classes.

CASCADE computes a budget for each grain size in each reach. This means that if the flux of sediment into an edge exceeds the transport capacity of that edge, part of the sediment will be deposited on the river bed. If, instead transport capacity is higher than the influx, new sediment can be entrained and transported, if available from the river bed or hillslopes contributions, generating a new cascade.

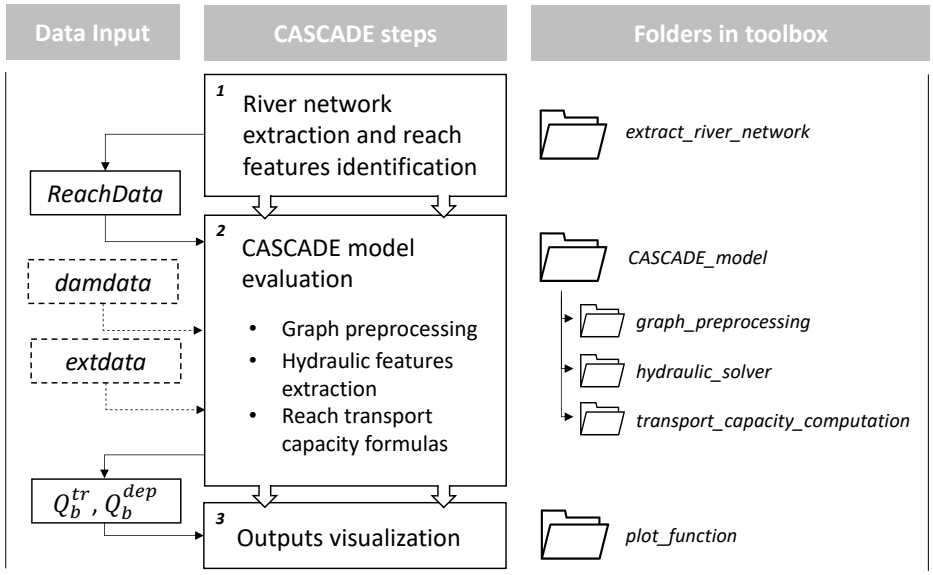

Figure 2.3: *Basic steps of CASCADE and corresponding output and folder structure in the Toolbox. Dashed box in the Data input column represent optional input data. The river network extraction step requires the use of functions from the TopoToolbox.*

2.3 Toolbox structure

Figure 2.3 shows the file structure of the CASCADE toolbox. The application of the CASCADE model is executed in three steps:

1. Extraction of the river network from a DEM, identification of the river network reaches and definition of the reach features (Table 2.1). This information is organized as a data structure named ReachData;

2. Evaluation of the sediment fluxes in the network with the CASCADE model;

3. Visualization and interpretation of the model outputs.

The functions in folder *extract_river_network* extract the river network and some morphologic parameters (length, slope) from a DEM. Users can customize the resulting river network by changing the inputs to the network extraction function (See list in Table 2.2).

The network is stored in the *ReachData* struct, the main input to the CASCADE model. Each row in *ReachData* represents a single reach in the network and columns contain reach features (listed in Table 2.1). Features not extracted

from the DEM are inserted by the user according to the case study. *ReachData* struct can be exported as shapefile for visualization and further processing in any GIS environment.

CASCADE uses *ReachData* to model sediment transport and connectivity. The main folder *CASCADE_model* contains the operations necessary for running CASCADE. The function in the folder requires as input the *ReachData* struct; if user-defined sediment sources are present, they are included in the model with the *damdata* and *extdata* struct, for dams and external sediment flow respectively. Refer to the user manual for additional information of the implementation of these data structures.

The CASCADE toolbox allows for the different customization options for the framework, including different methods of sediment transport capacity calculation and hydraulic features estimation, the possibility of limiting the sediment availability of the reaches, and thus the flow of sediment a reach can entrain in the model, and the incorporation of dams and additional sediment fluxes. Table 2.2 contains the full list of the customization options available in the released version of the CASCADE toolbox. A user interface with dialog boxes is also included, to guide in the selection of the different options of the model for first-time users.

Modelling step	Input options	Description	User-Options
Network extraction	Minimum Drainage Area	Minimum surface area a stream must drain to be included in the network. Changes the network complexity, the number of reaches and the amount of required input data.	
	Network Segmentation	Segmentation to approximate a fixed reach length (Schwanghart and Scherler, 2014), topologic (break at confluences), or based on user-defined breakpoints. It affects length and number of networks reaches.	• Constant length for uniform partitioning • User defined coordinates of the breaking points for manual partitioning.
CASCADE framework	Transport formula	Empirical sediment transport formula to calculate transport capacity.	1. Wilcock and Crowe (2003) 2. Engelund and Hansen (1967) 3. Yang (1973) 4. Wong and Parker (2006)
	Hydraulic parameter computation	Approach for approximating hydraulic conditions (flow depth and velocity) in each reach	• Hydraulic Solver, based on the iterative approach for flow depth computation (Schmitt, 2016). • Manning – Strickler formula (Manning, 1891).
	Dam implementation	Dams and barriers in the network.	Matrix of dam's location and inferred trapping efficiency.
	External sediment sources	External sediment supply	Matrix reporting the location and features of the supply.
	Erosion limit	Limits the quantity of sediment that can be eroded and entrained in a reach in case the transport capacity is higher than the supply (supply limited vs transport limited)	Scalar value from 0 to 1, defined as fraction of transport capacity for each grain size class. 0: no erosion. 1: erosion until transport capacity is matched.

Table 2.2: *List of main customization options available in the CASCADE toolbox*

2.4 Outputs and visualization options

The main CASCADE toolbox outputs are three-dimensional (nxmxc) m matrices representing sediment transport and deposition in the river network Q_b^{tr} and Q_b^{dep}. In this representation, n and m indicate the number of reaches and sediment sources in the network and c the number of sediment classes. Figure

2 c shows a graphical representation with n=4 and c=3. Each cell $[n, m, c]$, Q_b^{tr} and Q_b^{dep} stores the sediment flux and deposition (both in $[Kg/s]$) of sediment class c in reach m originating from source n (Figure 2.2 b). Through this structure, CASCADE allows to track the fate of each sediment class originating from any sediment source in the river network. Results can be aggregated on the scale of the single reach to analyse, e.g., how much sediment is transported in total and what the statistic properties (e.g., mean, median, percentile grain sizes) of transported and deposited sediment are.

The CASCADE toolbox provides the user with several functions which produce plots to visualize the outputs and aid in the understanding of the model results. The visualization tools in folder *plot_function* include the *Interactive connectivity assessment (ICA)* function, that guides the user in exploring the sediment connectivity on the scale of the a river network (Figure 2.4 a and Figure 2.4 b) and single reaches (Figure 2.4 d), including transported load, provenance and composition of the incoming cascades. Function *Connectivity Alteration Assessment (CAA)*, included in the same folder, provides, together with the options in ICA, a visual framework of sediment connectivity on which the user can interactively include or remove dams and external sediment contributions and visualize the changes in sediment transport, both at the whole network scale and at the reach scale (Figure 2.4 c).

2.5 Conclusions and outlook

The CASCADE toolbox was developed to facilitate access to the CASCADE model (Schmitt, 2016; Schmitt et al., 2018a,b), a computationally efficient, parsimonious and flexible tool for network scale assessments and management of sediment connectivity. The CASCADE toolbox contains customization options to adapt the model to the different requirements of the case study, data availability, the specific research and management objectives. The toolbox is supported with fully commented code and a comprehensive user guide. The toolbox is designed for easy data exchange between Matlab and a GIS environment for input data preparation, data sharing, and visualization. We encourage the use of CASCADE to evaluate for network and catchment-scale sediment management to leverage novel, network scale data of fluvial geomorphology for conceptualizing and quantifying river geomorphological processes at the basin scale. CASCADE toolbox is freely available from the CASCADE website (http://www.cascademodel.org/) and from the GitHub repository linked to the website, together with the user documentation.

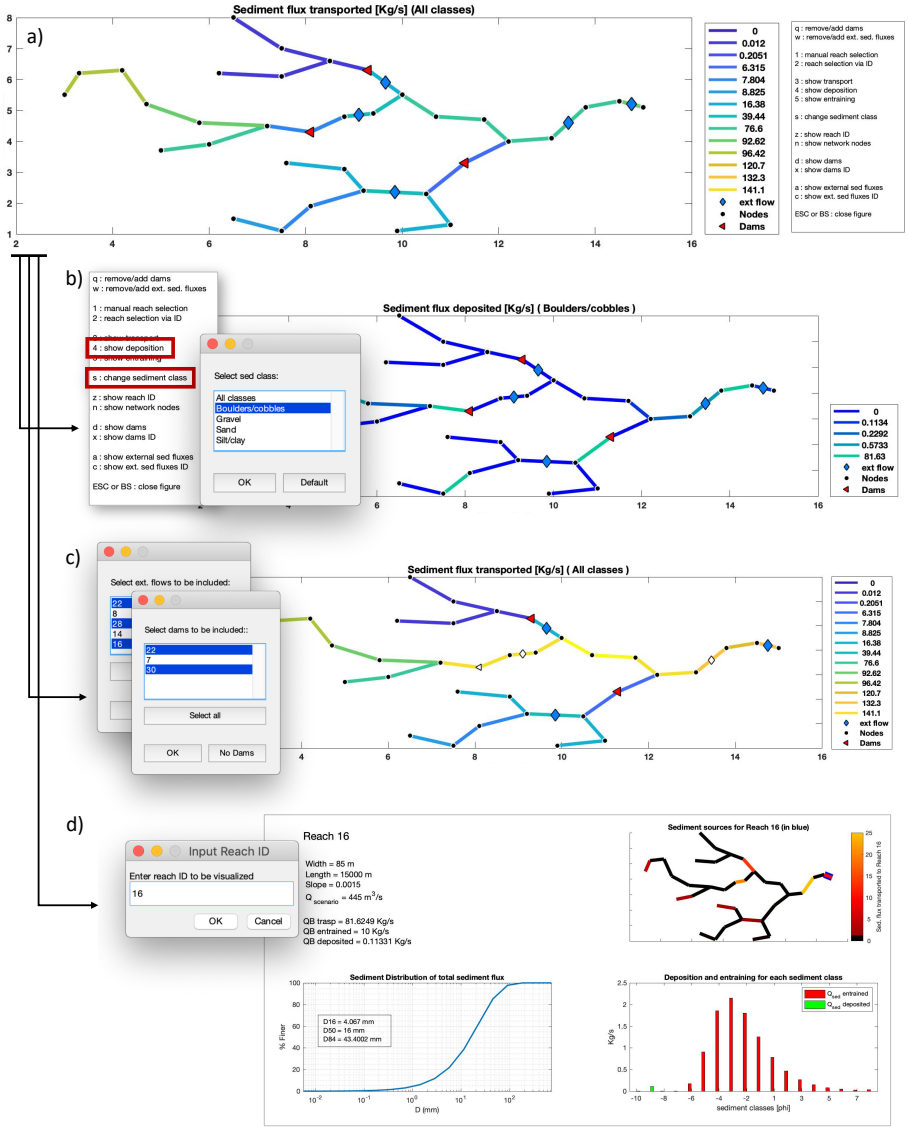

Figure 2.4: *Examples of plots obtained from the Connectivity Alteration Assessment (CAA) function for a synthetic network. CAA allows analyzing various properties of sediment connectivity in an interactive manner. Panel a shows the total sediment transported in Kg/s in the network. b visualizes patterns of deposition for a single sediment class out of the 18 considered in the model (in this case boulders/cobbles). c shows the changes in total sediment transport caused by the removal of one dam and two external sediment flows. d shows an analysis of grain size distribution, sediment sources and deposition and entrainment in a specific reach. Each step can be interactively controlled by the user using a graphical interface.*

3

Sediment transport at the network scale and its link to channel morphology in the braided Vjosa River system

In this chapter, we apply the CASCADE network-scale sediment connectivity model to the Vjosa River in Albania, one of the last un-impounded braided rivers in Europe. The river system is a data scarce environment, which limits our ability to model how this pristine river might respond to future human disturbance using traditional morphological modelling tools. To initialize the model, we use remotely sensed data and modeled hydrology from a regional model. We perform a reach-by-reach optimization of surface grain size distribution (GSD) and bed load transport capacity to ensure equilibrium conditions throughout the network. In order to account for the various sources of uncertainty in the calculation of transport capacity, we performed a global sensitivity analysis. The modelled GSD distributions generated by the sensitivity analysis generally match the six GSDs measured at different locations within the network. The modeled bed load sediment fluxes increase systematically downstream, and annual fluxes at the outlet of the Vjosa are well within an order of magnitude of fluxes derived from previous estimates of the annual suspended sediment load. We then use the modeled sediment fluxes as input to a set of theoretically derived functions that successfully discriminate between multi-thread and single-thread channel patterns. This finding provides additional

validation of the model results by showing a clear connection between modeled sediment concentrations and observed river morphology. Finally, we observe that a reduction in sediment flux of about 50% (e.g., due to dams) would likely cause existing braided reaches to shift toward single thread morphology. The proposed method is widely applicable and opens a new avenue for application of network-scale sediment models that aid in the exploration of river stability to changes in water and sediment fluxes.

This chapter is developed based on: Bizzi, S., Tangi, M., Schmitt, R.J.P., Pitlick, J., Piégay, H. & Castelletti, A.F. (2021) Sediment transport at the network scale and its link to channel morphology in the braided Vjosa River system. Earth Surface Processes and Landforms, 46(14), 2946– 2962. DOI:10.1002/esp.5225

3.1 Introduction

Understanding of sediment transfers in river networks is key to characterizing the spatial distribution and origins of fluvial forms, interpreting historical changes in channel patterns, and predicting future trajectories Fryirs (2013). The combination of processes regulating sediment production, routing, and deposition across space and time is commonly referred to as sediment connectivity Bracken et al. (2015); Wohl et al. (2019). Connectivity is the result of basin-scale processes which link the intrinsic structural properties of the landscape (structural connectivity) to the processes which function to carry water and sediment (functional connectivity) (Heckmann et al., 2018; Keesstra et al., 2018). Thus, studying river sediment connectivity requires a network scale consideration of the provenance, timing and quantity of sediment moving through the entire network Schmitt (2017). Recently, different definitions of sediment connectivity have been proposed and, and geospatial indices have been developed to quantify the magnitude and patterns of sediment connectivity (Cavalli et al., 2013; Heckmann and Schwanghart, 2013; Heckmann et al., 2015). However, our ability to quantify and simulate sediment connectivity in data-scarce settings is still quite limited (Keesstra et al., 2018).

In this study we focus specifically on modeling longitudinal sediment connectivity at the network scale. Network-scale river sediment connectivity describes how the sediment supplied to a river system is entrained, transported, and deposited throughout the channel network. Over the last decade, emerging remote sensing technologies have fostered the generation of network-scale geomorphic datasets concerning hydrology (Van Der Knijff et al., 2010) and geomorphology (Roux et al., 2015; Demarchi et al., 2017; Fryirs et al., 2019; Bizzi et al., 2019). The availability of this new information, along with advances in data processing capabilities, has led to the development of a new generation of sediment connectivity models that are capable of simulating sediment transfer at drainage basin scales (Czuba and Foufoula-Georgiou, 2014; Schmitt, 2016; Beveridge et al., 2020; Gilbert and Wilcox, 2020). These new sediment connectivity models require specification of not only the boundary conditions, and input information on hydrology, slope and channel geometry, but also formulation of computational routines for estimating source area sediment supply (both quantity and grain size). In most basins the source-area sediment supply is unknown, and this is a particularly important problem in reaches where the sediment transport capacity may not be in balance with the sediment supply. Model initialization is not the only challenge of such modelling exercises. Indeed, our ability to validate results and judge the veracity of simulated network fluxes has been limited because data on sediment transport at the network scale are often scarce or non-existent. Interestingly, recent findings (Schmitt et al., 2018b) have proven that even shown that even a few reaches with data

on transported grainsizes and fluxes can significantly constrain the scenarios of basin-scale sediment connectivity patterns. It is worth mentioning that most of the sediment connectivity models developed so far have focused on simulating the transport of bed-material and not on wash load. The latter is fine material that originates from sources other than the channel bed, and once entrained, travels out of the reach. The former is relatively coarse material that makes up the bed and lower banks of the channel and, consequently, it is of major importance in determining channel morphology (Church, 2006). For this reason, sediment fluxes computed in sediment connectivity models should be linked to river morphology. The river classification schemes that have been developed over the years (e.g.Schumm (1985); Church (2006)) have stressed the importance of sediment load (sediment size as well as mass flux) on channel patterns but functional links between sediment size and load and channel pattern have been quantified in relatively few studies. Indeed, sediment transport formulae and consequent bed load estimations have been developed more or less independently from the interpretation of channel patterns and processes (Church, 2006; Church and Ferguson, 2015). Notably, amongst the various studies of network-scale sediment connectivity (Schmitt, 2016; Czuba, 2018; Gilbert and Wilcox, 2020; Beveridge et al., 2020), none have investigated links between network sediment connectivity and reach-scale transitions in channel patterns. This limitation presents an opportunity to use sediment connectivity models to identify thresholds in water and sediment discharge which define a transformation in channel pattern. For instance, empirical evidence shows that, over the last century, braided rivers across the globe have shifted towards single-thread channels due to sediment starvation and construction of flood protection works (dams and levees) (Kondolf, 1997; Liébault and Piégay, 2001; Surian and Rinaldi, 2003; Piegay et al., 2009; Bizzi et al., 2019). Establishing a quantitative link between simulated sediment transport and observed river morphology would thus advance our ability to: i) validate the meaning and validity of simulated network-scale sediment transport values, and ii) to predict future channel morphological adjustments under various scenarios of sediment connectivity. In this paper, we implement the network-scale sediment connectivity model CASCADE (Schmitt, 2016; Tangi et al., 2019) for the Vjosa River basin, in Albania. The Vjosa River is one of the last un-impounded rivers in Europe, and is considered to be a hotspot for biodiversity. The Vjosa River is a free-flowing gravel-bed river that exhibits numerous transitions from braided to single-thread channel patterns along its course. It has some of the largest braided reaches still existing in Europe, but it drains a basin in which numerous hydropower projects are being planned (Schiemer et al., 2018; Peters et al., 2021). The objective of this paper is to implement CASCADE in a data-scarce environment to generate a network-scale assessment of sediment fluxes, and to

use this knowledge to link transitions in channel pattern to the quantity and grain size of the sediment transported. In detail, we test an optimization routine to define source area grain size distributions in the absence of field data, and we implement a sensitivity analysis to explore the main sources of uncertainty in calculating sediment fluxes across the network. We then link the modeled bed load fluxes to transitions in channel morphology observed across the network. To do so, we test an empirical model to discern between braided (Multi-Channels, MC) and Single Channel (SC) types based on sediment concentration, grain size, discharge and slope (Mueller and Pitlick, 2014). The empirical model is fed by CASCADE outputs in terms of sediment concentration and median grain size (D50), whereas channel patterns are observed by available orthophotos. Finally, we use the findings to assess the potential for the braided pattern of the Vjosa River to be lost if the construction of hydropower dams upstream results in reductions in sediment supply. Based on this case study, the paper also discusses broader challenges of initializing and validating network-scale sediment connectivity models in general. Our case study demonstrates the significance of having a few strategically but located field data for use in validating the model. In so doing, the paper points out the opportunity of network scale modeling to leverage limited sediment data to a develop a wider and more consistent understanding of network scale processes. This work also successfully links modeled sediment transport rates to channel morphology, opening up the possibility that we can predict channel planform sensitivity to alternative scenarios of water and sediment management.

3.2 Case Study

The Vjosa River is one of the last remaining free-flowing fluvial systems in Europe. The river originates in Greece, but most of its unimpeded 260 km course is in Albania. Almost all tributaries of the Vjosa are not regulated by any human infrastructures making the Vjosa stand out from other heavily modified Mediterranean rivers (Belletti et al., 2020). In Greece, the river, locally named Aaos, passes thought the Vikos-Aaos National park, where it forms impressive canyons. After entering in Albania, the Vjosa is joined by the Sarantaporos river, which displays wide braided channel patterns upstream of its confluence with the Vjosa (see Figure 3.1). The Vjosa then flows in a narrow valley, maintaining a relatively small width, incised in low terraces made of conglomerates deposits. After passing through the Dragot gorge, the river meets one of its two main tributaries, the Drinos. The valley then widens, the slope reduces and the river forms impressive braided sections up to two kilometers wide. The second largest tributary, the Shushica, enters the Vjosa near its delta. In total, the river drains an area of 6,700 km^2 and discharges in average 204 m^3/s at

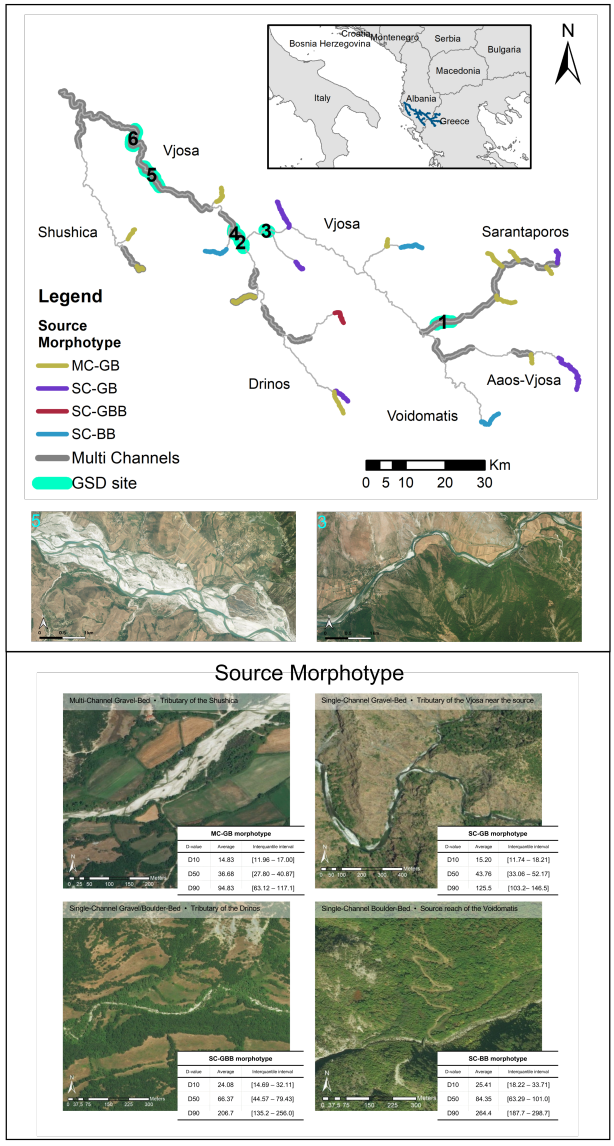

Figure 3.1: *Location of the Vjosa River, the grain size distribution (GSD) sites for samplings, and the network representation of the river used in this paper. Multi channels are highlighted with a grey bold line. Two images around GSD sites 5 and 3 show two typical examples of Vjosa channel patterns, a multi-channel braided section upstream of Kalivaç (5) and a confined single channel pattern east of the Dragot gorge (3) (satellite images: ©2021 Google/Airbus, Maxar Technologies). At the bottom, morphotypes are reported for source reaches: Multi-Channels Gravel-Bed (MCGB), Single-Channel Gravel-Bed (SC-GB), Single-Channel Gravel/Boulder-Bed (SC-GBB), and Single-Channel Boulder Bed (SC-BB)*

its mouth. The Vjosa falls into the pluvio-nival hydrological regime, with heavy rainfalls and consequent peak-flows in spring. While the average annual rainfall is around 1500 mm, in the upper, mountainous regions of the basin, where the coastal Mediterranean climate gives way to the continental climate, annual precipitations reach around 2500 mm/year (Schiemer et al., 2018). Geologically, the Vjosa River crosses the active graben system and the active frontal thrust system of the Albanides. The Vjosa River drains through ophiolites, flysch deposits, carbonate rocks, and Quaternary sediments. Limestone and sandstone represent the majority of riverbed sediment. The Vjosa River has various levels of alluvial terraces and recent analyses show that their formation is mainly controlled by climate changes which occurred during the Pleistocene (Carcaillet et al., 2009). In the middle part, the river flows over flysch deposits and the existing gorges follow an E-W transverse (E–W) along the frontal active trust, and then meanders on the coastal plain to the Adriatic Sea in the west.

Due to this geological context, channel types, as described, display a remarkable variety: the river forms gorges and incises the terraces in the upper and middle catchment, and braiding channel patterns are then observed when the valley widens with a transition to meandering towards the mouth. We assume that the transition between braiding and single channel patterns is regulated by the magnitude and grainsize of sediment supply, the stream power, and the degree of confinement. Using CASCADE outputs, we aim to establish quantitative links between those single versus multi-channel pattern.

3.3 Methods

3.3.1 The CASCADE model

The CASCADE model (CAtchment Sediment Connectivity And Delivery) (Schmitt, 2016) is a network-scale sediment transport model, which implements empirical sediment transport equations within a directed graph representing the river network (Tangi et al., 2019). CASCADE produces disaggregated information on sediment transport, deposition and delivery, allowing to track both the fate of sediment from a specific sediment source and the composition and origins of sediment in any downstream river reach. CASCADE has been applied in previous case studies to assess sediment connectivity in large river networks (Schmitt, 2016, 2017) and to evaluate alterations of sediment transport regime caused by anthropogenic alterations such as dams (Schmitt et al., 2018a, 2019). In the present study, we use the CASCADE toolbox (Tangi et al., 2019) to quantify bed load sediment fluxes in the Vjosa River network (Figure 3.1). CASCADE is a flexible and scalable tool to model network sediment connectivity using a relatively small number of remotely sensed and hydrological data to be calibrated. These include specification of the discharge, channel geometry

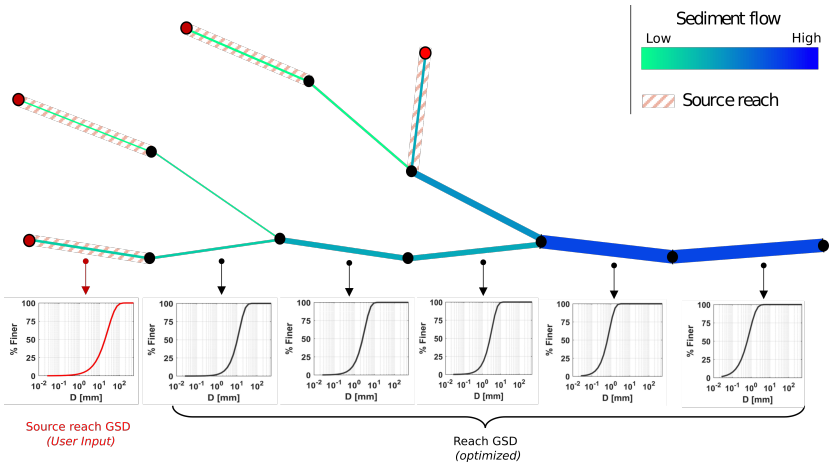

Figure 3.2: *CASCADE model conceptualization, for each reach the GSD are shown, source reaches are highlighted in red.*

and grain size distributions (GSDs) for each river reach (Figure 3.2). However, for the Vjosa, similar to probably most larger river systems worldwide, there are relatively few point measurements of GSDs. Here, we use an optimization routine, which was previously developed by Ferguson et al. (2015) for a single river channel. We expand the approach to an entire-network scale and use it to define bed GSDs in all river reaches. In the next sections, we describe how transport capacity is calculated in CASCADE and how we implement the optimization routine. Then, we describe how we derive the reach attributes needed to calculate transport rates at the network scale.

3.3.2 Transport capacity calculation

The bed load transport capacity is calculated using a function presented by Parker and Klingeman (1982) This function is used primarily because it is formulated for sediment mixtures, and thus can predict transport rates of individual size fractions; this is important when trying to predict the GSDs from one reach to another. The subsurface- and surface-based versions of this function fit field data very well when calibrated to a reference shear stress (Parker and Klingeman, 1982; Mueller and Pitlick, 2014). The bed load transport capacity for sediment size class i (Q_i^{sed}, [kgs^{-1}]) is defined as:

$$Q_i^{sed} = B_{at} W_i^* F_i \rho_s (\tau/\rho)^{(3/2)} (\Delta g)^{(-1)} \tag{3.1}$$

where B_{at} is the channel width [m] over which active transport (at) occurs,

W_i^* is the dimensionless transport rate for sediment size class i, F_i is the fraction of size class i in the bed surface sediment, ρ_s and ρ are the sediment and water density, respectively, g is the gravitational acceleration, and Δ is the submerged specific gravity of sediment. W_i^* is calculated using a function introduced by Parker and Klingeman (1982)

$$W_i^* = 11.2(1 - 0.853\tau_{r_i}/\tau)^{4.5} \tag{3.2}$$

where τ is the bed shear stress [$kgm^{-1}s^{-2}$]:

$$\tau = \rho g H S \tag{3.3}$$

and τ_{r_i} is the reference shear stress [$kgm^{-1}s^{-2}$] for an individual grain size, d_i [m]; τ_{r_i} is estimated from a hiding function:

$$\tau_{r_i} = \tau_{r_{50}}(D_i/D_{50})^{\gamma} \tag{3.4}$$

where $\tau_{r_{50}}$ is the reference shear stress [$kgm^{-1}s^{-2}$] for the median grain size, D50 [m] of the bed surface sediment; $\tau_{r_{50}}$ is estimated using an empirical equation presented by Mueller et al. (2005) that accounts for variations in the reference shear stress with increasing channel slope:

$$\tau_{r_{50}} = \rho g \Delta D_{50}(0.021 + 2.18S) \tag{3.5}$$

The other variables in equations 3.3, 3.4, 3.5 are the mean depth, H [m], the reach-average slope, S [-], and the hiding function exponent, γ. Values of γ close to zero are indicative of conditions, where transport is weakly size-selective (equal mobility), whereas values of $\gamma > 0.1$ are indicative of conditions where transport is predominantly size-selective. The average flow depth is found using the Manning-Strickler formula (Manning, 1891). The fraction of each size class in the bed surface sediment layer Fi is extracted from the reach GSD. The total transport capacity of the reach is found by summing the transport capacity across all size classes.

Initialization of GSDs for source reaches and routine for optimizing GSDs across the network Each first-order reach in the network is considered a source reach (these reaches are highlighted in red in Figure 3.2). To assign a grain size distribution (GSD) to each source, we visually classified the associated first-order reaches into four morphotypes as shown in Figure 3.1. Each morphotype was assigned a range of GSDs at the sources, based on Liébault's (2003) categorization and raw data of gravel GSDs in Mediterranean limestone mountain rivers. Morphotype MC-GB (D50 from 27 mm to 48mm) is characterized by a large active channel width (defined here as the flow channels and unvegetated exposed gravel bar width) and narrow, well-defined low flow channels (multiple channels) and gravel-bed; Morphotype SC-GB (D50 from 33 mm to 52

mm) is characterized by a single narrow low flow channel dominated by gravel (no boulders present) but with a narrower active width compared to Morphotype MC-GB; Morphotype SC-GBB (D50 from 44mm to 79mm) has an active channel width of less than about 20m, with bed material consisting of gravel mixed with boulders. Morphotype SC-BB (D50 from 63mm to 100mm) is single channel characterized by high density of boulders in the channel bed. Source morphotypes for the Vjosa network are indicated in Figure 3.1. The GSDs for each of the remaining reaches are generated using the optimization routine proposed by Ferguson et al. (2015), where the GSD is adjusted until the sediment transport capacity within a reach is in equilibrium with the upstream sediment supply. The sediment supply of the source reaches is derived as follows. First, we assign source GSDs according to the above classification. Then, we calculate the transport capacity for the GSD based on local GSDs and hydro-morphology. We finally assume that source reaches are in equilibrium too, i.e., sediment supply is equal to the local transport capacity. For the remaining downstream reaches, the GSD is then determined by modifying the parameters of the Rosin distribution (Ferguson et al., 2015) a cumulative distribution function used to represent the range in bed material grain size (Shih and Komar, 1990)

$$F(< D) = 1 - exp(D/k)^s \tag{3.6}$$

where k is the mode of the distribution and s an inverse measure of the spread. We then use the Genetic Algorithm toolbox in Matlab to minimize the difference between the local transport capacity in a reach and the incoming sediment flux from the upstream network by altering the two parameters s and k of the Rosin distribution. Each set of s and k results in a different set of frequencies, F_i (see eqn. 3.1), for each grain size class to be used in calculating the local bed load transport capacity. Thus, we assume that the local GSD in a reach will change to accommodate sediment supply from upstream under local hydromorphologic conditions (gradient, width, discharge). Thus, network sediment flux only increases at confluences. However, changing the GSD implies that there can be erosion or deposition of specific size classes, resulting in specific morphodynamics. For example, if the optimization for a reach results in a GSD that is finer than the incoming GSD this fining could be related to either fine material being eroded from the channel or to deposition of coarse material. In each reach, to maintain equilibrium, the deposition of some sizes is compensated by the entrainment of others. This process generates GSD patterns across the network.

3.3.3 Defining river network reaches

In this section, we define how the river network was extracted from the available Digital elevation Model (DEM), and how it was segmented into river

reaches with specific channel attributes, such as slope and channel type. For the Vjosa, we extracted the river network using the TanDEM-X DEM (Rizzoli et al., 2017; Wessel, 2018), with a pixel spacing of 0.4 arcsec, corresponding to a ground accuracy of approximately 10.9 m across the study area, with relative vertical accuracy of 2 m (slope < 20%) and absolute vertical accuracy of 10 m. The network was defined using a combination of the CASCADE toolbox (Tangi et al., 2019)and Topotoolbox (Schwanghart and Kuhn, 2010). We set a minimum drainage area of 100 km2 to identify the river network to be simulated. The river network is defined as a connected graph consisting of nodes linked to directed edges. Each edge represents a reach of the river network and is assigned a set of physical attributes including average slope, active channel width, channel roughness coefficient, bed material grain size distribution and discharge (Schmitt et al., 2016). These hydromorphic properties are then used to estimate the reach-scale sediment transport capacity, eqns. 3.1-3.5, from which we construct a reach-scale sediment budget, i.e., the balance between sediment supply and transport capacity, and the volume of sediment exported or deposited. Given that because each edge in the river network has a single set of attributes, the corresponding river reach should have quasi-uniform geomorphological features. We thus manually segmented the river network by visually identifying reaches with homogenous channel planform patterns, focusing particularly on differences in active channel width. Local channel widths were measured on available orthophotos from the most recent Google Earth images by selecting active sections of the riverbed with little or no vegetation. A total of 400 river width measurements were extracted from orthophotos before proceeding to network segmentation. The resulting river network is divided into 139 reaches, with average length of 4.3 km. Reaches with multiple channel width measures were attributed an active width equal to the average of these measures. Channel gradients were calculated from the DEM based on the elevation difference between the upstream and downstream node of each reach. Each reach was then classified as multi-channel or single thread, as shown in Figure 3.1. We also collected information on confinement, differentiating between confined or unconfined channels. Confinement was evaluated from orthophotos and reaches were classified as confined where terraces and hillslopes adjacent to the channels were visible. Channels bordered by floodplains were classified as unconfined.

3.3.4 River Network Hydrology

The magnitude and frequency of discharges used to calculate sediment loads for each river reach were estimated using a hydrological model. The dataset was generated by the LISFLOOD model, a rainfall-runoff model which provides daily flow data across a 5km x 5km grid (Van Der Knijff et al., 2010; Forzieri

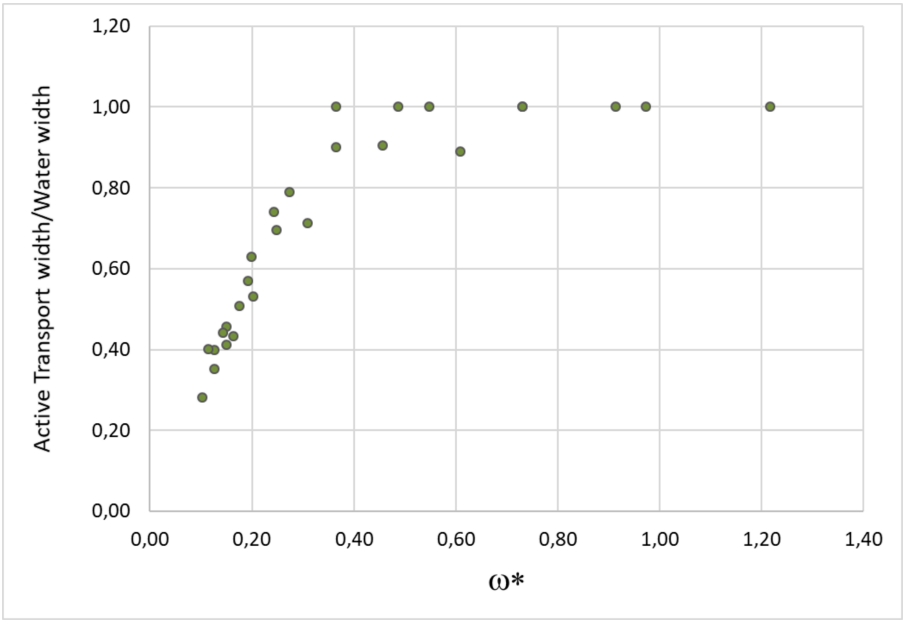

Figure 3.3: *The ratio of active transport width* (B_{at}) *with water width* (B_w) *plotted versus the dimensionless stream power* (ω^*). *Data from Lugo et al. (2015).*

et al., 2014). Model simulations provided daily discharge data from 1990 to 2014. We assigned each reach in the CASCADE model to the grid cell of the hydrological model with which it had most overlap. From that cell, we then extracted the hydrologic time series and divided it into eight discharge classes corresponding to specific percentiles (0, 0.1, 2.3, 15.9 ,50, 84.1, 97.7, 99.9, 100). We also determined the frequency with which discharge was in each percentile. Thus, we assigned eight discharge classes and time fraction to each reach, which we then used to simulate daily sediment loads (in kg/s), which are aggregated using the annual frequency of each discharge to obtain the annual sediment flux.

3.3.5 Relation between channel width and discharge

Active transport widths along the Vjosa River can vary appreciably with water discharge, particularly in braided reaches. To account for these variations, we developed a rating curve between active transport width and discharge that could be applied to each reach. A rating curve such as this is needed because the calculations of bed load transport capacity are sensitive to variations in channel width and depth. There is no detailed information on channel cross sections for the Vjosa. Thus, we took an empirical approach, forming a relation

between discharge and active transport channel width for each reach. (Lugo et al., 2015)presented a relationship between dimensionless stream power (ω^*) and the ratio between active transport width and water width (Figure 3.3):

$$\omega^* = \frac{QS}{(B_w\sqrt{(g\delta D_{50}^3)})} \tag{3.7}$$

where Q is the flow discharge, and B_w is the water width. The relationship calculated by interpolation of the data in Figure 3.3 is:

$$r = \frac{B_{at}}{B_w} = max(0.2, min(2.36\omega^* + 0.09, 1)) \tag{3.8}$$

where r is the ratio between active transport width (B_{at}) and water width (B_w).

In the flume experiments conducted by Lugo et al. (2015), the active transport width corresponds to the portion of the channel where bed load sediment transport occurs, whereas the water width refers to the portion of the channel covered by water. For our purposes, we assumed that the values of active channel width measured along the Vjosa on Google Earth images (see previous section) correspond with the water width of their flume experiments. This is likely reasonable only for discharges with return period of two or more years, whereas could be overestimating it for discharges that are big enough to transport sediment but not necessary flooding the entire active channel. We are aware of the inherent uncertainty related to this estimate of active transport width and also of its importance in the implementation of the sediment transport model and for this reason it will be included in the sensitivity analysis discussed below. Dimensionless stream power is computed within CASCADE and then a value of the ratio (r is derived for each reach and discharge scenario. The measured active channel width from orthophotos is then multiplied by this ratio (r) to obtain the active transport width (B_{at}) to be used to calculate transport capacity (see eqn. 3.1).

3.3.6 Sensitivity Analysis

We implemented a global sensitivity analysis on key parameters used in the CASCADE simulations, focusing on source GSDs, the hiding function exponent λ and the active transport width B_{at}. Source GSDs are not known and are provided in terms of plausible ranges for each morphotype (see tables of Figure 3.1). The hiding function exponent λ is allowed to vary from 0 to 0.1 to examine how differences in particle mobility affect downstream trends in GSDs. To consider the uncertainty in active transport width, B_{at} is randomly perturbed by a uniform distribution around plus or minus the 20% of the central estimates we

derived using Lugo et al. (2015) method. We aim at assessing how these ranges of parameter uncertainties simultaneously affect the modeled sediment fluxes and GSDs. In this analysis we do not investigate the relative importance of each of these factors, which would require additional consideration of parameter covariances. Here, we only assess the uncertainty in sediment transport measures (total load and GSD in each reach) as a cumulative result of uncertainty in individual parameters. For each parameter that is included in the sensitivity analysis (GSD, hiding factor and active transport channel width) values are sampled between the proposed ranges to best cover the parameter space. We use the Sobol's method, a technique to perform global sensitivity analysis which generates quasi-random low-discrepancies parameters sequences(Hadka and Reed, 2015). For our case study, this resulted in 2300 independent parameter sets, with each set containing a distinct value for each of the three parameters. For each of parameter set, we performed eight CASCADE runs, one for each discharge percentile, to generate the estimates of GSD and annual bed load transport rates in each reach estimates. The analysis of 2300 CASCADE simulations allow us to assess uncertainty domains for the estimated yearly sediment fluxes and associated GSD patterns.

3.3.7 Field Data for validation

We carried out field surveys and collected grain size data in 6 reaches in February 2018. We sampled the bed material in two braided reaches close the mouth of the Vjosa River (Pocem and Kalivaç), a more upstream single thread reach (Drinos), a confined reach in the Dragot gorge (Vjosa Gorge), a braided tributary reach with high sediment supply (Sarantaporos), and a single thread reach in another tributary (Drinos), see Figure 3.1 for site locations. We took between 5 and 10 pictures of the bed at different locations on exposed gravel bars. We took pictures by using a digital camera positioned vertically and about 1.5 m above the ground. We placed a scale bar in each frame to pinpoint the measurement scale. Picture resolution is 4032 x 3024 [px] resulting in an average pixel dimension of 0.5 [mm/px] for the selected 1.5 m distance from the ground. GSDs were calculated using Base Grain software (Detert and Weitbrecht, 2013), an object detection software tool for the analysis and extraction of granulometric information from images of non-cohesive gravel beds. Base Grain automatically separates grain areas (coarser than 8 mm) and interstices filled with finer sediment in the image using filtering techniques to identify the area of each gravel particle in the field of view. From there, the software extracts the grain size distribution of the coarser (>8mm) fractions of the surface sediment. The distribution is then completed with an estimation of the fraction of the finer, non-detectable particles, via Fuller curve estimation (Fehr, 1987). From the GSDs we can derive metrics such as D16, D50 and D84.

Test of the threshold between single-and multi-thread channels As noted in the introduction, links between network sediment connectivity and reach-scale transitions in channel patterns have not yet been studied. Here, we propose to calculate a channel pattern threshold using CASCADE outputs to discern single and multi-thread-channels. Mueller and Pitlick (2014)modified the approach developed by Millar (2005)and Eaton et al. (2010) to derive an equation that predicts the threshold between single- (SC) and multi-thread channels (MC) on the basis of a threshold in sediment concentration, and an assumption that braided channels will form at width to depth ratios greater than 50. The Mueller-Pitlick threshold is based on a regime relation (eqn. 3.12) presented by Mueller and Pitlick (2014):

$$\frac{B_{bf}}{H} = 425 Q^{*0.12} C'^{-2.30} \mu'^{-2.9} \tag{3.9}$$

where B_{bf} is the bankfull river width and H is the flow depth at bankfull discharge. μ' is a dimensionless ratio of the relative erodibility of the bank versus the bed material. Q^* is the dimensionless discharge defined as

$$Q^* = \frac{Q_{bf}}{\sqrt{(s-1)gD_{50}}D_{50}^2} \tag{3.10}$$

$C' = -\log_{10} C$, where C is bed load sediment concentration, defined as the ratio of bankfull volumetric bed load discharge, Q_{bf}^{sed} (m^3/s), to bankfull water discharge (m^3/s), Q_{bf} ($C = Q_{bv,bf}/Q_{bf}$) (Mueller and Pitlick, 2014). Equation 9 can be rearranged and simplified to find the critical sediment concentration, C_t, under the assumption of $B_{bf}/H = 50$:

$$C_t = 10^{(-2.54 Q^{*0.052} \mu'^{-1.26})} \tag{3.11}$$

Equation 3.11 defines the threshold between MC and SC patterns. We applied this formula to all alluvial unconfined or semiconfined reaches present within the Vjosa network. We neglected confined reaches because, in most cases, channels in these reaches are nonalluvial. Sediment concentration and grain size values for implementing equation 3.11 are derived by CASCADE simulations. In order to further test the validity of CASCADE outputs, we also plot the braiding threshold proposed by Eaton et al. (2010) which is based on slope (S) not on sediment concentration:

$$S_t = 0.4 Q^{*-0.43} \mu'^{1.41} \tag{3.12}$$

where S_t is the critical slope derived for the threshold case where $B_{bf}/H = 50$. We then calibrated these thresholds (eqn. 3.1 and 12) altering the value of μ' to find the threshold that best discerns SC from MC patterns in the Vjosa basin,

as also proposed by Millar (2005). The value of μ'so obtained incorporates all errors, including systematic errors in the theoretical relations. However, this approach is necessary to include how vegetation density and bank material affect the resistance to erosion. μ' near 1.0 is used for the most sparsely vegetated categories, indicating that bed and banks are approximately equally erodible, and progressively increase with vegetation density or changes in bank material towards more resistance texture to between 1.5 and 1.9 for the most densely vegetated channels.

3.4 Results

3.4.1 CASCADE validation

Figure 3.4 shows the pattern of mean D50 generated by CASCADE (the average value over 2300 simulations) for the entire network. In general, modelled grain size distributions are coarsest in headwater reaches and in single-thread reaches upstream of the Vjosa Gorge. An overall pattern of downstream fining is evident at the network scale. Figure 3.4 compares the GSDs generated by the 2300 CASCADE simulations for each reach (red lines) with the measured GSDs for the same reaches (green lines). In general, the CASCADE generated GSDs match the patterns observed in the field (Figure 3.4 and Table 3.1): the coarser grain sizes which are located along the Drinos and Sarantaporos tributaries and in the Vjosa Gorge are well-differentiated from the finer grain sizes in the downstream braided reaches, Vjosa-Drinos, Kalivac, and Pocem, respectively. The modeled GSDs broadly overlap with the measured GSDs, particularly in the four reaches above the Vjosa-Drinos confluence. In the two downstream reaches– Kalivac and Pocem– the modeled GSDs are generally finer than the measured GSDs, although the mean distributions (indicated by the bold solid lines) are quite close (Fig. 5). The percentile values listed in Table 3.1 suggest that the modeled D84 and D50 are comparable to Base Grain estimates across all sites. In contrast, it appears that the finer grain sizes simulated by CASCADE, e.g. D16, are biased, overestimating their sizes in comparison to Base Grain estimates.

The simulated annual bed load fluxes for the entire network are presented in Figure 3.5, which shows average values amongst all the 2300 simulations. Figure 3.5 shows also a series of box plots indicating the range of simulated fluxes for selected locations, including the outlet of the Vjosa River and its main tributaries. Bed load estimates from our sensitivity analysis indicate that the median annual bed load at the outlet of the Vjosa is approximately 0.58 Mt/yr with 50% of the simulated fluxes falling between 0.25 and 0.86 Mt/y. The simulated sediment fluxes can be validated only at the outlet, where a few published estimates of the annual suspended sediment load are available. **?** Milliman and

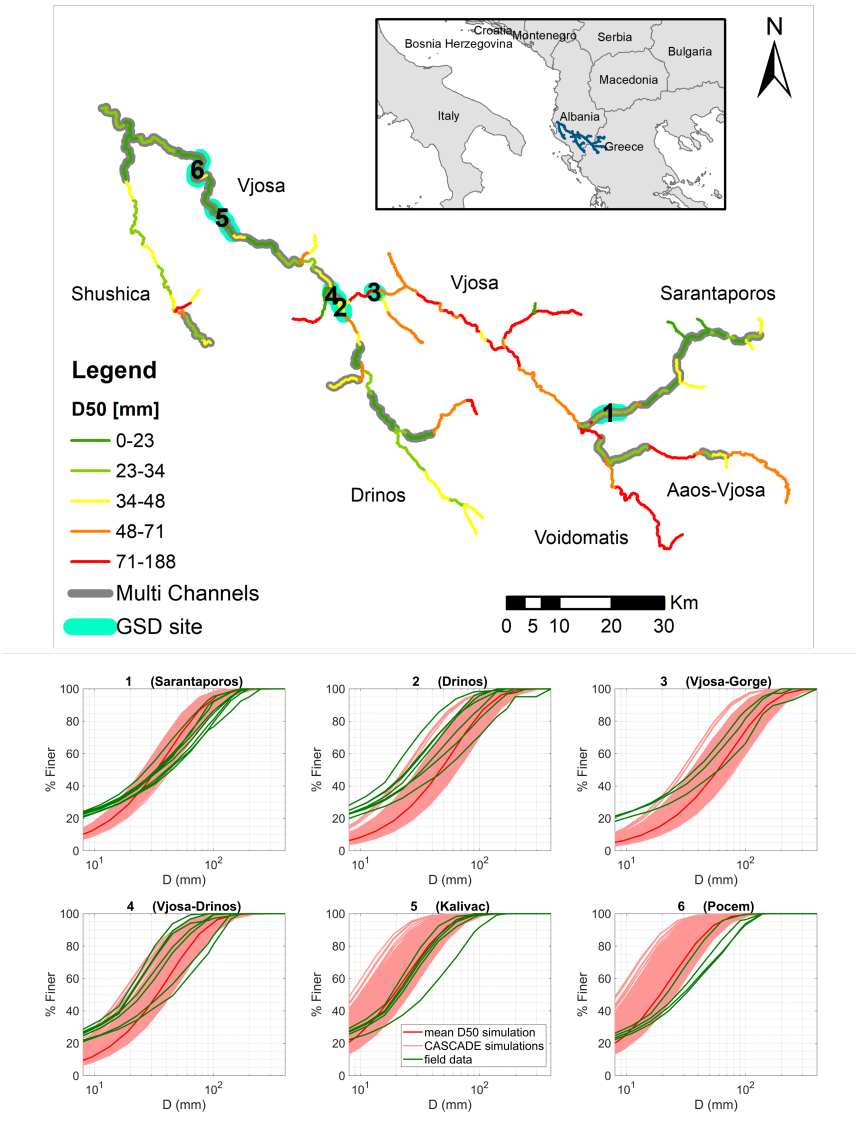

Figure 3.4: *At the top the river network shows range in mean D50, amongst all the 2300 simulations. GSD sampling locations are shown together with multi-channel patterns. At the bottom GSD sites show the grain size distributions modelled and observed (the numbers in the graph titles match the GSD site numbers in the top map). Green lines are GSD for each picture derived by Base Grain, in red the CASCADE set of simulated GSDs, bold red line shows the mean among all the simulations.*

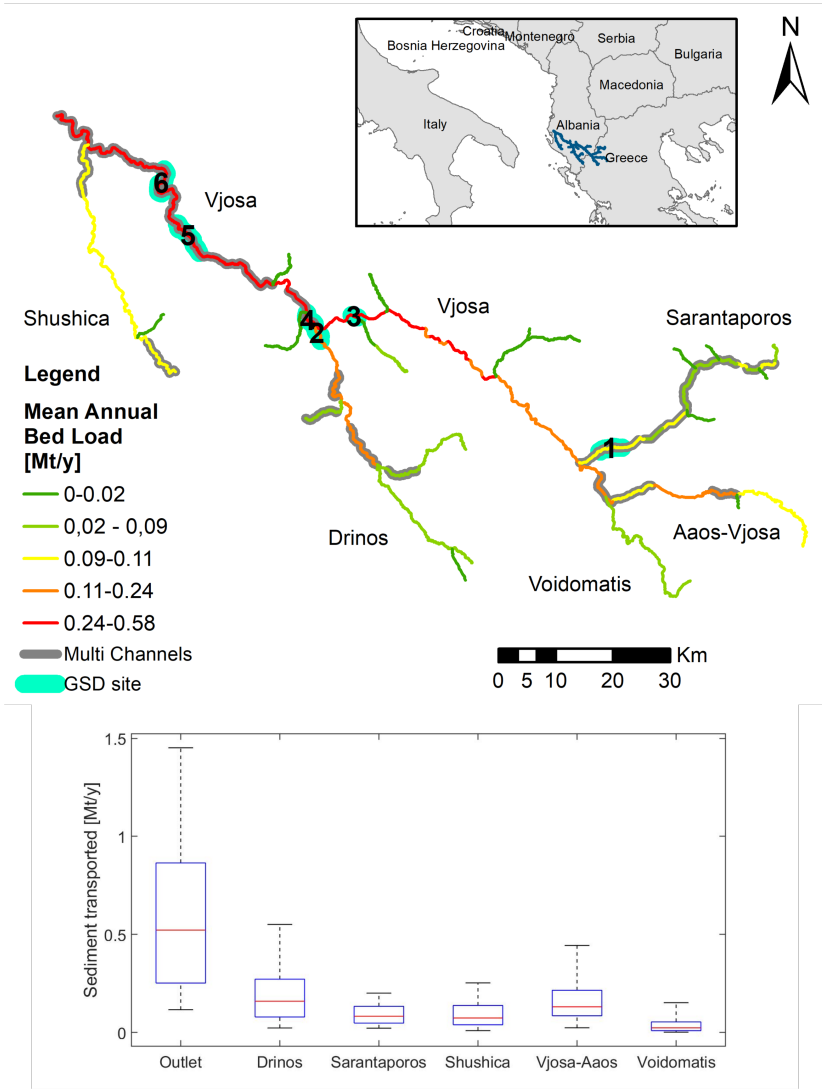

Figure 3.5: *Top figure: mean (across the 2300 simulations) yearly bed load transport values are reported across the network for all reaches, multi-thread channels (MC) reaches are represented by double lines in gray. Bottom figure: the boxplots report the range of yearly bed load values generated by CASCADE simulations at the outlets for the Vjosa and its main tributaries (the values correspond to the fluxes of the last reach of the tributary before the confluence with the Vjosa River). The red central mark in the boxplot indicates the median, and the bottom and top edges of the box indicate the 25th and 75th percentiles, respectively. The whiskers extend to the most extreme data points not considered outliers.*

	D16	D50	D84	Source
Sarantaporos	11	33	72	Modelled
	4	36	97	Observed
Drinos	16	47	98	Modelled
	3	31	83	Observed
Vjosa-gorge	20	58	125	Modelled
	4	41	100	Observed
Vjosa-Drinos	11	33	70	Modelled
	3	27	61	Observed
Kalivac	6	19	40	Modelled
	2	20	42	Observed
Pocem	6	26	40	Modelled
	3	27	66	Observed

Table 3.1: *Modelled and observed D84, D50 and D16 values for 6 reaches are reported in mm. Modelled values report the average amongst the 2300 CASCADE simulations (red bold lines in Figure 3.4, bottom figure). Observed values the average between the Base-Grain estimations from pictures (green lines in Figure 3.4, bottom figure). For site locations Figure 3.4, top figure.*

Farnsworth (2011) report that the annual suspended sediment load of the Vjosa River is approximately 8.3 Mt/y; in a separate study, Fouache et al. (2001) report a slightly lower load of 6.7 Mt/y. The bed-load fraction in the Vjosa is reported in the range of 15-20% of the total load (Ciavola, 1999). If we assume a somewhat broader range, e.g., that bed load is 10-20% of the total load (bed load plus suspended load), then the annual bed load flux should fall in the range of 0.7-2.1 Mt/yr, depending on which values of suspended load we use, and what assumptions we make about the fraction of bed load to total load. The differences between bed load fluxes estimated from suspended sediment measurements and the fluxes generated by the CASCADE simulations (0.58 Mt/yr at the Outlet) are not large and suggest that the simulated fluxes are within an order of magnitude of the expected fluxes.

3.4.2 Multi-channel / single channel threshold

We further analyzed results for a possible correlation between modelled bedload transport and observed channel patterns. The channel pattern threshold given by eq. 3.11 (Mueller and Pitlick, 2014) indicates that the distinction between MC and SC reaches depends on various factors, including sediment concentration, C, relative bank strength, μ', and dimensionless discharge, Q^* (which in turn depends on Q_{bf} and D50). Using average values amongst the

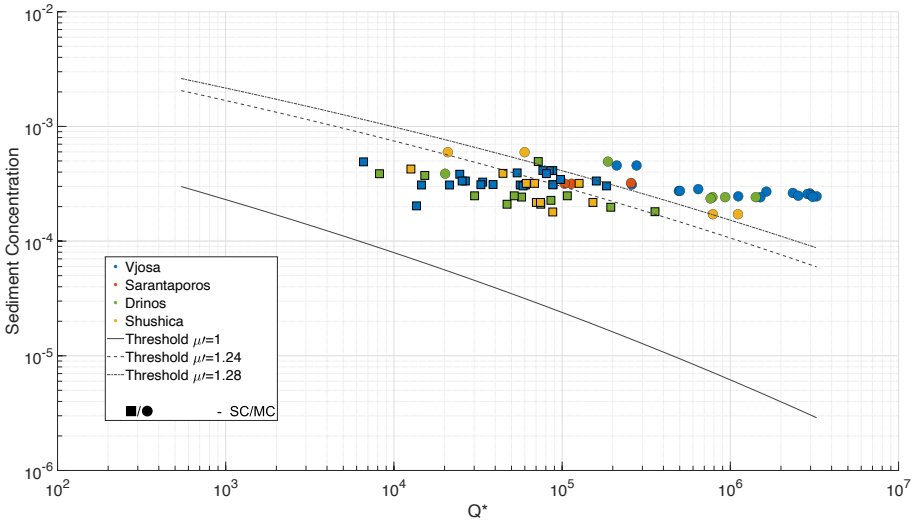

Figure 3.6: *Relation between sediment concentration and* Q^* *for all unconfined reaches. Circles represent multi-channel reaches (MC) and rectangles single channel reaches (SC). Colors refer to different sub-basins. Lines show alternative thresholds for braiding for different values of the relative bank strength parameter,* $\mu' = 1$ *(solid line),* 1.24 *(dashed line) and* 1.28 *(dash-dot line).*

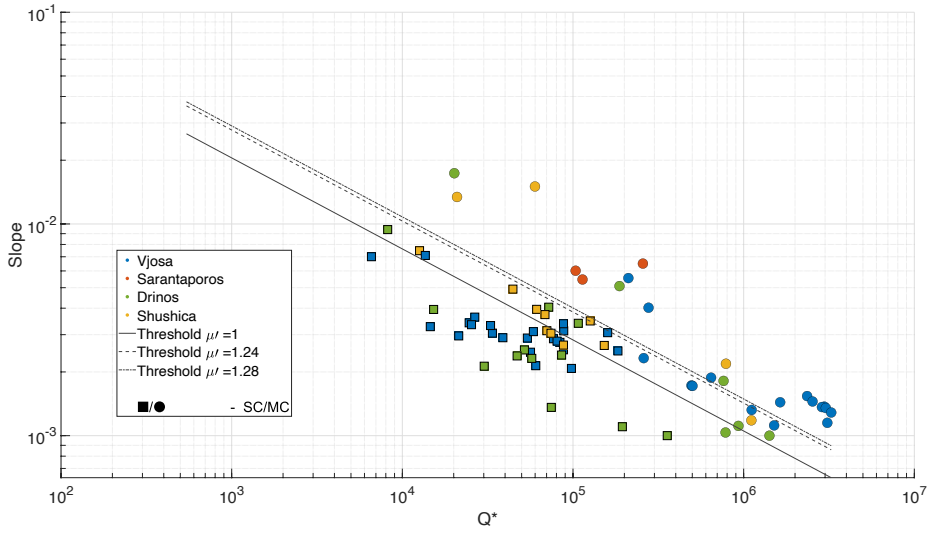

Figure 3.7: *Relation between slope and Q* for all unconfined reaches. Circles represent multi-channel reaches (MC) and rectangles represent single channel reaches (SC). Lines show alternative thresholds for braiding for different values of the relative bank strength parameter μ'= 1 (solid lines), 1.24 (dashed line) and 1.28 (dash-dot line).*

2300 simulations of sediment fluxes and D50 generated by CASCADE, we can plot sediment concentration versus Q* for all the unconfined reaches, and compare with the threshold relation, eqn. (11). The results are shown in Figure 3.6. Rectangles correspond to SC reaches and circles correspond to MC reaches. Colors refer to specific sub-basins, and the diagonal lines indicate thresholds corresponding to three assumed values of μ': 1.0, 1.24 and 1.28. With few exceptions the SC reaches are well-discriminated from the MC reach for an assumed valued of $\mu' = 1.28$. The value of 1.24 is an example of a different threshold which could apply to reaches in the Shushica basin (light orange points). In order to further explore the threshold between SC and MC patterns, Figure 3.7 plots the slope-dependent threshold given by eqn. 12. Using this threshold, SC reaches (squares) are relatively well-discriminated from MC reaches (circles). Figure 3.7 plots the same three thresholds shown in Figure 3.6 for μ' equal to 1.0, 1.24 and 1.28. Compared to the concentration-based threshold, the slope-based threshold has a wider zone of overlap. Indeed, SC and MC reaches coexist primarily in between μ' values of 1 and 1.28.

A third plot illustrating the combined influence of slope and grain size on channel pattern is shown in Figure 3.8. Here the symbol colors and sizes have the same meaning as in Figures 3.6 and 3.7, but D50 is plotted instead of Q* on

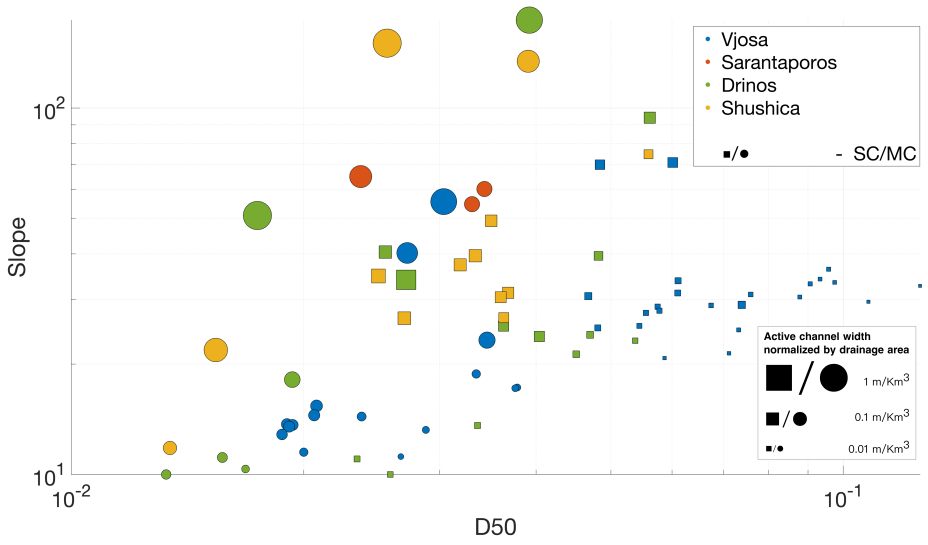

Figure 3.8: *Slope and D50 are plotted for all unconfined reaches: circles represent multi-channels (MC) and rectangle single channel (SC). Colors refer to different sub-basins, dot size is proportional to the active channel width normalized by drainage area. i.e., very large dots indicate reaches which are very wide relative to their drainage area.*

the x axis, and dot sizes are proportional to active channel width normalized by drainage area. This latter parameter provides information on active channel width once the size effect of drainage area is removed (Piegay et al., 2009; Bizzi et al., 2019). The results shown in this figure indicate that, for similar values of channel slope, SC reaches are characterized by coarser D50 and lower values of normalized active channel width, whereas for similar values of D50, MC reaches have higher slope and higher values of normalized active channel width. These observations suggest that the formation of MC patterns is likely driven by floodplain availability and degree of confinement. Indeed, when the channel can widen into the floodplain, it develops a MC pattern characterized by a wider active channel, which may in turn reduce the average depth, and thus lower the sediment transport capacity compared to SC reaches. The lower transport capacity may in turn trigger a condition for aggradation, as well as finer D50. In such cases, the MC reach needs a much higher slope than the SC reach to transport the same grain size.

It is evident from the results presented above that the discriminations between SC reaches and MC reaches are sensitive to the relative bank strength parameter, μ'. In addition, as explained in the Methods, we considered how uncertainties in other parameters (γ, source GSDs and active width, B_{at}) might

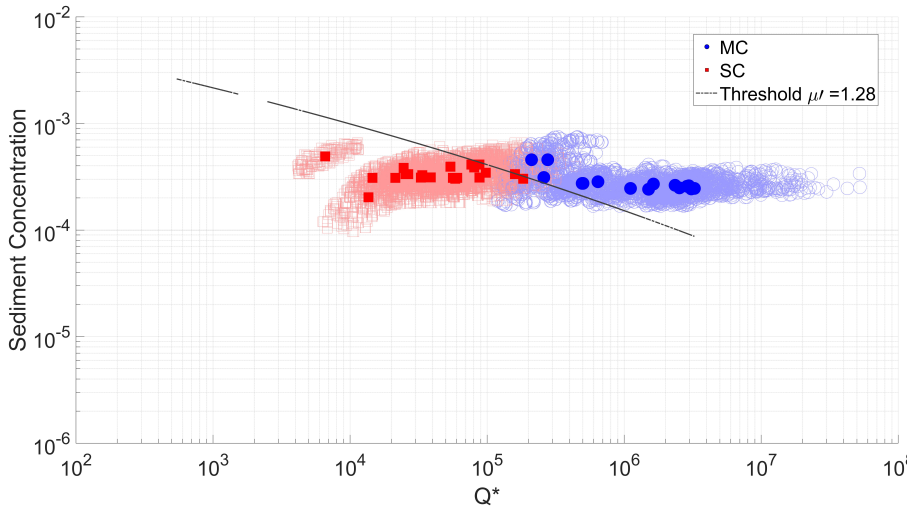

Figure 3.9: *Sediment Concentration and* Q^* *are plotted for all unconfined reaches along the main stem of the Vjosa. Red rectangles show single-channel (SC) reaches and blue circles multi-channels (MC) reaches. Filled markers indicate the mean value for each reach. The grey line indicates the braiding threshold calculated with* μ' *equal to 1.28.*

affect CASCADE outputs, and the discrimination between SC reaches and MC reaches. The results of our sensitivity analysis are summarized in Figure 3.9, which plots the 2300 simulated values of sediment concentration versus Q^* for only the main stem reaches of the Vjosa River. The red rectangles are SC reaches and the blue circles show MC reaches. Filled markers indicate the mean values amongst the 2300 simulations for each type of reach. The line indicating the braiding threshold corresponds to $\mu' = 1.28$. The cloud of red and blue points indicating the CASCADE simulations shows that even when we include uncertainty in key parameters there is a clear separation between the two channel patterns along the Vjosa. An important trend that emerges, which was also evident in Figure 3.6, is that the range in simulated sediment concentration is relatively narrow. It appears, therefore, that concentration is less important compared to Q^* in discerning SC from MC. This result is mostly driven by the modelling hypothesis that the sediment transport capacity within a reach is in equilibrium with the upstream sediment supply. This point is discussed further in the Discussion section.

Another practical result that emerges from this analysis is that once the SC-MC threshold is defined, river reaches close to the threshold are more likely to shift from one pattern to another compared to reaches further away from

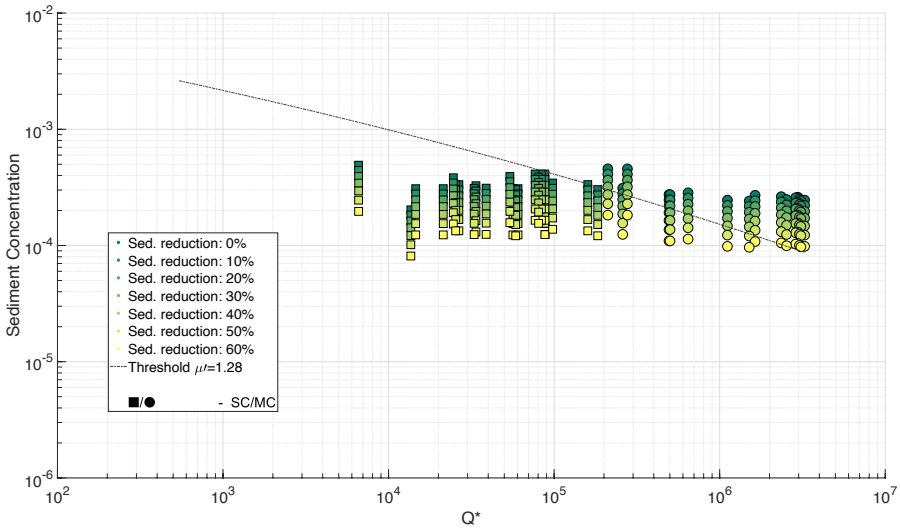

Figure 3.10: *Sediment Concentration and Q* are plotted for all unconfined reaches along the main stem of the Vjosa: rectangles show single-channel (SC) and circles multi-channels (MC) reaches. Point color is proportional to the sediment reduction applied to each reach. The braiding threshold (grey line) has μ' equal to 1.28*

the threshold. Focusing on the Vjosa reaches and using average values amongst all the simulations, Figure 3.10 shows how reductions in sediment concentration could produce a channel-pattern shift with respect to the braiding threshold. The MC reaches along the main stem of the Vjosa (circles in Figure 3.9 and 3.10) are all located downstream of the Drinos confluence (see Figure 3.5 or Figure 3.1) and Q^* increases moving downstream. For the first six braided reaches downstream the Drinos confluence a sediment reduction of 40% would be sufficient to locate them near the braiding threshold, whereas the most downstream ones would reach the threshold for a sediment reduction around 50-60%. This suggests that a sediment reduction of about half of the yearly sediment load would likely threaten the existence of the entire Vjosa braided system.

3.5 Discussion

3.5.1 Model initialization and validation with GSD and sediment fluxes

In this paper we assessed longitudinal sediment connectivity in one of the last un-impounded braided rivers in Europe. We developed an approach to robustly initialize and validate a network scale sediment connectivity model in a data

scarce environment. The proposed approach demonstrates the importance of a few specific steps in model initialization which affect our system functioning hypotheses. First, we developed a hypothesis about the range of possible GSDs and sediment supply in source reaches (see Figure 3.1 at the bottom). We then assumed that subsequent reaches are in a morphodynamic equilibrium, i.e., that the transport capacity of the reach balances the upstream supply, similar to what Ferguson et al. (2015) proposed for the Fraser river. In addition, we performed a more in-depth sensitivity analysis. The significant degree of uncertainty in local sediment transport calculations is well known(Ancey, 2020a,b) and this is even more critical in a data scarce environment. In the Vjosa River, detailed data on channel geometry is not available and hydrology is derived from a spatially distributed model with a coarse spatial resolution. In addition to the uncertainties in hydrology and channel geometry, the sediment flux within a reach depends on sediment supply from upstream, so these uncertainties propagate and possibly amplify through the network. For this reason, we explored results based on a wide range of possible combinations of source GSDs and different parameterizations of two key variables in the sediment transport formula calculation: the hiding function exponent and the width-discharge relationship.

Despite the wide uncertainty in parameter values and scarce field data on grain size and sediment fluxes, the CASCADE simulations generate plausible and coherent patterns of sediment fining that match observed sediment size distributions along the Vjosa River and its tributaries (see Figure 3.4 and Table 3.1). The CASCADE-generated estimates of D50 and D84 are comparable to those observed in the field, whereas the model overestimates the size of the finer fractions. The bias in finer sizes is mostly a numerical effect related to the difficulty of resolving grain sizes finer than 8 mm with the Base Grain software. In the two most downstream reaches, Pocem and Kalivac, the modeled GSDs are overall finer than the measured GDS, but the averages are similar. This effect for the downstream reaches is mostly due to two aspects of the modelling framework: 1) CASCADE simulates transport across all sediment size classes defined in the network and finer sediment might be underestimated in our observed measures of surface grain sizes, e.g., because of armoring; and 2) as mentioned earlier the fine tail of the distribution cannot be easily compared. Volumetric sampling would be required in this situation.

The hydrologic model adopted is validated at the European scale but without data from this basin (Van Der Knijff et al., 2010). In the absence of long-term hydrological data, it is not possible to even speculate how uncertainty in hydrologic drivers affects model results. With this in mind, our modelled sediment fluxes at the outlet of the Vjosa network are in the same order of magnitude as previous estimates (Fouache et al., 2001; Milliman and Farnsworth, 2011; Covault et al., 2013).

In the present study, the hypothesis about the morphodynamic equilibrium state of the river is the most critical and the least generalizable to other studies. Given that the Vjosa River is a pristine river system, where human influence had limited impacts, the hypothesis of morphodynamic equilibrium is reasonable. However, In many settings, sediment connectivity has been altered by human disturbance, e.g., through the construction of dams and diversions, in-stream gravel mining and increases in sediment supply caused by changes in land use (deforestation and cultivation). In rivers with a legacy of (dis)connectivity driven by human disturbance, or a landscape legacy of natural disturbance (e.g., landslides), equilibrium assumptions may not be valid (Brierley and Fryirs, 2005; Rinaldi et al., 2013; Gurnell et al., 2016). In such circumstances, the process of initializing models such as CASCADE can be improved by measuring source-area grain sizes, and, if possible, source-area sediment supply (Tangi et al., 2019). In addition, hillslope sediment supply can be derived from stochastic models of mass wasting (Beveridge et al., 2020), and river bed surficial grain size availability along river networks can be inferred from empirical relationships based on slope, drainage area, and river morphology (Snelder et al., 2011). For these reasons, even in contexts where morphodynamic equilibrium cannot be assumed, models such as CASCADE, when integrated with a sensitivity analysis, allow us to test multiple hypotheses on sediment supply and transport capacity, and to select the subset of model results which best reproduce the observed data.

As presently structured, CASCADE does not model the direct influence of hillslope processes on sediment connectivity. For this reason, the integration of sediment connectivity indices with models focusing on geomorphic processes occurring on hillslopes and floodplains (Cavalli et al., 2013; Heckmann et al., 2015) represent an important next step for generating information on sediment supply from sources outside the channel (Beveridge et al., 2020; Gilbert and Wilcox, 2020). Further developments may also better integrate channel-floodplain interactions including river lateral mobility and bank erosion modelling (Gilbert and Wilcox, 2020; Lauer et al., 2016). However, for a network-scale sediment connectivity model to be efficient, it is important to simplify local-scale processes without losing the ability to represent the main driving forces and connectivity patterns. In many circumstances, as this study demonstrates, trends in bed surface GSDs, represent a first order and effective way to infer sediment supply in network-scale sediment connectivity models.

3.5.2 Linking sediment fluxes and GSDs with river morphology

In spite of limited data availability, the Vjosa River basin provides a valuable opportunity to evaluate the link between modelled sediment fluxes and river morphology. The link between sediment loads and channel morphology has

been discussed in a number of papers (Schumm, 1985; Knighton, 1998; Kondolf et al., 2003; Buffington and Montgomery, 2013), but a quantification of these physical links is often missing (Church, 2006). To this aim, we applied a threshold formula to discern MC from SC based either on sediment concentration as proposed by Millar (2005) and Mueller and Pitlick (2014), or slope, as proposed by Eaton et al. (2010). Such a threshold is particularly meaningful for the Vjosa basin since here the river network experiences various transitions throughout its course from multi-thread to single-thread channel patterns. Our findings support previous models developed to discriminate between multi- and single-thread channel patterns and show that the MC/SC transition can be robustly modelled even under uncertainty (Figure 3.9). Our results suggest that the transition between MC and SC patterns is well defined by a threshold that varies with sediment concentration and relative bank strength, μ'. We treated μ' as a calibration parameter but note that it incorporates all errors, including systematic errors in the theoretical relations. The importance of this parameter in discerning SC from MC patterns has been discussed in a recent review (Candel et al., 2021). Analyzing what differentiates MC from SC reaches (Figure 3.8), we observed a clear pattern that can be interpreted as follows. The channel's ability to widen into the floodplain is a primary driver of the formation of MC reaches, which are characterized by a higher channel width, lower channel depth, finer grain sizes, and possibly higher slopes compared to adjacent lowland SC reaches. This interpretation reinforces the idea that bank strength, floodplain extent, and sediment composition are critical parameters in the formation of braided reaches, as discussed in the work of Candel et al. (2021) and Hohensinner et al. (2021).

We have shown that CASCADE modelling outputs can be used to establish thresholds between multi- and single-thread channels. To our knowledge, this is the first time that such thresholds are used in a dynamic context with simulated data and not field data. This is also the first time that the threshold theory has been applied to alluvial reaches in an entire river network. This has not been done previously because the data needed to implement the underlying equations (Eaton et al., 2010; Millar, 2005) are generally not available continuously across the network. This is an important step towards quantifying the link between connectivity and fluvial forms at the basin scale and in assessing channel sensitivity to change.

The results shown in Figures 3.6-3.8 merit further comments about CASCADE simulations, which are not obvious when looking only at GSDs and fluxes at the outlet. The Sarantoporos is a braided tributary of the Vjosa represented by red dots in Figures 3.6-3.8. We note that these reaches have geomorphic characteristics that are consistent with MC reaches, whereas in Figure 3.6, they plot close to or just below the braiding threshold due to low values of sedi-

ment concentration. This inconsistency suggests that simulated sediment fluxes for this basin are likely underestimated. This could be due to: i) underestimation of discharges generated by the hydrological model and/or ii) inadequacy of the sediment equilibrium hypothesis, particularly in a very dynamic and sediment rich sub-basin, such as the Sarantoporos. This latter point has probably likely has wider implications beyond the Sarantoporos reaches. We have suggested that the range of sediment fluxes generated by CASCADE is likely narrower than in reality. This is evident particularly in Figures 3.9 and 3.10 when comparing the range of sediment concentration values compared to the range of Q^*. This result is due in part to the equilibrium hypothesis which allows sediment fluxes to increase only at confluences. Other hypotheses on sediment transport mode and availability, as previously discussed, could be tested in the future following a more exhaustive and field-based river geomorphic analysis.

3.5.3 Assessing river morphology sensitivity and implications for management

A planform shift from braided or wandering channel patterns to single-thread patterns is a well-known consequence of alterations in water or sediment supply. In sediment starved rivers the changes can trigger a chain of reaction from river-bed incision, bank and infrastructure destabilization, aquatic and riparian habitat degradation and groundwater table alterations (Surian and Rinaldi, 2003; Kondolf, 1997; Bizzi et al., 2015, 2019). For this reason, being able to predict river channel response to alteration in sediment delivery is of paramount importance to support river management activities. Recent studies focusing on river sensitivity to changes in water and sediment supplies (Reid and Brierley, 2015; Fryirs, 2017) have highlighted the importance of understanding these links to be able to predict future channel change and better support river management strategies.

In the present study, we used average values of CASCADE simulations to calibrate the braiding threshold with $\mu' = 1.28$, then determined how different degrees of sediment reduction would move MC reaches toward and perhaps across the threshold for SC reaches. This perspective is relevant for the Vjosa where hydropower development might alter one of the last undammed braided rivers in Europe (Schiemer et al., 2018; Peters et al., 2021). We have shown that cutting the annual sediment load in half could transform the Vjosa from a braided river system to single thread. This information is critical for future management decisions regarding the Vjosa River since damming of upstream tributaries or sediment mining often reduces the amount of sediment delivered to reaches downstream (Liébault and Piégay, 2001; Simon and Rinaldi, 2006; Kondolf et al., 2018).

Further studies are needed to assess the degree of accuracy of such a thresh-

old. At what point in the sediment concentration-Q* plane would a river that today is braided turn into a river that is single channel? This is untested at the moment. A distinction between MC reaches and SC reaches clearly emerges but the distinction is based on the validity of model estimates and on the spatial distribution of reaches. What is needed is information on some reference reaches for which we can determine their trajectories over time. To build such historical trajectories we need data on sediment loads and grain size for the past, which often do not exist. What is more achievable is to start monitoring these trajectories in the future by mapping changes in channel morphology with respect to new positions in the sediment concentration-Q^* plane. Such knowledge could then be integrated into more comprehensive assessments of how alterations in sediment load and hydrology, translate to changes in channel form and function. Those assessments can then be used to inform management strategies such as mining regulations or the strategic siting or removal of dams.

3.6 Conclusion

This paper presents the application of the CASCADE model to the Vjosa River. We demonstrate how to initialize a network-scale sediment connectivity model in a context where data on hydrology and sediment information are scarce. In order to include how various source of uncertainties about key river attributes affect the calculation of transport capacity, we performed a global sensitivity analysis. The GSDs generated by the model generally match observed GSDs, except in the two downstream-most reaches where the finest modeled sizes are underrepresented. The modeled bed load sediment fluxes increase systematically downstream, and annual fluxes at the outlet of the Vjosa are well within an order of magnitude of fluxes derived from previous estimates of the annual suspended sediment load.

In addition to these results, we link simulated sediment fluxes and grain size across the network to observed river channel planform types. We used published braiding thresholds, which require information on water and sediment discharges, to discern MC from SC patterns. Feeding the empirical threshold model with CASCADE outputs we are able to discern these two patterns after calibrating the relative bank strength parameter. This is a remarkable result because it is an additional form of validation which supports the hypothesis that simulated sediment fluxes and their size distributions across the network are realistic and coherently linked to observed channel patterns. It is the first time that the adopted braiding threshold is calculated with data generated by a sediment transport model and not with field data. It is also the first time that such model output is applied and validated continuously at the scale of an entire river network. Inconsistency in these relationships also highlights some rele-

vant limitations of the model, related to discharge estimation and the sediment equilibrium hypothesis adopted.

The findings presented herein advance our ability to link sediment connectivity to river planform patterns and the sensitivity of the patterns to sediment management. For example, a 50% reduction of sediment transport along the main stem of the Vjosa, e.g., because of the proliferation of hydroelectric dams (Peters et al., 2021), would likely alter the unique braided character of the river. Future applications can develop more informed strategies for sediment management and tools to assess the consequences of network-scale alterations in sediment connectivity and channel planform stability.

4

The Dynamic CASCADE model

Modelling network-scale sediment (dis)connectivity and its response to anthropic pressures provides a foundation understanding of river processes and sediment dynamics that can be used to forecast future evolutions of the river geomorphology. However, this requires a solid understanding of how a system is currently operating, and how it operated in the past. In this chapter, we present the basin-scale, dynamic sediment connectivity model D-CASCADE, which combines concepts of network modelling with empirical sediment transport formulas to quantify spatiotemporal sediment (dis)connectivity in river networks. D-CASCADE accounts for multiple factors affecting sediment transport, such as spatiotemporal variations in hydrological regime, different sediment grainsizes, sediment entrainment and deposition. Add-ons are included in the D-CASCADE environment to model local changes in river geomorphology driven by sediment-induced variations in features such as channel gradient and width.

This chapter is developed partially based on: Tangi, M., Bizzi, S., Fryirs, K., & Castelletti, A. (2022). A dynamic, network scale sediment (dis)connectivity model to reconstruct historical sediment transfer and river reach sediment budgets. Water Resources Research, 58. DOI: 10.1029/2021WR030784

4.1 Introduction

Sediment (dis)connectivity is a fundamental property of river networks, emerging from temporal and spatial interactions (or the lack thereof) among sediment of different composition and grain sizes, delivered to the river from sources with varying supply rates, timing, and spatial distribution. Hydromorphological properties of river channels (e.g. width, gradient, and discharge) regulate sediment transport capacity and entrainment, transport, and deposition dynamics and rates. Spatiotemporal variability in the magnitude, frequency, and location of flood events that drive basin-scale patterns of discharge will also change the distribution and strength of these processes (Fryirs, 2013; Bracken et al., 2015; Sklar et al., 2017; Heckmann et al., 2018). To adequately and realistically model natural systems, these dynamics need to be properly accounted for in sediment transport models. Direct or indirect anthropic alterations disrupt sediment (dis)connectivity, leading to major shifts in the morphology of river channels at both the local (e.g. reach) and network scale. As (dis)connectivity is a distributed property of river systems, multiple drivers, whose intensity and effects may be spatially and temporally heterogeneous, may produce positive or negative feedbacks that alter the operation of the sediment cascade (Surian and Rinaldi, 2003; Vörösmarty et al., 2003; Fryirs, 2013; Bizzi et al., 2015; Wohl et al., 2019; Gregory, 2019). Thus, the characterization of basin-scale sediment (dis)connectivity is critical to improving our capacity to quantify possible future alterations following anthropic disturbances, whether direct (e.g. construction and management of a reservoir, or removal of vegetation), or indirect (e.g. land use change, climate change, or implementation of restoration), and determine how to manage them (Kondolf et al., 2014a,b; Wohl et al., 2019). Currently, available models and tools struggle to account for the complexity of these processes when applied at large temporal and spatial scales. Traditional morphodynamical models allow for detailed modelling of river processes with high accuracy, but, due to high computational demand and in-situ data requirements, analysis is often limited to short and well-studied river reaches or segments, where the boundary conditions can be defined precisely (Briere et al., 2011; Lammers and Bledsoe, 2018). However, such models do not take into account the (dis)connected nature of sediment transport that occurs at the whole basin-scale (Merritt et al., 2003). Recently, the increased availability of remotely sensed datasets of hydromorphological networks has allowed characterization and interpretation of geomorphic processes at the entire river network scale (Schmitt et al., 2014; Demarchi et al., 2017; Bizzi et al., 2019).This has led to the development of novel numerical models of network-scale sediment (dis)connectivity (Heckmann and Schwanghart, 2013; Schmitt, 2016; Czuba et al., 2017; Gilbert and Wilcox, 2020; Wild et al., 2021). These models trade part of the local-scale accuracy of more traditional models for a wider scale frame-

work that can run over longer timeframes and over larger areas to produce results that characterize (dis)connectivity patterns among different components of the river network. The CASCADE model (Schmitt, 2016) is a network scale sediment connectivity model that describes the movement of material from many individual sources across a network as separate transport processes called "cascades". Each cascade is identified by its provenance and carries a specific sediment volume that can be partly or completely deposited as it moves downstream, and interacts with other cascades. In this way, CASCADE can be used to quantify the rates at which each sediment source is connected with downstream reaches and to calculate the statistical properties of connectivity between different sediment sources and sinks. Therefore, CASCADE can evaluate (dis)connectivity alterations due to changes in both sediment sources and network hydro-geomorphic features for any given type of disturbance event (whether natural or anthropic) (Schmitt et al., 2018a, 2019). Tangi et al. (2019) expanded the description of the sediment cascade by defining sediment cascaded not by a single grain size, but by multiple grain size classes each carrying different volumes, to allow for a more thorough representation of sediment supply and transport (Bizzi et al., 2021). CASCADE, however, is a static model that can only represent spatial (dis)connectivity at one point in time, under static network properties and features. In this chapter, we present D-CASCADE, a new dynamic, network-based sediment (dis)connectivity model that can be used to explore the spatiotemporal evolution of sediment supply and delivery across a basin. D-CASCADE maintains all the properties of the original CASCADE model, but includes a temporal representation of sediment processes that is able to trace the position and movement of cascades over time, as well as across space. Thus, D-CASCADE can investigate the effects of multiple heterogeneous drivers of change that vary in magnitude, location, duration, or timing, as well as pinpoint and characterize the contribution of each driver to the cumulative change. D-CASCADE is designed to be a flexible and highly customizable modelling environment that can be adapted for different purposes, data availability, and level of detail needed. The model structure allows for the inclusion of multiple modelling add-ons that are designed to simulate 2D and 3D processes that the 1D structure of the basic D-CASCADE framework cannot capture.

4.2 Model structure

The structure, core components, and procedures of the D-CASCADE model are shown in Figure 4.1. The model setup is divided into two phases: initialization, and main D-CASCADE loop.

D-CASCADE shares the same graph structure which constituted the basis of the original CASCADE model (Schmitt, 2016) and the CASCADE toolbox

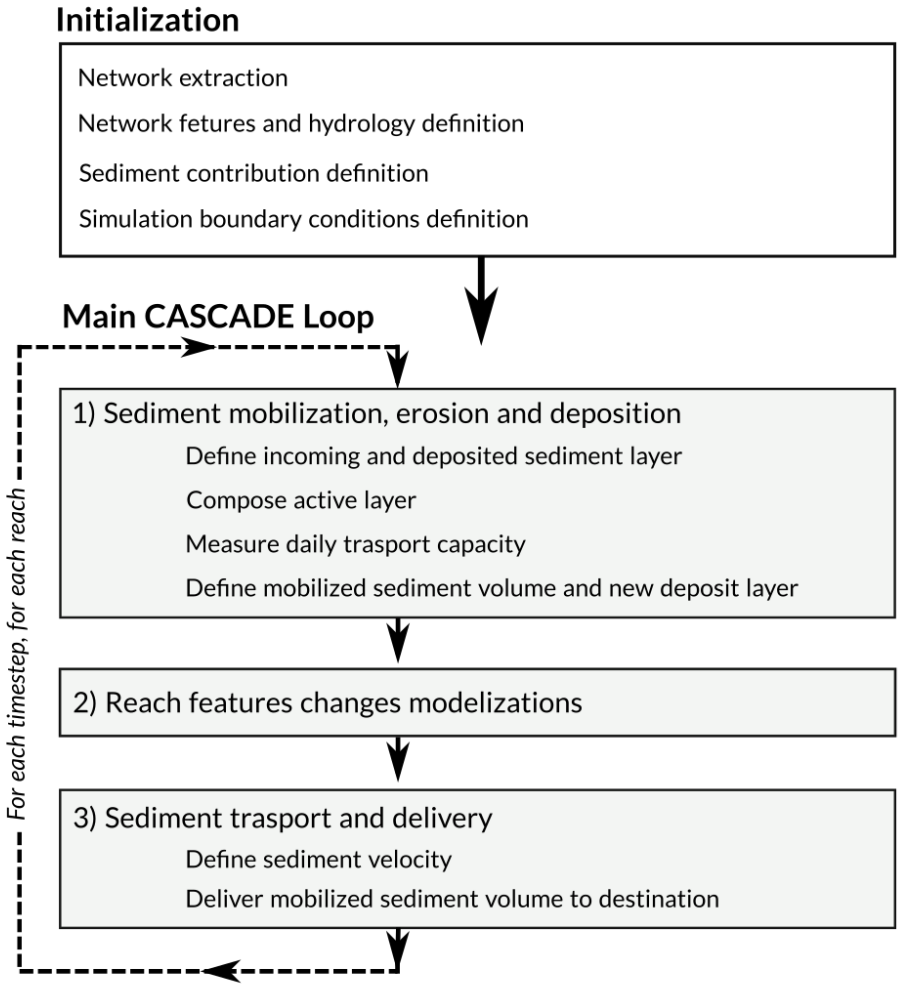

Figure 4.1: *D-CASCADE framework modelling steps*

(Tangi et al., 2019). Thus, the initialization phase includes the network extraction and reach features characterization. However, as detailed in the following section 4.3 D-CASCADE dynamic structure and morphological features modelling means network features may need to be either characterized for each modelling timestep, or initialized for the first timestep, according to the presence of specific add-ons components for modelling reach features response to changes in sediment delivery.

As described in Sections 1.4 and 2.2, in the original CASCADE framework the operations to determine sediment transport capacity, cascade delivery, deposition and routing are repeated for each network reach. The order of the reaches in the loop is determined by the reach hierarchy, i.e. the number of upstream reaches; therefore, source reaches are processed first, while the outlet reach is the last. the D-CASCADE modelling approach expand this structure by including two nested loops. The reach loop, which also integrates reach deposit stratigraphy and morphological features modelling, is repeated for each daily timestep, as detailed in Section 4.4.

4.3 Initialization

The initialization phase defines the input data necessary to run D-CASCADE and delineates the structure of the simulation itself. The model's primary input is the river network, represented as a graph comprised of nodes and reaches, like in the static CASCADE model (Tangi et al., 2019). The reach is the core modelling unit in both versions of CASCADE and is defined as a section of the river network between two nodes characterized by homogeneous geomorphic and hydraulic features. Each reach is defined by a unique set of geomorphological features, which are used by the modelling framework to derive information on sediment transport (such as transport capacity and velocity) via empirical formulas. In the modelling framework, these features fall into three categories:

1. Static features, which are kept fixed for the entirety of the simulation and must be defined once for each reach;

2. dynamic features, whose values may change in each timestep, and are defined a priori for each reach and for each timestep by the user;

3. modelled features, whose changes are simulated in each timestep by a specific component in the modelling framework, and thus only require initialization for the first timestep.

The reach features used by D-CASCADE are reported in Table 4.1. Depending on the confidence limits of knowledge of the study system and the data available, a feature may be better implemented as static, dynamic or modelled. For

Features	Description
Slope [m/m]	Channel slope. Derived from data surveys or Digital Elevation models (DEMs)
Length [m]	Desired length of individual reaches. Depends on the partitioning method used on the network.
Q [m^3/s]	Discharge in the timestep. Obtained from interpolation of gauging station datasets (Schmitt et al., 2016) or spatially distributed hydrological models (Schmitt et al., 2018a).
Active channel width [m]	Width of the channel section in the timestep. Obtained from satellite imagery (Schmitt et al., 2014, 2016, 2018b), field studies, or global data (Yamazaki et al., 2014; Frasson et al., 2019)
Grain size distribution (GSD)	Grainsize distribution parameters of sediment in the river bed. Interpolated from available point sediment samples, expert-based assessments, or based on hypothesis regarding river sediment transport regimes.
Manning's n	Manning's roughness coefficient for the bed material in the channel. Obtained from field data or estimated from the literature.
Sediment deposit [m^3]	Total amount of sediment stored in each reach, in each timestep. Initialized from data from by field surveys or expert assessments, and modelled directly in D-CASCADE.
External sediment inputs [m^3]	External sediment contributions from the watershed in each reach, in each timestep. Estimated by field surveys, empirical soil loss equation (USLE, RUSLE) or large-scale, grid based erosion models.

Table 4.1: *Key input features and possible sources for deriving their values on network scales in D-CASCADE*

example, the active channel width may be kept constant (static), or changed in each timestep by the user (dynamic), e.g. according to the discharge, or be simulated by a specific component in the modelling framework to reproduce channel width changes due to sediment erosion (modelled), as in the case of the Bega case study. Moreover, the initialization phase also includes the definition of the boundary conditions of the simulation, such as its time horizon, the numerical precision in the measurement of the sediment volumes, and the provenance and quantity of sediment routed in the model.

Sediment volumes routed through the network may be derived from material initialized in the reaches as a sediment deposit, or as external, user-defined sediment contributions supplied to individual reaches in specific timesteps, e.g. to reproduce sediment delivery from the hillslopes. Cascades are defined by the ID of the reach where the volume was initially delivered or stored, and the total sediment volume transported [m3], subdivided into different grain size classes. The size and composition of the sediment classes are pre-determined and defined in the initialization phase, and are selected according to the composition of the material transported and the level of detail desired.

4.4 Main D-CASCADE loop

The main D-CASCADE loop, which constitutes the core of the modelling framework, is comprised of a series of operations, broadly described in Figure 4.1, which are repeated for each reach and for each timestep as: i) mobilized sediment definition, ii) change in geomorphic features, iii) and sediment delivery.

4.4.1 Mobilized sediment definition

In each reach, the total volume mobilized and transported downstream in each timestep is comprised of cascades either delivered from upstream in the previous timestep, stored in the deposit layer or both. The deposit layer is conceptualized as a series of distinct tiers stacked on top of each other, with each tier comprised of a single cascade (Figure 4.2a and 4.2b). This modelling structure guarantees that newly deposited cascades form a tier above the previously deposited material, and at the same time entrained sediment is removed from the upper tiers of the deposit first. At any timestep t, the total sediment volume [m^3] in the deposit and the incoming cascades layers of a reach is measured as:

$$V_{d,t} = \sum_{\substack{\text{all cascades} \\ \text{in the deposit} \\ \text{layer at time t}}} V_{c,d,t} \qquad (4.1) \qquad V_{i,t} = \sum_{\substack{\text{all cascades in} \\ \text{the incoming} \\ \text{layer at time t}}} V_{c,i,t} \qquad (4.2)$$

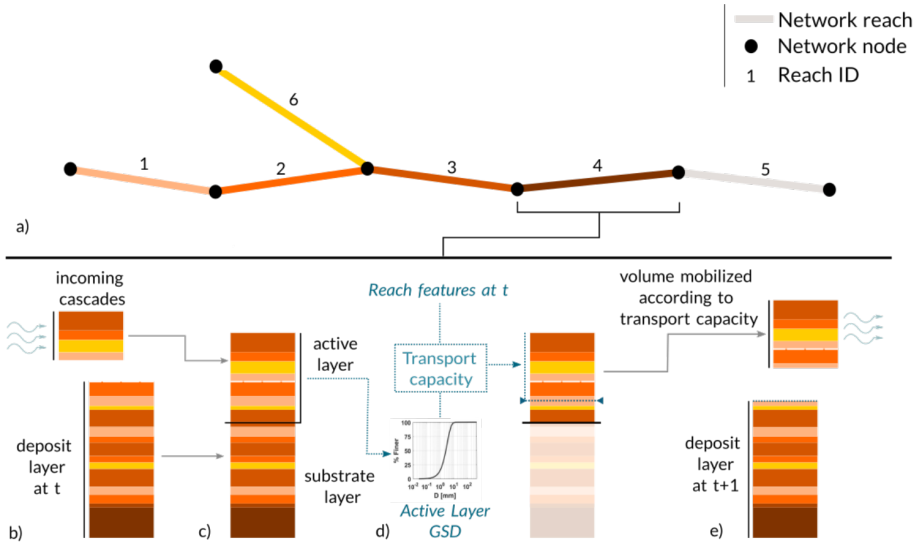

Figure 4.2: *An example of how the mobilized sediment volume is defined in a reach in a single model timestep. a) shows the modelled network as a graph composed of reaches and nodes, b) to e) show the passages to define the mobilized sediment volume for reach 4. The colours of the tiers indicate the reach of provenance in the network. In b) the model extracts the incoming cascades and deposit layer in the timestep, in c) the deposit is divided into active and substrate layer, in d) the model calculates the transport capacity for the sediment in the active layer, according to the layer Grain Size Distribution (GSD). Finally, in e) the mobilized volume and new deposit layer are defined.*

Where $V_{c,d,t}$ and $V_{c,i,t}$ are the total volumes transported by individual cascades located respectively in the deposit and incoming layers at time t, given by the sum of sediment volumes for each sediment class. As illustrated in Figure 4.2c, the upcoming sediment cascades are stacked above the deposit layer to form a single column, with volume $V_{f,t} = V_{d,t} + V_{i,t}$. This volume is then divided into an active layer $V_{a,t}$ and a storage/subsurface layer, according to the maximum active layer volume $V_{a,t}^{max}$ (similar to the procedure used in Czuba et al. (2017) and Czuba (2018), measured as:

$$V_{a,t}^{max} = W_t d_a l \tag{4.3}$$

where l is the reach length [m], W_t [m] is the channel width at time t. d_a [m] is the active layer thickness, which indicates the depth of the sediment layer that can be mobilized in a single daily timestep, defined either as a constant or as a variable in space and time according to the hydraulic and geomorphic

conditions of the network. Cascades in the top part of the column are put in the active layer until its volume $V_{a,t}$ reaches the maximum volume $V_{a,t}^{max}$ or there are no more cascades available. If a cascade is situated on the boundary between active and substrate layers, it is divided according to the remaining available volume in the active layer.

The volume $V_{m,t}$ mobilized in the reach at time t is determined by the sediment transport capacity, i.e. the maximum sediment discharge passing through a section allowed by the hydromorphological characteristics of the reach in the timestep considered. The instantaneous transport capacity Q_s $[m3/s]$ can be calculated using empirical formulas, which requires a definition of the grain size distribution (GSD) or the median grain size (D50) (Jr and Yang, 1989). The GSD used in the sediment transport is relative to the sediment volume in the active layer (Figure 4.2d). The instantaneous transport capacity is then converted into daily transport capacity to determine the mobilized volume $V_{m,t}$ for timestep t. Thus, the cascades in the active layer are mobilized starting from the top layer, until a volume equal to the $V_{m,t}$ is reached or the active layer is emptied. These cascades will be transported downstream. Conversely, the volume not mobilized in the active layer is stacked on top of the storage layer to form the new deposit layer (Figure 4.2e).

4.4.2 Change in geomorphic features

Selected modelling add-ons can be used to quantify changes in modelled geomorphic features between timesteps from the variation of sediment storage defined in the previous step. These add-ons can include traditional 2D or 3D morphodynamical modelling techniques, or a simplified model calibrated on observed historic channel evolution.

For example, (Czuba et al., 2017) uses a simple components to model changes in channel slope due to sediment accretion or entrainment in the channel which takes advantage of the graph structure of the river network, and can be easily repurposed in D-CASCADE. Sediment volumes added or removed from a reach are placed in its own reach and in the reaches immediately upstream. This is done to adjust bed elevation and thus slope, according to the equation:

$$\eta_{i,t+1}^{(u)} = \eta_{i,t}^{(u)} + \frac{(V_{d,i,t+1} - V_d, i, t)}{(W_{i,t} l_i + \sum_{u=U} W_{u,t} l_u) * (1 - \phi)} \tag{4.4}$$

Where $\eta_{i,t}^{(u)}$ is the elevation of the upstream node of reach i at time t, $W_{u,t}$ and l_i are the reach width and length, U is the set of reaches directly upstream and the $(1 - \phi)$ term accounts for the sediment porosity of the deposit. Channel slope is then calculated as:

$$S_{i,t+1} = \frac{\eta^{(u)}_{i,t+1} - \eta^{(d)}_{i,t+1}}{l_i} \tag{4.5}$$

Where $S_{i,t+1}$ is the channel slope of reach i at time $t+1$ and $\eta^{(d)}_{i,t+1}$ is the elevation of the downstream node of reach i at time $t+1$. This methodology generates a negative feedback loop, where erosion decrease slope, and thus transport capacity, and this in turn decreases the volume eroded in future timesteps. Conversely, deposition increases slope and transport capacity, leading to more sediment entrainment the next timestep.

4.4.3 Sediment delivery

The mobilized volume in each reach is delivered downstream according to the characteristic velocity of sediment $v_{s,i}$ of each reach i. The rate of transport of a mobilized sediment volume in the i-th reach is defined as:

$$v_{s,i} = \frac{Q_{s,i}}{W_i H_a \phi} \tag{4.6}$$

where $Q_{s,i}$ is the instantaneous transport capacity of the mobilized sediment in reach i [$m3/s$], W_i is the channel width [m], ϕ is the sediment porosity and H_a is the characteristic vertical length scale for sediment transport [m], which can be a function of the water height or kept constant. In reality, the characteristic velocity varies substantially depending on a variety of factors including the composition of the solid material transported and the hydromorphological conditions of the river reach. This formulation has been used in other distributed sediment models (Hassan et al., 1991; Czuba and Foufoula-Georgiou, 2014) and guarantees an estimate of sediment velocity that is useful for large-scale modelling efforts. However, it provides a single estimation of sediment velocity for the mobilized sediment volume, without discriminating between different sediment classes. An alternative approach to derive sediment velocity for each grain class is to assume sediment velocity is independent from grain size distribution, i.e. interactions between grains of different classes do not influence sediment velocity. Therefore:

$$v_{s,c,i} = \frac{Q_{s,c,i}}{W_i H_{a,c} \phi} \tag{4.7}$$

Where $v_{c,s,i}$ is the velocity of sediment movement for grain class c in reach i, $H_{a,c}$ is the characteristic vertical length of sediment transport for grain class c, $Q_{s,c,i}$ is the transport capacity for that sediment class, measured using empirical transport capacity formulas, assuming uniform sediment size and thus equating the D50 in the formula to the mean grain class diameter. While both

these approaches are based on empirical equations which provide simple estimates of virtual velocity of sediment load, the first assume the sediment mixture to move as a single entity, while the second consider each grain size class independently, Therefore, the choice of velocity formula depends on the modelling goals and the type of sediment class considered. The first equation may be more suited for modelling efforts in rivers with uniform or semi-uniform grain size distributions, where the sediment classes are few and close between. On the contrary, the second formula may be more appropriate if the model accounts for sediment of widely different sizes, which are bound to move at vastly different velocities.

For each sediment volume $V_{m,t}$, the model first derives sediment velocity for all the downstream reaches (and for each sediment class), from which it obtains the daily travelling distance, and then the destination reach, where the material will be delivered in the next timestep from the incoming layer $V_{i,t+1}$. Sediment leaving the network through the outlet is stored in an appropriate, out-of-bounds layer.

4.5 Conclusion

In this chapter, we presented the new dynamic D-CASCADE framework as a promising tool to explore the complex dynamics and patterns of river sediment (dis)connectivity across a catchment and over time. The inclusion of addons in its modelling environment allows for the evaluation of more complex and localized multidimensional morphological processes, which the basic 1D model structure cannot capture. The flexible and adaptable potential of the D-CASCADE framework allows for a wide array of future applications, including more complex representations of local morphological processes associated with sediment (dis)connectivity and integration with other large-scale models, e.g. distributed hydrological and morphological models. Limited data requirements and computational time also promote its use for relatively quick testing of model uncertainties and parameter sensitivity for use in final simulations. As with the original CASCADE model, D-CASCADE is also designed to be employed in strategic decision-making contexts, to provide indicators of sediment (dis)connectivity alteration as part of a multiple decision portfolio (Schmitt et al., 2018a, 2019). The novel dynamic framework also allows for the exploration of the competing or compounding effects of time-varying sediment management strategies, e.g. basin-wide water release and sediment flushing strategies for multiple reservoirs in different part of the network (Kondolf et al., 2014b, 2018; Wild et al., 2021). Both uncertainty analysis and portfolio performance exploration are supported by the limited computational requirement and scalability of the D-CASCADE modelling environment, which allows

for fast and repeatable model simulation.

5

D-CASCADE application to reconstruct historical sediment transfer and river reach sediment budgets

This chapter presents an application of the D-CASCADE modelling framework to the well-documented Bega River catchment, NSW, Australia, where significant geomorphic changes to rivers has occurred post European colonization (after 1850s), including widespread channel erosion and sediment mobilization. The Bega catchment also provides a useful case study to test D-CASCADE, as original source data on the historical sediment budget are available. By introducing historic drivers of change in the correct chronological sequence, the D-CASCADE model successfully reproduced the timing and magnitude of major phases of sediment transport and associated channel adjustments over the last two centuries. With this confidence, we then ran the model to test how well it performs at estimating future trajectories of basin-scale sediment transport and sediment budgets at the river reach scale.

This chapter is developed based on: Tangi, M., Bizzi, S., Fryirs, K., & Castelletti, A. (2022). A dynamic, network scale sediment (dis)connectivity model to reconstruct historical sediment transfer and river reach sediment budgets. Water Resources Research, 58. DOI: 10.1029/2021WR030784

5.1 Introduction

To validate the effectiveness of D-CASCADE in reproducing major patters of sediment (dis)connectivity, sediment delivery and morphological change, we apply D-CASCADE to the Bega River network, NSW, Australia, with the objective of reproducing the known geomorphic changes and trajectories of river adjustment that have occurred due to anthropic disturbances post-European settlement (ES). The Bega catchment case study was chosen to test D-CASCADE because of the wealth of well-documented and published data on river change and sediment budgets (e.g. see Brooks and Brierley (1997); Fryirs and Brierley (2001); Fryirs et al. (2007); Brierley and Fryirs (2013)). We return to the historical record and use the original source data to reconstruct the pre-ES river morphology. We then define the magnitude, timing, and location of dominant historic drivers of geomorphic change over the last 170+ years to set the boundary conditions for the simulation. Given the large uncertainties in the reconstruction of some historical parameters, a sensitivity analysis is used to explore different scenarios of geomorphic change in response to different hydraulic conditions over time. Knowledge of system evolution is then used to delineate possible trajectories of future geomorphological adjustments across the river network.

5.2 Case study

The Bega River catchment is located on the south coast of NSW, Australia, and drains an amphitheater-shaped area of 1930 km^2, divided into six different subcatchments, namely Wolumla, Candelo, Tantawangalo, Sandy, Bemboka and Brogo (Figure 5.1a). An escarpment encircles the catchment on three sides, rising to 1200 m asl, which abruptly gives ways to elevated uplands, and after the confluence with Wolumla Creek, a lowland plain, where Bega township, the largest settlement in the area, is located. The climate is characterised as temperate but there can be prolonged period of drought and no-flow that are abruptly broken by intense rain events that produce floods (Brooks and Brierley, 1997). The largest flood on record, in February 1971, had a discharge of 1800 m^3/s at Morans Crossing. A technical report by Cardno (2018), estimated that a flood event with 1% of annual exceeding probability, similar to the 1971 flood, could have a discharge of 10400 m^3/s near the outlet.

Rivers in the Bega catchment underwent catastrophic geomorphological changes following the establishment and expansion of European settlements, starting from the XIX century, as described in the timeline in Figure 5.1b. Brooks and Brierley (1997); Fryirs and Brierley (1998, 1999, 2001). Prior to European settlement, the Bega catchment was dominated by open woodland with

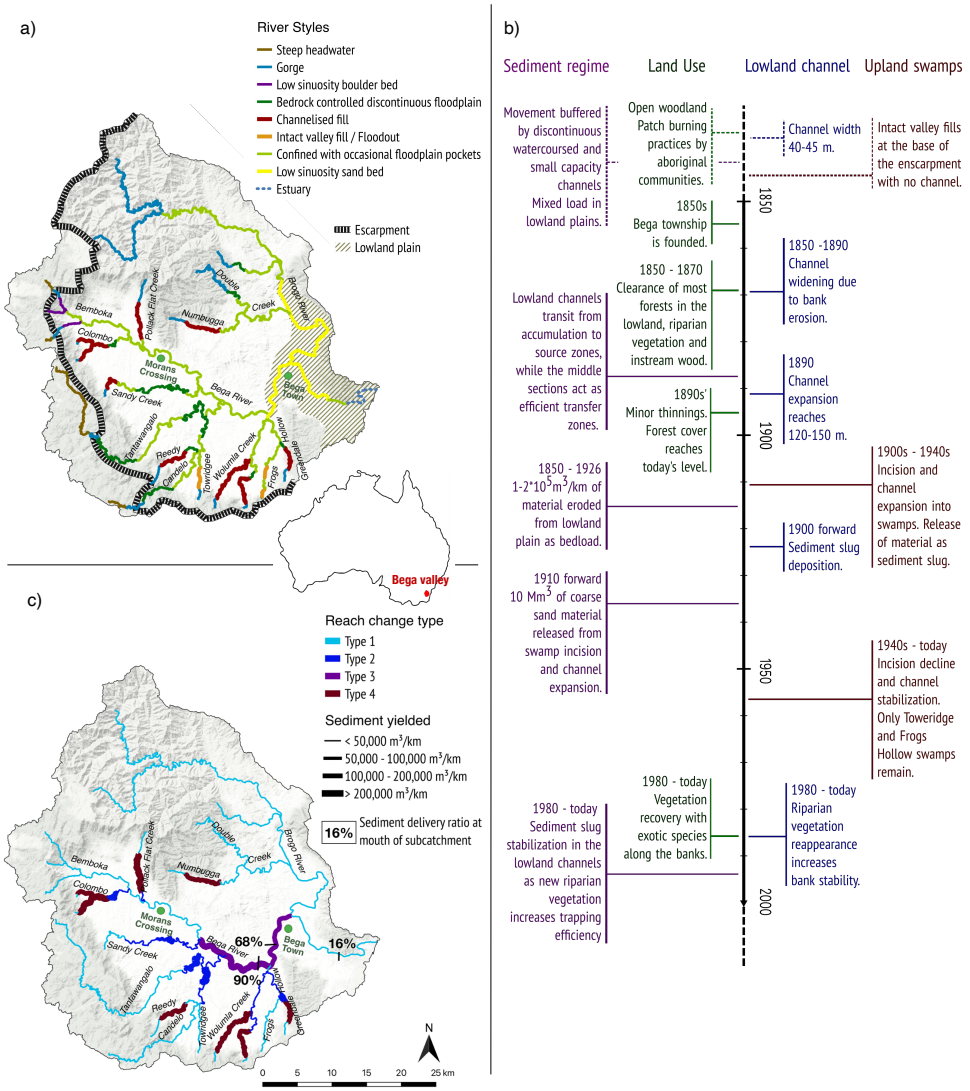

Figure 5.1: *Features and timeline of changes in the Bega River valley. a) Present-day River Styles (Fryirs and Brierley, 2001)in the Bega catchment, NSW, Australia; defined by Brierley and Fryirs (2000). Channelized fills were originally intact valley fills or swamps, but due to anthropic interference have experienced widespread erosion, incision and sediment release. b) Timeline of the major geomorphological changes in the Bega catchment from 1850 to 2020. c) Classification and sediment yielded since European settlement for the reaches of the Bega river network (in m3/km) as defined by Fryirs and Brierley (2001). The amount of sediment yielded is represented by the line thickness. Sediment delivery ratios used for validation of the model outputs are also displayed.*

scrubby undergrowth and intact valley fills (swamps) at the base of the escarpment. Many parts of the Bega tributary networks were characterized by discontinuous watercourses with no well-defined channels (Brierley et al., 1999) which greatly limited sediment transport and produced significant buffers and barriers to sediment (dis)connectivity (Fryirs et al., 2007; Poeppl et al., 2020).

The river along the lowland plain was likely a suspended or a mixed load system (Brooks and Brierley, 1997). Early European settlements are dated to 1840's and 1850's, with Bega township being founded in the early 1850's. By the 1890's, around 90% of the lowland vegetation cover was removed from the floodplains (70% of the total vegetation cover of the basin) and riparian vegetation and wood was removed from the river channels (Brooks and Brierley, 1997). The channel expanded from around 40 - 50 m in the 1850s to 120 – 150 m by 1890, before being stabilized by exotic willows on the banks by 1926 (Brooks and Brierley, 1997). The material released by bank erosion was around 100,000 – 200,000 m^3/km of fine to medium sand (mean grain size 350 – 500 μm) (Brooks and Brierley, 1997; Fryirs and Brierley, 2001). Channel expansion to varying degrees also occurred along large sections of the middle reaches of the Bega and Brogo trunk streams.

At the base of the escarpment, incision and channel expansion into formerly intact valley fills (swamps) occurred from about 1900 (Brierley and Fryirs, 1998; Brierley et al., 1999; Fryirs and Brierley, 1998, 1999, 2001). In total, around 10 million m3 of material was released. Today, intact valley fills persist in only two locations in the network (Towridgee Creek and Frogs Hollow). The release of material from these valley fills was rapid, producing a sediment slug composed mostly of coarse granular sand (mean grain size 1 – 2 mm) which travelled downstream through the middle reaches of the system and was deposited in the lowland channels and floodplains (Fryirs and Brierley, 2001). This supply changed the sediment regime of the lowland plain river to a sand-dominated bedload system (Brooks and Brierley, 1997). Sediment released by these river changes created a large sediment slug that still remains in the system today.

During the last decade, it has been observed a reappearance of vegetation, mostly non-native species, alongside the banks of most of the downstream reaches. The recovery of vegetation cover along the banks and on the sediment bars both contribute to increase bank stability and consolidating the position of the sediment slug in the lowland reaches. (Fryirs et al., 2018).

Using the D-CASCADE modelling framework we aim to test whether the most impactful geomorphic changes observed in the basin, i.e. erosion and sediment release from the valley fill swamps, channel expansion along the lowland plain, and sediment slug formation and movement can be recreated and modelled.

5.3 Methods

Using the D-CASCADE modelling framework, we aim to test whether the most impactful geomorphic changes observed in the Bega River basin post European settlement can be recreated and modelled. These include erosion and sediment release from valley fill swamps, channel expansion along the lowland plain, and sediment slug formation and movement, as well as the sediment budget alterations. For the model parameterization, we first define the network features and the historic hydrology. We then introduce the modelling components for the geomorphic changes and the simulation structure. Finally, we define validation parameters for the model outputs based on literature and available data.

5.3.1 Network features definition

Table 5.1 describes the main D-CASCADE features, their source and their modelling type, according to the classification described in Section 4.3. River networks of the Bega catchment were extracted using a Digital Elevation Model (DEM) provided by Geoscience Australia, with 2 meter resolution, using the Topotoolbox software(Schwanghart and Scherler, 2014). Uniform reaches with an average length of 2 km were extracted, excluding reaches corresponding to former swamps, which are considered sediment sources and were therefore extracted as a single reach without segmentation. This helps to avoid sediment stagnation between consecutive source reaches. In total, the network is partitioned into 263 reaches. To model the historic geomorphological changes in D-CASCADE, reaches are classified into 4 categories according to the type and magnitude of geomorphic changes experienced (Figure 5.1c):

- Type 1 reaches are located above the escarpment line or along still vegetated river stretches that experienced no significant morphological changes.
- Type 2 reaches are in the middle portion of the basin and have experienced minor channel expansion.
- Type 3 reaches are in the lower part of the basin and have experienced substantial channel expansion.
- Type 4 reaches are the valley fill reaches at the base of the escarpment that were affected by incision into swamps.

Modern day values of channel width, bed grain size distribution, and channel roughness coefficient are obtained from satellite images and field surveys, and historical data is drawn from the published literature. The original sediment budget data from Fryirs and Brierley (2001) have also been used. Elevation

Features	Description	Classification for the Bega case study
Slope [m/m]	Channel slope. Derived from the Digital Elevation models (DEMs) provided by Geoscience Australia	Static feature
Length [m]	Desired length of individual reaches. Defined by the reach classification in Fryirs and Brierley (2001)	Static feature
Q [m^3/s]	Discharge in the timestep. Obtained by combining gauging station datasets with a spatially distributed hydrological model (see section and Appendix A1.	Dynamic feature
Active channel width [m]	Width of the channel section in the timestep. Initialized by field studies and hystorical reconstructions.	Modelled feature
Grain size distribution (GSD)	Grainsize distribution parameters of sediment in the river bed. Initialized by field studies and hystorical reconstructions.	Modelled feature
Manning's n	Manning's roughness coefficient for the bed material in the channel. Obtained from field studies.	Dynamic feature
Sediment deposit [m^3]	Total amount of sediment stored in each reach, in each timestep. Initialized by sediment budget estimations in Fryirs and Brierley (2001).	Modelled feature

Table 5.1: *Key input features, sources for deriving their values on network scales and how these features are reproduced in D-CASCADE for the Bega river network case study.*

data from the DEM are used to derive channel slope; as no data on pre-ES channel gradient are known, we assumed slope to be a static network feature. For type 2 reaches, the pre-ES channel width is set equal to 80% of the current value, to account for a 20% width expansion. For type 3 reaches, the channel width is expanded from 40 m to 135 m before 1890, while the original bed grain size is assumed equal to the estimated pre-ES bedload (Brooks and Brierley, 1997). For type 4 reaches, the last remaining intact swamps in the network are used as pre-ES analogues. These swamps are relatively wide (150-180 m) and steep (0.02 – 0.028). The types of sediment released from type 4 reaches is medium

to coarse sand (1 - 1.4 mm) as documented in Fryirs and Brierley (1998) for the valley fill stratigraphy. Due to the lack of historical datasets, grain size distribution for type 1 and 2 reaches are assumed equal to present day value. For the pre-ES condition, we assigned a relatively high roughness coefficient for all reaches, given the known presence of dense riparian vegetation and wood in the channels, equal to 0.2 for type 4 reaches and 0.1 otherwise. Roughness coefficients associated with vegetative recovery after 1980 have been defined using expert judgement as well as historic and contemporary satellite images. For example, in the lowland channels, roughness shifts from 0.1 pre-ES, to 0.04 after riparian vegetation removal, to 0.08 today with vegetative recovery. By 2001, around 90% of the mobilized volumes were delivered to the lowland plain channels. Only around 16% of the released material has been delivered to the estuary (Fryirs and Brierley, 2001) (Figure 5.1c). These volumes are used in the simulation to initialize the pre-ES sediment deposit in each reach, assuming uniform grain size distribution.

5.3.2 Reconstruction of hydrology

As D-CASCADE models daily timestep, a complete simulation of the full time horizon would require continuous daily discharge data for all 263 reaches over 170+ years, which are not available. Therefore, given that most of the sediment movement along the Bega River network occurs during intermittent flood events, we chose to simulate only the daily timesteps when historic flood events with a 1-year relative flood return period (RP) or more occurred, and assumed sediment transport to be nil or negligible otherwise. For detailed information on the hydrology reconstruction, refer to Appendix A.1.

In total, 168 daily flood events have been identified. Historical hydrological dataset from 1850 are only available for gauge height and relative flood RP in specific locations. To account for uncertainty in the correlation between gauge height, flood RP, and discharge, we defined four scenarios that are designed to cover a wide range of possible discharge conditions. Each scenario classifies each flood events into a RP class (1-, 2-, 5-, 10-, 20-, 50-, 100-year flows) correlated to a specific discharge for each reach. The scenarios are: Medium discharge scenario (MedQ), High discharge scenario (HighQ), Low discharge scenario (LowQ), and Mixed discharge scenario (MixQ). The MixQ scenario is designed to account for higher flood magnitude in upstream reaches compared to lowland ones, and then to increase sediment erosion and release in the type 4 reaches: the same flood event is classified in a higher PR class in type 4 reaches, and in a lower class otherwise.

To explore future sediment transport trajectories in the network, we created 100 scenarios lasting 100 years each, assuming a maximum of one flood event per year, by generating independent flood events extracted from the yearly

probability distribution of the historical dataset.

5.3.3 Add-ons modelling components

For the Bega case study, we introduce two add-ons to D-CASCADE to reproduce changes in channel width and the effect of overbank floods on the in-channel sediment storage. These components are described in detail in Appendix A2

The channel expansion add-on simulates channel width change caused by bank erosion, by increasing its value proportionally to the erosion of the initialized reach sediment budget, up to observed present-day conditions. The overbank flooding component accounts for part of the discharge going overbank during particularly large floods, which decreases the potential for sediment erosion on the channel bed. This is especially important in the lowland reaches, where overbank flooding has historically led to sediment deposition on the floodplains and lower erosion potential of the channel bed. In each timestep, this add-on reduces the value of the discharge used to quantify the erosion of the deposit layer to a value corresponding to the highest non-overbank flood, while sediment transport and velocity remain unaltered.

5.3.4 Simulation structure

	Phase 1 (1850 - 1900)	Phase 2 (1901 - 1910)	Phase 3 (1911 - 1980)	Phase 4 (1981 - 2020)
Type 1	• Channel roughness decreased linearly to pre-vegetative recovery values	• Overbank flood add-on component is active	• Overbank flood add-on component is active	• Channel roughness increased linearly to present day values where vegetative recovery is observed • Overbank flood add-on component is active
Type 2-3	• Channel roughness decreased linearly to pre-vegetative recovery values • Sediment deposit made available for erosion proportionally to the changes in channel roughness • Channel width increased up to present day value as modelled by the channel expansion add-on	• Overbank flood add-on component is active	• Overbank flood add-on component is active	• Channel roughness increased linearly to present day values where vegetative recovery is observed • Overbank flood add-on component is active
Type 4	No changes	• Channel roughness decreased linearly to pre- vegetative recovery values • Channel width decreased linearly to 10 m	• Channel width increased up to 50 m as modelled by the channel expansion add-one	• Channel roughness increased linearly to present day values where vegetative recovery is observed

Table 5.2: *Timeline of morphological drivers introduction and add-ons activation in the historic simulations for each reach types and temporal phases.*

We introduced the drivers of geomorphological change in the modelling environment in a temporal sequence relative to known phases of change from the historical record. Table5.2 describes the structure and length of each phase and summarizes how and when the different drivers of change are introduced to the simulation. The temporal phases are:

- Phase 1 (1850 – 1900): vegetation removal along lowland river that resulted in bank instability and channel expansion.
- Phase 2 (1900 – 1910): valley fill incision and channel expansion along type 4 reaches.

- Phase 3 (1911 – 1980): delivery and stalling of the sediment slug along the lowland plain channel and floodplain.
- Phase 4 (1981 – 2020): vegetation recovery and subsequent decrease in sediment mobilization.

In this study, we consider seven sediment classes from very fine sand to pebbles (-5.5, -4, -2.5, -1, 0.5, 2 and 3.5 φ in Krumbein logarithmic scale, corresponding to 45, 16, 5.6, 2, 0.70, 0.25, 0.088 mm). As we reproduce the movement of mostly sand in the network, we applied eq 4.6 for measuring virtual sediment velocity independently from the grain size classes considered. The active layer thickness d_a (see eq. 4.3) and the vertical length for sediment transport H_a (see eq. 4.6) are kept constant in all reaches and equal to 1 m and 0.1 m respectively (Czuba, 2018), and the sediment porosity ϕ = 0.4 (Wu and Wang, 2006). To avoid excessive computing time and data storage, new sediment cascades are defined only if they carry at least 0.1 m^3 of sediment in at least one grain size class. The transport capacity is calculated using the Ackers-White formula (Ackers and White, 1973), the bedload transport capacity formula also employed in Fryirs and Brierley (2001). The formula requires estimation of D35, obtained via interpolation of the grain size distribution of the active layer, and values of water height and velocity, derived using the Manning-Strickler formula (Manning, 1891). Ackers-White is a total transport capacity formula, so the Molinas and Wu partitioning formula (Molinas and Wu, 2000) is used to derive fractional transport capacity for each sediment class.

5.3.5 Validation parameters

To quantify how the D-CASCADE model simulation performs at reproducing quantifiable effects of major historical changes observed in the network, we defined four indicators based on field data and historical reconstruction, which compare the model outputs for the 2000s with field data collected in the same years (Brooks and Brierley, 1997; Fryirs and Brierley, 2001):

1. **SedDelRt**: Fryirs and Brierley (2001) extrapolated from field data the sediment delivery ratio (labelled *SedDelRt*) of the mobilized deposit at the mouth of different subcatchments since ES. We can derive sediment delivery ratio (SDR) from the model outputs by comparing the amount of sediment, deposited or mobilized, present in a subcatchment at time t with the same value at t=1

$$SDR_{i,t} = \frac{\sum_{j=ur\_i}(V_{d,j,t} + V_{m,j,t})}{\sum_{j=ur\_i}(V_{d,j,1} + V_{m,j,1})} \tag{5.1}$$

Where $SDR_{i,t}$ is the sediment delivery ratio in reach i at time t and ur_i is the set of all reaches situated upstream reach i,i included. In particular, we used the sediment delivery ratio in 3 different downstream locations as indicators (see Figure 5.1c): at the Bega River just before the Wolumla Creek confluence (SDR = 90%), the Bega River at Bega township (SDR = 68%), and just before the estuary (SDR = 16%). The sharp decrease in SDR between these sections is indicative of one of the major morphological changes observed, i.e. the trapping of material released as a sediment slug in the lowland sections of the river.

2. Type 4 - % incised: According to the historic reconstruction (Fryirs and Brierley, 2001), sediment material initialized in the deposit layer of type 4 reaches (Figure 5.1c)should have been completely transported downstream by 2001. By measuring the percentage of total sediment initialized along these reaches eroded by 2001, we can validate if the methodology used to model sediment erosion is sufficiently able to reproduce incision of the valley fills and subsequent channel expansion.

3. Type 3 – Width: validated whether the channel expansion add-on is able to reconstruct the historic changes in channel width along the lowland plain (Brooks and Brierley, 1997) by comparing the modelled average channel width with present day field-measured values.

4. Type 3 – D50: checked whether the model is able to replicate the coarsening of bed material grain size in the lowland reaches, and therefore the change in sediment regime from mixed load to bedload, by determining whether the average D50 of the modelled bed material matches the field-measured present day average of 1.4 mm (Brooks and Brierley, 1997).

5.4 Results

5.4.1 Historical sediment transport trajectories

Figure 5.2 shows the D-CASCADE simulation outputs for the MedQ scenario, for selected sections of the river network. Lowland reaches are classified into 8 different sections (Figure 5.2a, from A to H), each of which is comprised of 2 to 4 reaches. Total sediment volume in each timestep is defined as the sum of the mobilized volume $V_{m,t}$ and the deposit layer $V_{d,t}$ of all reaches in a section. Figure 5.2b shows the evolution of total sediment volume and channel width for the lowland sections in the simulation horizon. D-CASCADE provenance tracing allows us to categorize the total volume according to the original supply location. In this case, we distinguish between provenance from type 2 and 3 or type 4 reaches.

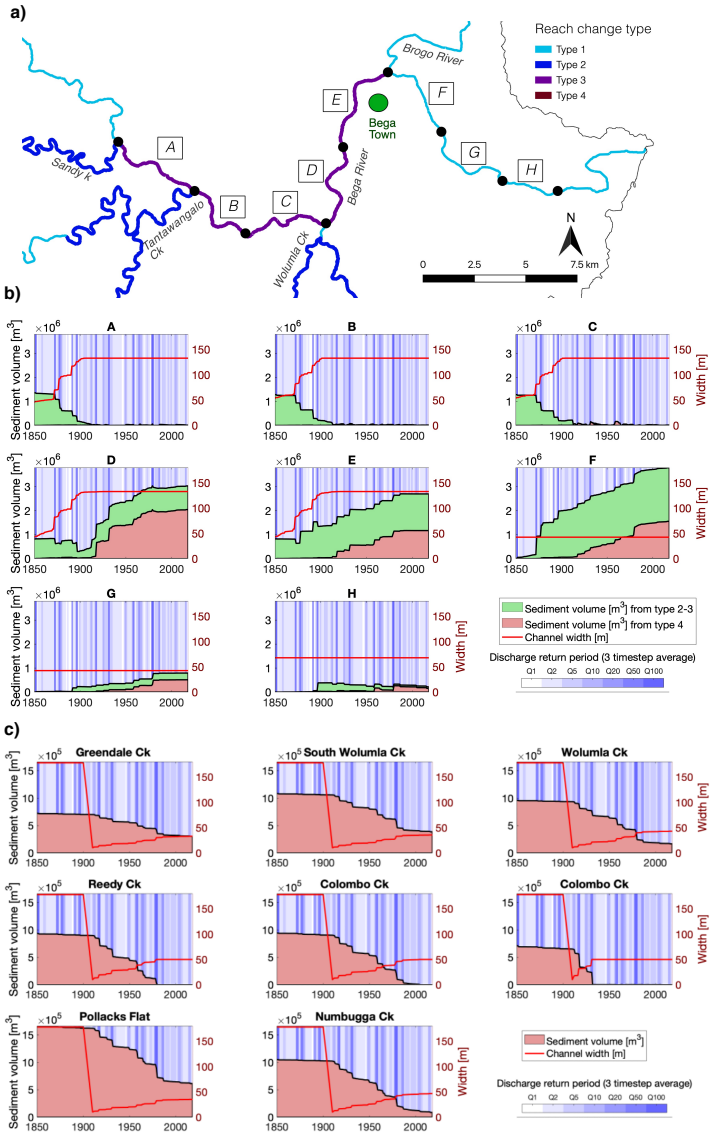

Figure 5.2: *Variations in total sediment volume and network features in different locations in the river network for the MedQ scenario. Sections in the downstream reaches are identified in figure a). Bars on the background of b) and c) indicate the flood RP each year, with a 3 timestep average. Figure b) show trajectories for the downstream reaches, separating sediment from channel expansion (type 2 and 3, in green) from material from incision of valley fills (type 4, in orange). The figure also shows channel expansion due to bank erosion (red lines). Figure c) shows the decrease of the original sediment budget in type 4 reaches, following swamp drainage, incision and channel expansion.*

According to the model, channel expansion in type 2 and 3 reaches occurred between 1850 and 1900, mostly driven by large flood events. Before 1900, all the bank material that was available has been eroded and channel width increases to present-day values. Most bank material is transported downstream, depositing mostly in section D-F. After 1900, sediment released from incision of the valley fills transits easily through sections A to C, before accumulating mostly in sections D to F. Figure 5.2c shows trajectories for type 4 reaches for the MedQ scenario. Before 1900, all simulations show that sediment release from type 4 reaches is almost non-existent due to the unincised nature of the valley fills, characterised by no channel and high surface roughness that greatly reduces transport capacity. After 1910, swamp drainage and channelization led to channel incision and sediment slug formation, which continues for the rest of the simulation horizon. Variations in the hydrology of each reach explains why sediment is released at different rates, e.g. Reedy and Colombo Creeks are mostly emptied before 1950, while Pollacks Flats, Greendale and South Wolumla Creek retain material past the year 2000.

After 1980, the increase in riparian vegetation and channel roughness leads to a visible decline in sediment mobilization in both upstream and downstream reaches, even during large floods.

Figure 5.3a shows sediment delivery and deposition in the lowland reaches for the four hydrological scenarios. Most noticeably, under the HighQ and MedQ scenario, less sediment is stored in section E, and more in section F downstream of the Brogo confluence. Channel expansion rates remain largely the same across all scenarios.

The performance of the four scenarios for the four validation parameters are shown in Figure 5.3b. Sediment delivery of the material initialized follows similar patterns, as all scenarios present sediment sinks along the lowland plain (section D-G) while upstream sections function as sediment source and transfer zones. Consequently, all scenarios show a clear decrease in sediment delivery between sections C and H.

Conversely, lowland channel expansion in all scenarios follows the pattern defined by historical observations, with channel width reaching present-day conditions around 1890-1900. All simulations reproduce the coarsening of bed material along the lowland plain.

Scenarios with the highest discharge in type 4 reaches (HighQ and MixQ) exhibit more pronounced erosion of valley fill sediment and higher sediment delivery ratio to the lowlands, while LowQ and MedQ are associated with lower percentages in both parameters.

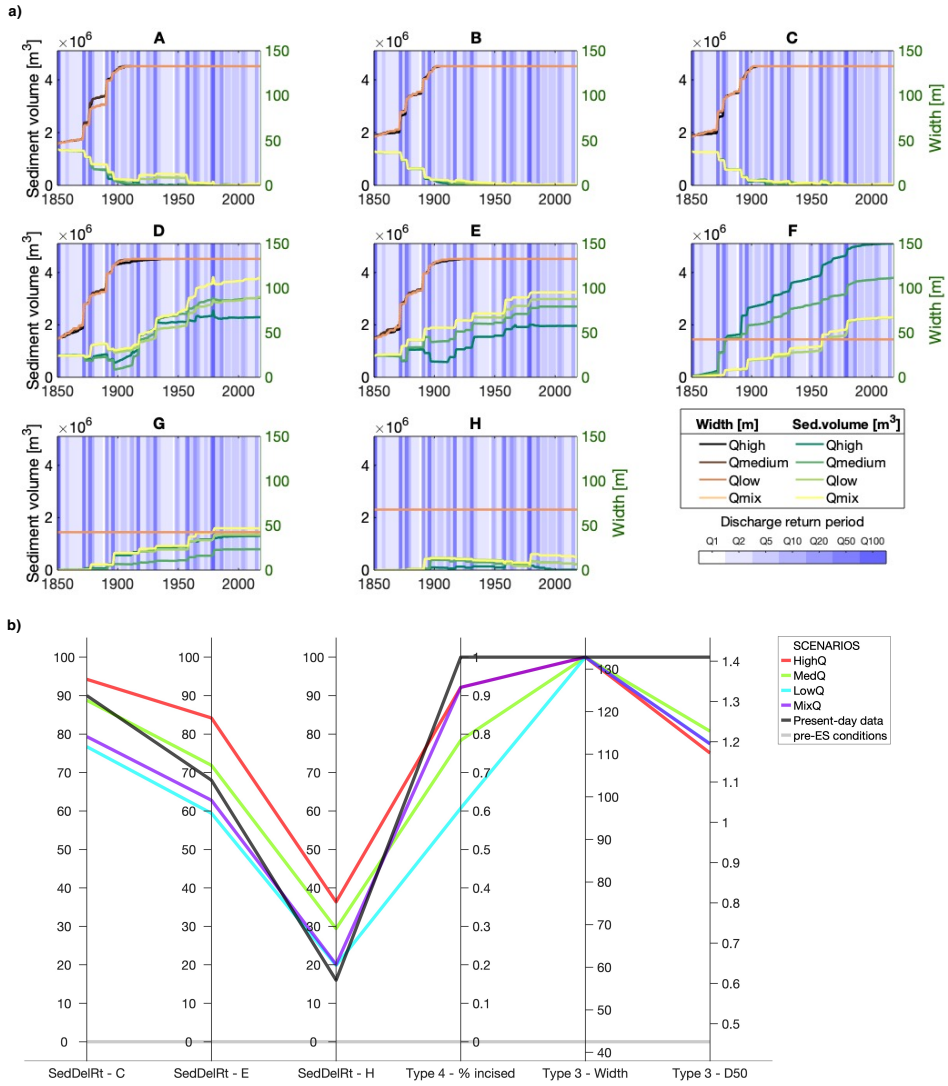

Figure 5.3: *D-CASCADE model output and performances for the different hydrology scenarios. a) Variation of total sediment volume and channel width along the lowland plain, for the four hydrological scenarios. Discharge is shown for the HighQ scenario. b) Performance of the four hydrological scenarios for the four validation parameters. The grey and black lines represent, respectively, the pre-ES and the present-day values for the parameters. Scenarios closer to the black line have better performances.*

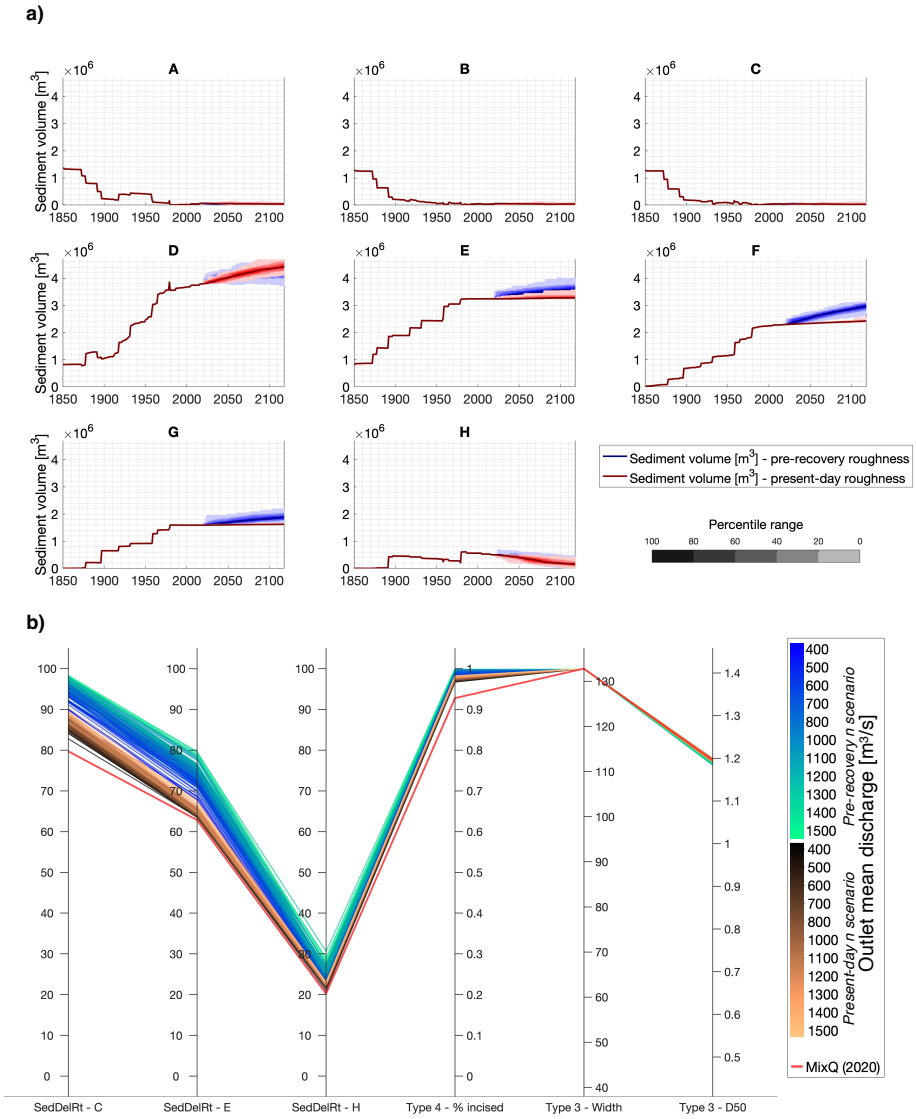

Figure 5.4: *Trajectories and performances of future hydrology scenario, in the pre-restoration and present-day roughness scenarios. a) Variation of total sediment volume for the downstream reaches identified in Figure 5.2a, from 1850 to 2120, for the two future scenarios. Trajectories from 1850 to 2020 are relative to the MixQ scenario. A Montecarlo fan chart is used to visualize the future trajectories of the parameters after 2020. Each color gradient defines a 20% frequency range of future trajectories. b) Performance of the two future hydrology scenario, for the last timestep of the simulation. The red line represents the performance of the MixQ scenario relative to the final year of the historic horizon (2020). The color gradient indicates the mean yearly flood discharge at the outlet for the future trajectories.*

5.4.2 Forecasting future sediment transport trajectories

As the MixQ scenario is performing the best relative to the majority of the validation criteria, we used this classification method to generate discharge values for 100 future discharge scenarios with which to run forecasting exercises.

The red lines in Figure 5.4a show the projected range of variation of sediment volume and sediment delivery ratio for the downstream reaches as defined in Figure 5.2a. This simulation runs for 100 years from 2020 to 2120. Type 4 reaches provide little further insight on the system evolution because they are largely already depleted of sediment. However, for the lowland plain reaches, it is forecasted that the trend of sediment delivery from upstream will persist into the future, as any remaining material from upstream is delivered. However, a noticeable increase in sediment delivery only occurs in section D. Sections E to F experience a remarkable lack of sediment mobilization as all material is retained and stored in section D. Over the next 100 years a slow increase in sediment delivery ratio is forecast (brown lines in Figure 5.4b). This trend is more pronounced in upstream sections, as sediment from upstream is delivered to section D. While the majority of sediment remains trapped in sections E to F, a small fraction does exit the system, as shown by the very small increase in sediment delivery ratio to the outlet.

The stagnation of the sediment slug that has been simulated is most likely a consequence of the high channel roughness associated with vegetative recovery. To check whether removal of riparian vegetation in the future would affect sediment transport, we ran the same future discharge scenarios, but with channel roughness across the whole river network set to pre-vegetative recovery values (blue lines in Figure 5.4a). The results show an increase in mobility in this scenario, and a subsequent increase in sediment delivery ratio along the lowland reaches and to the basin outlet (blue lines in Figure 5.4b).

5.5 Discussion

5.5.1 Reconstruction of historical sediment storage and reworking

The model outputs show that D-CASCADE is able to reproduce historical morphological changes in the Bega River network and reconstruct reach (dis)connectivity roles with suitable accuracy. By defining pre-ES boundary conditions and introducing selected drivers of change in the correct temporal sequence, all simulations reproduce both patterns of lowland channel expansion and valley fill incision and material release (Brooks and Brierley, 1997; Fryirs and Brierley, 2001). In particular, lowland channel expansion is accurately reconstructed both in timing and location. By using different discharge scenarios, we can explore and simulate different sediment transport and

(dis)connectivity patterns that are driven by different sequences of flood magnitude and frequency.

All simulations also correctly reproduce the role that downstream reaches have played in driving the sediment (dis)connectivity of the basin identified by Fryirs and Brierley (2001). Reaches upstream of the confluence with Wolumla Creek (A-C) experience rapid bank erosion and channel expansion after 1850. Moderate channel gradient and limited overbank flooding facilitates the transport of newly released sediment downstream. After the initialized sediment deposits have been eroded around 1900, these sections switch to transfer zones, where sediment from upstream is quickly conveyed downstream with little or no deposition. The receiving reaches along the lowland plain (D-G) behave like sediment sinks, displaying a high degree of sediment deposition due to low gradients and a high frequency of overbank flooding that limits transport capacity in the channel. Any sediment that does make it to the gorge in section H is quickly delivered to the basin outlet. After 1910, material supplied from the incision of valley fills is deposited mostly in sections D to F. This retention effect is greatly exacerbated by the increase in roughness due to vegetative recovery that has occurred since about 1980, as the decrease in transport capacity in the lowland channels leads to less material being mobilized even during large flooding events. Figure 5.3 shows that the role of the different sections in the sediment connectivity of the basin remains largely the same across the scenarios, with section A, B, C and H as a transfer zone, and D to G as a sediment sink. This pattern is also confirmed by the sharp decrease in sediment delivery ratio at the lowland plain (Figure 5.3b).

For type 4 reaches, all simulations reproduce the high sediment retention rate in valley fill reaches before 1910. However, differences between hydrological scenarios are more evident in the reconstruction of valley fill incision and subsequent sediment release. Only simulations with high discharge for type 4 reaches (HighQ and MixQ) guarantees that most of the material stored in valley fills is mobilized and delivered downstream between 1910 and 2001 (around 92%, in comparison to the 60% ratio of LowQ). Even in these scenarios, sediment release is noticeably slower when compared to the historic reconstruction. The 1944 aerial photos show that most incision had already occurred, and in the same year MixQ simulation presents a rate of erosion of 43%. This is probably due to simplifications introduced when modelling sediment entrainment, which is designed to reproduce bank erosion controlled by the transport capacity. This approach may not be suitable for simulating complex dynamics of channel incision and gullies formation in eroding valley fills. For future applications, new add-on components for modelling gully formations and channel incision could be implemented to better simulate these processes. Similarly, the observed massive channel adjustments likely affected the channel gradient, thus

an add-on design to model channel slope variations due to sediment accretion and entraining could be added in future research.

Overall, the MixQ scenario seems to perform the best for the validation criteria defined. This was expected, as MixQ has the multiple advantage of ensuring frequent high discharge on type 4 reaches that guarantees a high incision rate and sediment supply upstream, while also reducing flood event intensity in the lowlands to produce lower rates of sediment mobilization and a low sediment delivery ratio to the outlet. While more exhaustive information on the past hydrology of the basin may have led to better representation of the historical trajectories, the implementation of hydrological scenarios has still yielded satisfactory results, while also providing insight into the sensitivity of geomorphic processes to changes in flood frequency and intensity.

5.5.2 Future sediment release and transfer

For this system, the model does not suggest that there will be dramatic changes in the role of the reaches in network (dis)connectivity in coming decades, should the current conditions prevail. The lowland plain will continue to function as a sediment sink, storing the remaining sediment delivered from upstream and across sections A to C. By 2120, assuming negligible alterations to present-day riparian vegetation in the lowlands and not accounting for climate change induced hydrological alterations, it is forecasted that the increase in sediment delivery ratio will be higher in the reaches located directly downstream of the Wolumla confluence.

These forecast patterns could indicate that while there may be visible variations in sediment delivery along more upstream sections as the tail of the sediment slug reaches the lowland plain, the function of the lowland plain as a sediment sink seems to intensify further downstream. By sections F and G this trend is so pronounced that these sections appear mostly insensitive to variation of discharge, significantly stalling the amount of material that can escape to the outlet. The high channel roughness brought by vegetative recovery after 1980 traps virtually all sediment slug material in the lowland plain for the foreseeable future. These results also suggest that should vegetation be removed from the riparian or in-channel zones of the lowland plain, either from wildfires or anthropic interventions, it would trigger a new period of sediment slug mobilization and delivery to the estuary.

5.5.3 Opportunities and limitations for further research

The application of D-CASCADE to the Bega River network showcases the potential of a network-scale dynamic and distributed sediment connectivity model to aid in the reconstruction of historical sediment (dis)connectivity pat-

terns and sediment budget trajectories (Schmitt et al., 2016; Gran and Czuba, 2017; Murphy et al., 2019; Beveridge et al., 2020). The new dynamic framework allows for the exploration of more complex sediment connectivity processes and how the interactions between different hydromorphological components that are disaggregated in time and space guide their evolution over time (Czuba, 2018; Wild et al., 2021). This, in turn, makes D-CASCADE a useful instrument for modelling future trends of sediment (dis)connectivity dynamics, that can be used to forecast and quantify possible future alterations in time and space resulting from multiple anthropic disturbances in a system.

Furthermore, the flexible and open-ended structure of the D-CASCADE modelling environment allows for the inclusion of multiple add-ons components and to integrate the large-scale 1D structure of the model with specific tools that can account for more localized and multidimensional processes. Dynamic and two-directional interactions between the D-CASCADE model and additional components guarantees that local changes modelled by add-ons may influence basin-wide (dis)connectivity, and vice-versa (Fryirs, 2013; Bracken et al., 2015). These components may be based on traditional physically-based models, or, as in the case of the Bega River case study, simplified relations based on, and calibrated with, historical observations. This provides the advantage of both reducing complexity and uncertainty while producing results that match observed local conditions and known past morphologies.

The adaptability of D-CASCADE allows us to test hypothesis regarding sediment (dis)connectivity in data-scarce environments where limited data for validation are available. However, modelling complex processes at large spatial and temporal scales does lead to multiple sources of uncertainty, either from the lack of data on boundary conditions, or the modelling parameters necessary to run such large-scale frameworks. Therefore it is important that multiple hypothesis are tested with each simulation (Tangi et al., 2019). Stochastic approaches, like the one used in Schmitt et al. (2018b), and multiple scenario explorations are necessary to test hypothesis on network scale processes and make the results more transparent while "embracing" the uncertainties in modelling sediment (dis)connectivity (Heckmann and Schwanghart, 2013; Shrestha et al., 2021).

The Bega case study offered a unique opportunity to test D-CASCADE, given that so much was already known about the evolution of the rivers and the impact of post-ES disturbance on the morphology of the system over a 170+ year timeframe (Brooks and Brierley, 1997; Fryirs and Brierley, 1998, 1999, 2001; Brierley and Fryirs, 1998; Brierley et al., 1999; Brierley and Fryirs, 2000) . This meant that both the boundary conditions and validation parameters could be readily identified and used in the modelling. Despite this, there are still assumptions built into the simulations. Work is needed to establish appropriate discharge estimates to run in a place where the length of record is short and

patchy. However, the Bega study did allow us to explore the extent to which flows of different magnitude influence different sediment delivery processes and the performance of the model in validation (Frasson et al., 2019). Other complexities include the definition of both sediment transport capacity and sediment velocity and how this can alter spatial and temporal patterns of sediment (dis)connectivity. Moreover, future studies could differentiate between deposition in the channel and on floodplains, by modelling two different sediment layer structures for each reach that store sediment independently, while interacting and exchanging materials to reproduce channel-floodplain interactions (Beveridge et al., 2020; Gilbert and Wilcox, 2020).

The simple formulation of sediment velocity, while already used in other distributed sediment models (Czuba et al., 2017; Czuba, 2018; Murphy et al., 2019), has never been explored exhaustively. Given the importance of this parameter for the representation of the movement of sediment volumes, and its inherit complexity and dependence on multiple hydromorphological features (Ferguson et al., 2015; Gran and Czuba, 2017), further studies on this parameter and how to derive it are necessary. Finally, there is work to be done on evaluating the effectiveness of different sediment transport formula at producing sensible and realistic results, particularly if forecasting work is being undertaken and used for river management decision-making.

5.6 Conclusion

This chapter showcases the first application of the D-CASCADE modelling framework, and demonstrate its potential for large, scale dynamic modelling of sediment delivery and transport to reconstruct the past morphological history of the river network and indicate future pathways under different basin evolution scenarios.

D-CASCADE model successfully reproduced the timing and extent of major morphological processes caused by anthropic disturbance of rivers in the Bega valley, NSW Australia, which included channel expansion, sediment release from upland valley fills and sediment slug formation along the lowland plain. The sediment transport pathways generated by the model generally match the historical reconstruction of sediment supply and delivery ratio. Future trajectories of sediment transport have been conducted to forecast how this system may operate into the future. The data and codes used in this chapter are available at https://doi.org/10.5281/zenodo.5067940.

Appendix A

In this appendix, we provide more detailed information on the techniques used in the model to generate hydrological scenarios (A.1) and on the functioning and integration of the add-ons component in the model (A.2) in chapter 5.

Appendix A.1 includes the description of the techniques used to reconstruct the flood hydrological record for the historic simulation for each network reach, as well as to generate future hydrological scenarios for the future (dis)connectivity trajectories analysis.

Appendix A.2 provides information on the channel expansion and overbank flooding add-ons components included in the framework for the simulation of network features alterations brought by sediment delivery and erosion.

A.1 Hydrology reconstruction

The definition of the hydrology for the historical simulation in D-CASCADE requires information of water discharge in each reach for each daily timestep. Given the hydrological regime of the Bega river network, which is characterized by long periods of drought alternated by intermitted flood events where most of the sediment transport occurs, we chose to simulate only the daily timesteps when historic flood events with a 1-year RP or more occurred, assuming sediment transport to be nil or negligible otherwise.

The only complete historic flood record extending back to the 1850's is a stage height dataset located at the North Bega gauge near Bega township (Figure A.1a). This gauge did not start recording discharge until 1997. To produce discharge data for all reaches in the network, we first 1) correlated the recorded stage heights at North Bega with the discharge and return period (RP) of flow recorded at the upstream Morans Crossing gauging station where discharge data is available from 1942. An exponential law ($R^2 = 0.46$, Figure A.1b) was used. This correlation was then used 2) to calculate for each flood in the height record a discharge and RP. We then assumed that each flood event has the same RP for all reaches. We then 3) determined for each reach the discharge for 1-, 2-, 5-, 10-, 20-, 50-, 100-year flows, using the dataset employed by (Fryirs and

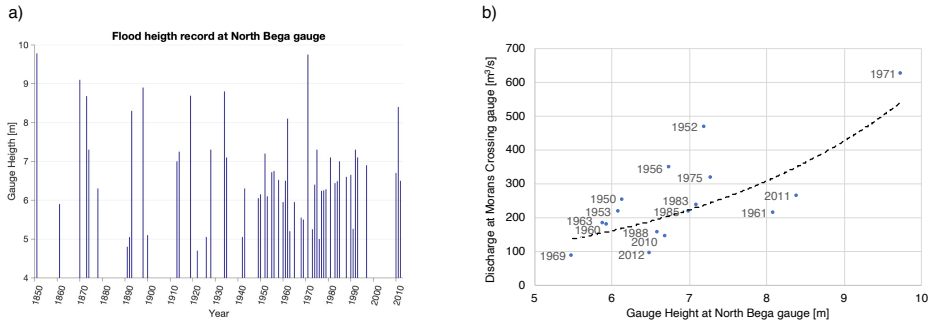

Figure A.1: *a) Flood height record at North Bega gauge from 1850 to 2012; b) correlation between recognizable flood discharge data from Morans Crossing gauge and flood height from North Bega gauge, with exponential interpolation curve* ($R^2 = 0.46$).

Brierley, 2001). That dataset was generated using the Australian Rainfall and Runoff (ARR) Rational method hydraulic model (Pilgrim et al., 1987) Finally, 4) we reconstructed the historic flood discharge for all reaches by attributing to the RP found in step 2) to the reach-specific RP and discharge obtained in step 3).

The flood height record shows a lack of small to medium floods until 1940. This inconsistency is also verified by the difference in frequency of 1y to 5y RP before and after 1942. To account for this, 1y, 2y and 5y RP floods are added randomly in the period from 1850 to 1942, so that the frequency of floods matches the period after 1942. Given the high frequency and relatively low discharge of minor floods, this randomness is not expected to add significant uncertainty to the model results. In total, 168 daily timesteps corresponding to floods higher then 1y RP have been identified for the simulation horizon.

To account for the large uncertainty in the reconstruction of the hydrology, we defined four different scenarios for discharge that were designed to cover a wide range of possible discharge conditions. The scenarios are differentiated by how the RP for each flood is associated to a class of discharge in step 4). In the Medium discharge scenario (MedQ) the discharge is attributed according to the closest RP class to the historic RP, e.g., a flood with 30y RP is attributed 20y RP discharge data series. In the High discharge scenario (HighQ) and Low discharge scenario (LowQ) the discharge is attributed according to the highest, or lowest, respectively, RP class between the two closest to the historic RP, e.g., a flood with 30y RP is attributed a 50y RP discharge in HighQ, a 20y RP in LowQ. Finally, Mixed discharge scenario (MixQ) is a scenario designed to increase sediment erosion and release in the type 4 reaches. Here, discharge is attributed to

Return Period	Discharge scenario HighQ	MedQ	LowQ	MixQ (type 4)	MixQ (others)
1	0	50	84	0	84
2	88	73	56	88	56
5	51	25	13	51	13
10	12	8	4	12	4
20	4	4	8	4	8
50	8	6	2	8	2
100	3	2	1	3	1

Table A.1: *Number of flood events in each discharge scenario for the modelling horizon 1850-2020, divided for return period (RP).*

the highest RP class for type 4 reaches and the lowest for all other reaches. Table A.1 shows the number of flood events for RP in each of these scenarios.

To explore future sediment transport trajectories in the network, we generated 100 scenarios lasting 50 years each, assuming a maximum of one flood event per year. Random RPs of floods are selected from a yearly probability distribution extracted from the Morans Crossing gauging station that also includes years without flood. Then, each RP is classified into a RP class, or as a no-flood year, according to one of the classification methods used in the scenario generation. Finally, discharge data for each timestep are extracted for each reach using the value from the ARR model, or considered nil for no-flood timesteps.

A.2 Add-ons components

Channel expansion is simulated by correlating the erosion of the reach sediment budget with the increase in channel width. The difference between pre-ES and present-day channel width is added to the original width proportionally to the decrease of the original sediment deposit, with the formula:

$$W_t = W_{preES} + \frac{(1 - (V^{(i)}_{d,i,preES}) - V^{(i)}_{d,i,t})}{(V^{(i)}_{d,i,preES})}(W_{present} - W_{preES})$$

Where W_{preES} and $W_{present}$ are the channel width of reach i before and after channel expansion, respectively, as observed by field data and historic reconstructions. $V^{(i)}_{d,i,t}$ is the portion of the deposit layer $V_{d,i,t}$ composed by the volume $V^{(i)}_{d,i,preES}$ initialized in the reach at the start of the simulation. With this formulation, only erosion of the original sediment layer triggers channel

expansion. The formula also implies that, when energy for sediment erosion is available, bank erosion is prioritized with respect to bed erosion, i.e., erosion triggers widening of the channel as observed historically. Thus, the sediment layer $V_{d,i,t}^{(i)}$ is always prioritized while filling the active layer not occupied by the incoming cascades (step c of Figure 4.2). As $V_{d,i,t}^{(i)}$ can only decrease with time as sediment is delivered downstream, channel expansion is irreversible.

During large flood events, part of the flow and discharge may go overbank, and thus reduce the potential for sediment entrainment on the channel bed. For each reach, we can estimate which RP class leads to overbank flooding by comparing channel width with flooded width for each RP class, derived from flood risk evaluations of the basin. If the flow causes overbank flooding, the model limits the volume of sediment added to the active layer from the deposit layer. This volume is defined by the transport capacity relative to the discharge of the highest RP class not associated with overbanking. This step is performed before defining the mobilized sediment volume (between step b and c in Figure 4.2). However, the model still uses the original discharge associated to overbanking to estimate both the transport capacity used to define the mobilized sediment volumes (step c in Figure 4.2) and the sediment velocity in equation 4.6. In this way, the model limits the potential for bed erosion during overbank flood events, while ensuring that the sediment budget for transport and the sediment velocity still reflects the actual flooding event.

6

Sediment management in reservoirs operational strategy

River sediment (dis)connectivity plays a fundamental role in the conservation of fluvial ecosystems and the goods and services they provide for human use. Dams profoundly alter the natural processes of sediment delivery and transport, and due to these processes' interconnected nature, the impacts of these infrastructures may be displaced in time and space and not limited to the construction site. This chapter presents a novel application of the D-CASCADE model to assess the impacts of reservoirs and their management strategies on river sediment connectivity. The model is applied to the 3S river system, a tributary of the Mekong river, which is interested in large-scale dam development plans. First, reach sediment budget, and network sediment yield for different sediment sizes are estimated with D-CASCADE for the no-dams scenario, and the results are validated with previous estimates from the literature. Then, the effect of reservoir management is explored with D-CASCADE by including four downstream dams on the river network and assessing daily sediment transport and delivery with specific dam release strategies. Planned reservoir configuration would reduce sediment yield to the Mekong river by 50%. Reservoirs features (i.e., Volume, area, height, and sediment deposit) are dynamically modelled via a compartment representation. Finally, sediment management techniques are introduced via the inclusion of periodic drawdown flushing in the simulation.

This chapter is developed based on: Tangi, M., Bizzi, S., and Castelletti, A. (2022). Sediment connectivity conservation in the Mekong via strategic reservoirs water and sediment management. (In preparation).

6.1 Introduction

Worldwide, the construction of dams on river systems is progressing at a fast pace, in particular in developing areas where the hydropower potential is still untapped (Imhof and Lanza, 2012; Zarfl et al., 2015). Major river systems, like the Irrawaddy (Schmitt et al., 2021) and Amazon (Latrubesse et al., 2017; Arias et al., 2020) are now interested in large scale dam development plans, with hundreds of barriers of various sizes planned on the fluvial network. A significant example of this development is the Mekong river, one of major fluvial system in the world. On the Lower Mekong basin alone, 43 reservoirs have been built over the last 20 years, with other 104 planned or in construction (MRC (Mekong River Commission), 2014a)

The construction of reservoirs breaks the natural river connectivity patterns which characterize the movement of water, sediments, and organisms (Ligon et al., 1995; Kondolf, 2000). In particular, sediment movement is halted by the low hydraulic forces inside the reservoirs, resulting in sediment sequestration to the main stream. This so-called trapping potential of reservoirs varies according to the dam features, e.g., location, size, impoundment volume and surface, and the type of sediment considered. In general, however, the presence of dams typically leads to material deposition in the reservoir(Vörösmarty et al., 2003) and sediment starvation downstream (Kondolf, 1997). The first reduces reservoir total storing capacity, and in turn, energy production, with losses up to 30% of annual costs (Palmieri et al., 2001; Ansar et al., 2014), and it may decrease efficiency or even damage hydroelectric equipment and pose safety hazards Annandale (2013); Wisser et al. (2013). The second impact is more insidious since it is not constrained to the reservoir's boundaries, but it has the potential to affect the river system as a whole, with impact displaced in time and space from the dam site. The sediment sequestration from the water stream constitutes an element of strong disconnectivity in the basin-scale sediment transport network that could have significant detrimental consequences on the fluvial hydromorphological processes (Sholtes and Doyle, 2011; Bizzi et al., 2015; Wyżga et al., 2016), riverine ecosystems (Wild and Loucks, 2012a; Gilvear et al., 2013) and human infrastructures and livelihood (Kondolf, 1997).

Given the distributed and connected nature of sediment delivery processes, the presence of series of dams on the same system could lead to cumulative unfavorable effects which may surpass the sum of the individual impacts (World Commission on Dams, 2000; Ziv et al., 2012; Kondolf et al., 2014a). This is especially valid in systems where the number of dams and barriers on a river number by the hundreds. Nevertheless, few attempts have been made to assess basin-wide negative externalities on sediment connectivity of multi-dams systems (Kondolf et al., 2014b; Jager et al., 2015; Schmitt et al., 2019). The reason for that can be found in both the inherent complexity of quantifying the

effects, distributed in time and space, of disruptions on such large-scale properties like river sediment (dis)connectivity (Bizzi et al., 2012), and the difficulties in identifying a complete and comprehensive planning and management strategy agreed upon by all the stakeholders invested in the project, whether they be private individual, companies, groups of interest and sovereign States. Thus, risk assessment analysis on dam projects focuses in the overwhelming majority of cases on single projects, ignoring basin-scale and cumulative effects (Jager and Smith, 2008; Orr et al., 2012).

For the Mekong river, while the cumulative impact of these project is largely unknown, a great number of the study indicates risks of major alterations in the hydrology Lauri et al. (2012), morphology Kummu et al. (2010); Kondolf et al. (2014b) and ecology (Burnhill, 2009; Ziv et al., 2012) of the river system, which threatens the productivity of the river and the livelihood of the local population. Blocking of fish migratory pathways is likely to decrease the abundance of many fish species that constitute a primary source of protein in their diet of approximately 60 million people living in the Mekong basin (Hortle, 2009). The decrease in sand yield to the delta, combined with rising sea level and sand mining on the river (Hackney et al., 2020), threatens the survival of the Mekong delta itself, home to around 17 million peoples, which could subside below ocean levels by the end of the century (Syvitski et al., 2009; Schmitt et al., 2017).

A variety of sediment management strategies can be implemented in reservoirs to preserve reservoir capacity or combat sediment depletion downstream, which have been proven effective in a number of case studies around the world (Vischer, 1997; Kokubo, 1997; Jansson and Erlingsson, 2000; Stevens, 2000; Sumi, 2008; Wang et al., 2018). An in-depth look at these techniques is provided in Section 1.1. However, these techniques are not implemented broadly nor consistently in reservoirs, possibly due to the difficulties in comparing the short term costs of these approaches versus the long term consequences of sediment (dis)connectivity disruptions or the specific design requirements needed for an effective implementation (Kantoush and Sumi, 2010; Kondolf et al., 2014a). On the Mekong, there is no recorded evidences of planned sediment management strategies in the reservoirs, as no dams have currently been constructed or designed with any kind of sediment pass or bottom outlet, nor any plan have been devised to retrofit existing ones where possible(Kondolf et al., 2014b).

Even in the rare case of documented applications of sediment management approaches, the research focuses the benefits on single reservoirs, ignoring the network-scale implications of sediment (dis)connectivity disruption caused by the reservoir water and sediment management strategies (Kondolf et al., 2014a). The complexity of the problem increases further when considering multiple dams on a single river network. In this case, the dams siting, their design features, the timing and frequency of the application of sediment management

techniques, and the hydromorphological characteristics of the river network all concur in creating a complex and interconnected web of causes and effects which may lead to unforeseen impact on the river network and on the efficacy of the management techniques themselves. Thus, coordination between dams when planning comprehensive sediment management strategies on the same river is vital for the success of said operations (Kondolf et al., 2014a).

In this chapter, we present a novel application of the D-CASCADE modelling framework on the 3S river network, a tributary system of the Mekong composed of the Se Kong, Se San and Sre Pok rivers, to quantify the sediment depletion to the outlet caused by the combined trapping of a series of dams located in the lower sections of the system and evaluate the effect of coordinated reservoir flushing on the basin cumulative sediment yield. The original CASCADE model, on which D-CASCADE is based, has already been applied on the 3S case study (Schmitt et al., 2018a,b), to quantify network sediment transport and delivery under different dam development scenarios, using an optimization-based frameworks for strategic sequencing of dam development to identify trade-offs between hydropower production and sediment connectivity conservation. However, the static structure of the CASCADE framework prevents its application for evaluating the spatiotemporal effects of dynamic water management strategies. The dynamic structure of the D-CASCADE model prevents this issue and hence is much more suited to assess spatiotemporal variations of sediment delivery patterns bought by both the siting and the management of multiple reservoirs on a rivet network, including the effect of different sediment management techniques. Multiple grain size classes ranging from gravel to silt are considered in the analysis, to analyse the effects of reservoirs on the composition of the sediment load.

This study represents a never before seen application of a distributed sediment transport model for the quantification on impacts on sediment connectivity brought not only by the inclusion of dams on the network (as was the case in Schmitt et al. (2018a, 2019)), but by the dynamic and time-varying water and sediment management strategies of multiple reservoirs on a single river network. This research open up possibility for integrating D-CASCADE in optimization-based, multi-objectives strategic planning and management frameworks, to extract sediment connectivity indicators and identify trade-offs and synergies between multiple objectives for competing dam planning and management portfolios.

6.2 Case study

The river network composed of the Se Kong, Se San and Sre Pok rivers, often referred to as 3S, is one of the major tributaries of the Mekong river. The

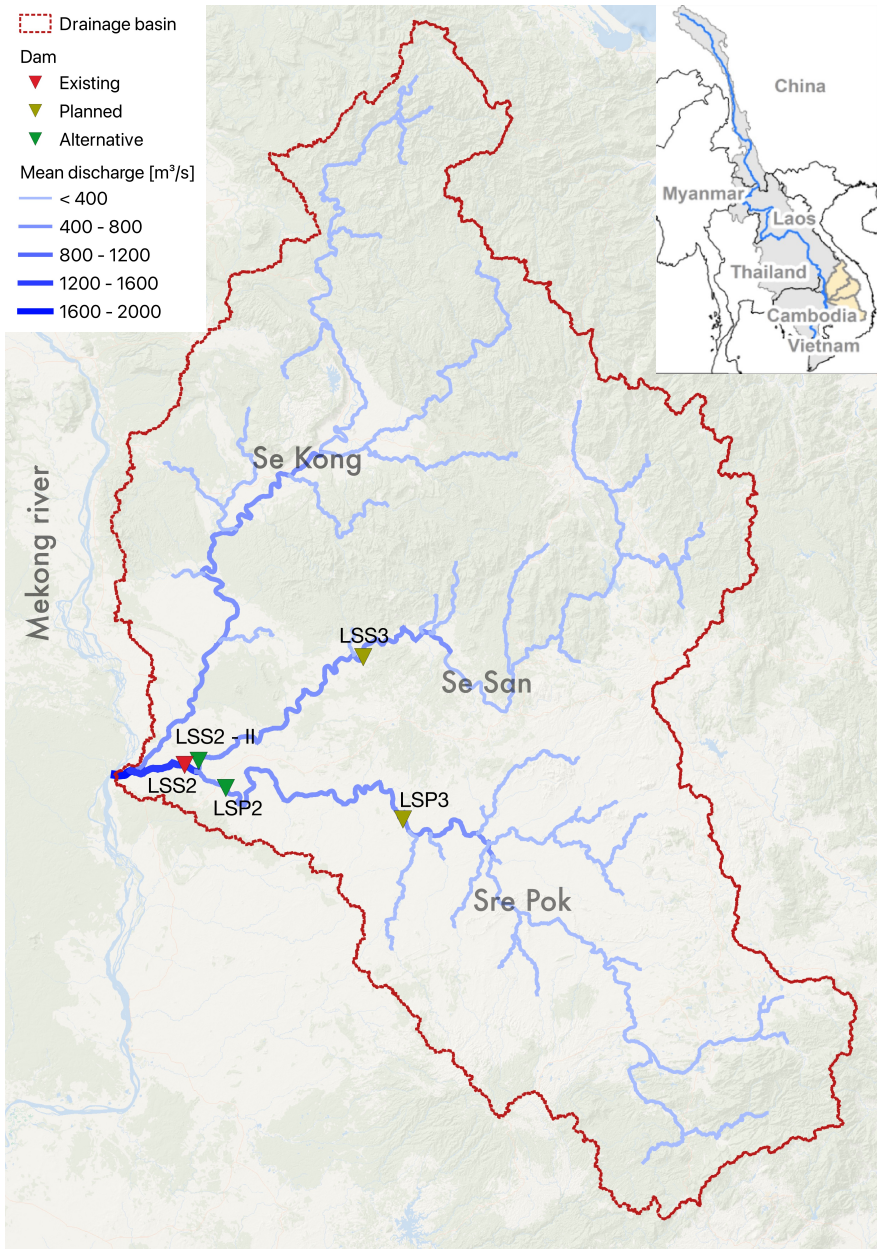

Figure 6.1: *The 3S river network as represented in the D-CASCADE modelling framework, including reservoir location and average reach water discharge. The study focuses on the five reservoirs shown in picture: the Lower Se San dam (LSS2) already constructed, the planned LSS3 and LSP3 dams, and the alterative configuration for the LSS2 dam proposed by Annandale (2013) consisting in the two dam LSS2-II and LSP2.*

three rivers converge together just before joining the main river near the city of Strung Treng, at roughly 500 Km upstream the Mekong delta (Figure 6.1). The 3S river system drains 82,500 km^2 across Vietnam, Laos, and Cambodia (Se Kong: 30,400 km^2; Se San: 20,000 km^2; and Sre Pok: 32,000 km^2). The three systems combined contribute to 17%-20% of the annual discharge of the Mekong river (Sarkkula et al., 2010a). The climate of the Lower Mekong is charcterized as hot and humid, with the annual monsoon season occurring from mid-May to mid-October. The annual hydrological regime is controlled by monsoon-induced floods, which carry up to 75% of the total annual flow (Piman et al., 2016). This distinct seasonality also characterizes the hydromorphological and biological cycles of the river, with sediment transport processes and life-cycle, grow rhythm, and migration of fluvial species synchronizing with the seasonal hydrological variations (Piman et al., 2013).

While direct measurement of sediment yield and grain size distribution are not available on the 3S, empiric evidence based on field data on the Lower Mekong characterize the 3S basin as one of the principal contributors of sediment to the main river, especially sand, which plays a vital role in the morphodynamic stability of the river and its delta (Bravard et al., 2014; Kondolf et al., 2014b; Piman et al., 2016). Wild and Loucks (2014) estimates total sediment yield from the 3S to be around 25 Mt/yr, based on the residuals of the sediment budgets of the Mekong estimated before and after the 3S confluence (Koehnken, 2012). Kondolf et al. (2014b) delineated nine geomorphic provinces, based on rock type, uplift, land-use, and available sediment transport data, and attributed to each province an annual sediment yield (t km^{-2} y^{-1}). The 3S system is located primarily on the Tertiary Volcanic Plateau (TVP) province (290 t km^{-2} y^{-1}), with part of the upper Se Kong and Se San touching the Kon Tum Massif (KTM) province (280 t km^{-2} y^{-1}). These estimates put the total sediment yield of the 3S system to around 24 Mt/yr. However, by its own design, this method of predicting sediment yield ignores conveyance losses due to sink areas and choke points. Other models (Carling, 2009; Sarkkula et al., 2010b) used as a baseline by the Mekong River Commission (Koehnken, 2014), lower the estimated sediment yield to 16 -18 Mt/yr, based on 1990 – 2000 modelling results.

Rapid development in the counties sharing the Mekong river basin meant growing interest in exploiting the estimated 235,000 GWh/yr of the hydroelectric potential offered by the river and its tributaries. Dam construction is progressing at a fast pace all through the basin, driven by energy demand (International Energy Agency, 2015). The 3S river system is also interested in this large-scale dam development effort, with 20 large dams already built or under construction and around 20 dams planned on the network. At the moment, the majority of the reservoirs are located on the upper Se San and Sre Pok. (Schmitt et al., 2018a) identified the impacts of sediment delivery of the

Lower Se Kong, Lower Se San 3 (LSS3) , Lower Sre Pok 3 (LSP3), and Lower Se San 2 (LSS2) dams (shown in Figure 6.1) to be especially critical due to their downstream location and high trapping potential. In particular, the LSS2 dam is shown to have a disproportionate impact on suspended sediment transport to the Mekong compared to its hydropower potential.

The impact of dam construction on the total sediment yield delivered to the Mekong is debated. Koehnken (2014) estimated sediment delivery to be around 8-11 Mt/yr based on 2009-2013 measurement with 16 active hydropower impoundments, mostly located upstream the Se San and Sre Pok. However, the completion of the LSS2 dam, operative from 2018, is bound to reduce the sediment yield further. Schmitt et al. (2018a) estimated a 97% reduction in the 3S sand sediment budget if all planned dams are constructed.

The reduction in sediment delivery form the 3S system, especially sand, is especially significant in our case study, as it would contribute to the cumulative sand starvation which currently threatens the Mekong Delta. Thus, in our analysis, we focused primarily on changes in the quantity and type of material delivered to the network outlet as indicators of sediment connectivity alteration brought by competing dam development scenarios.

6.3 Methods

To achieve our research objectives, we applied the D-CASCADE model as described in chapter 4 to the 3S river system. Given the scope of our analysis and the lack of available data on the morphological changes in the river network, we characterized all reach morphological features as static. Channel width, depth, and velocity are, however modelled in flooded reaches inside dams' impoundment, thanks to a specific add-ons component for dynamic reservoir modelling presented in section 6.3.3 and Appendix B).

To derive estimates of daily network sediment yield for the 3S river system under downstream dam development scenarios, and evaluate the effects of drawdown flushing on sediment trapping and delivery, a 4-step methodology was implemented:

1. Initialization: we defined the direct graph representing the 3S system, and characterize each reach static and dynamic morphological features using available information on channel morphology. The daily hydrological database is instead derived from the VIC hydrological model(Dang et al., 2020) for the period 1995-2005. The specific parameters for the measurement of sediment transport rates and velocity. Sediment yields from the watershed to the network are extracted from large scale morphological estimates (Kondolf et al., 2014b);

2. Sediment budget definition: D-CASCADE is applied on the entire 3S river network without reservoirs, to quantify reach sediment budgets and transport rates for the unimpeded river system. The model outputs are validated using the estimates of average annual sediment yield available from literature. A sensitivity analysis is performed on the grain size distribution of the catchment sediment yield;

3. Reservoir impact assessment: D-CASCADE is applied on the 3S for different scenarios of dam development. Reservoirs are integrated on the modelling framework via specific add-ons components. To decrease computational time, the model run is performed on a smaller river network which only includes reaches affected by the reservoirs placement, i.e. flooded sections and reaches downstream the dams. Sediment input to the reduced network is derived from the model runs on the unimpeded network;

4. Effects of drawdown flushing on sediment trapping and delivery: Finally, we evaluated the effects on reservoir sediment storage and network sediment yield of repeated and coordinated flushing operations.

6.3.1 Initialization

The 3S river network was extracted from a 90 m void-filled, digital elevation model (Consultative Group on International Agricultural Research, 2008), via the standard extraction algorithm implemented in Topotoolbox (Schwanghart and Kuhn, 2010). The minimum drainage area of the network notes was set to 500 km^2. In total, 463 reaches were extracted averaging 7 km in length. Channel gradient for each reach is consider static and derived from the DEM. Outliers given by grid elevation errors in the DEM were corrected via interpolation. Channel width and roughness coefficient are obtained from the dataset used in Schmitt et al. (2018b,a) for the application of the original CASCADE model on the 3S system.

The daily hydrological record from 1995 to 2005 was obtained via the grid-based VIC hydrological model (Dang et al., 2020). Reaches are attributed to a single cell in the VIC grid, and thus a single hydrological series, while matching errors at the confluences are corrected manually.

Sediment supply from the watershed to the network, which constitutes the only sediment source of the model, was derived from distributed annual sediment yield estimates by Kondolf et al. (2014b). The volume delivered to each reach is given by the yield reported for the morphological region encompassing the reach (t km^{-2} y^{-1}), multiplied by the reach direct drainage area to obtain annual sediment yield. Daily sediment delivery is obtained by assuming constant sediment contribution throughout the year, and is represented in the model as

a sediment cascade attributed to the input reach, which is included among the incoming sediment cascades from upstream at the beginning of each timestep.

To consider the entirety of the sediment transport delivery to the Mekong, we defined five different sediment classes in the study, corresponding to gravel, coarse sand, fine sand, coarse silt and fine silt. (-1.5, 0.5, 2.5, 4.5 and 6.5 φ in Krumbein and Aberdeen (1937) logarithmic scale, corresponding to 2.8, 0.71, 0.16, 0.044 and 0.011 mm). These classes are the most representative of the grain size distribution of the sediment transport in the Lower Mekong river, as reported by field measurement on the main channel (Koehnken, 2014).

The reach transport capacity is calculated using the Engelund & Hansen equation (Engelund and Hansen, 1967) for total load (i.e., both suspended and bed load). As this formula returns the total transport capacity, we obtained fractional transport rates for the five classes considered via the Bed Material Fraction (BMF) approach (Molinas and Wu, 2000) described in section 2.2.1. Given the wide range of classes considered in the simulation, we applied the sediment velocity equation described in eq 4.7 in section 4.4.3, which returns different sediment movement rates according to the reach features and the grain size considered. Other parameters for the quantification of the mobilized sediment load are defined as follows: both active layer thickness d_a (see eq. 4.3) and vertical length for sediment transport H_a (see eq. 4.6) are kept constant and set equal to 1 m and 0.1 m respectively (Czuba, 2018). Sediment porosity ϕ is set to 0.4 (Wu and Wang, 2006). To avoid excessive computing time and data storage, the numerical precision used ot describe sediment volumes in the network is set equal to 10^{-1} m^3.

6.3.2 Sediment budget definition

To assess the spatiotemporal input of dam inclusion and management on the 3S, first we need to reconstruct reach sediment budgets and sediment delivery for the pristine, unimpeded river network. Multiple D-CASCADE runs are performed to account for the uncertainty in the GSD of the sediment yield delivered from the watershed. The outputs of these simulations are then used to validate the modelled catchment sediment yield with available field data and provide boundary conditions for the subsequent D-CASCADE simulations with the inclusion of reservoirs.

The estimation of sediment yield by Kondolf et al. (2014b) does not include values of grain size distribution for the sediment input. Therefore, we run multiple CASCADE simulation over 3 years with different initializations of D50 for the external sediment cascades. Given the lack of data on the river network, we assumed all external sediment inputs to have the same sediment class distribution. The GSD to the chosen D50 is obtained via interpolation using the cumulative Rosin distribution function (Shih and Komar, 1990) (eq 3.6). The

Reservoir and dam features	LSS2	LSS3	LSP3	LSS2-II	LSP2
Name	Lower Se San 2	Lower Se San 3	Lower Sre Pok 3	Lower Se San 2 - II	Lower Sre Pok 2
Full Supply Level (m)	26.3	12.2	13.2	16.3	13.6
Reservoir storage capacity at FSL (Mm^3)	1,793	231.5	204	136.9	258.6
Design Discharge (m^3/s)	2,119	864	1,000	966	1,123
Catchment Area (Km^2)	51,850	16,200	27,750	19,550	31,800
Mean annual unregulated inflow rate (m^3/s)	452	789	647	1382	527

Table 6.1: *Reservoir and Dam Features at currently built or planned LSS2, LSS3 and LSP3 dams (MRC (Mekong River Commission), 2014b), as well as the proposed alternatives to the LSS2 dam: LSS2-II and LSP2 (Annandale, 2013; Wild and Loucks, 2014).*

distribution spread is kept constant and equal to 0.8 for all simulations, while the D50 of the sediment yield is simulated for 5 scenarios (1 mm, 0.5 mm, 0.1 mm, 0.05 mm, 0.01 mm). Regardless of the sediment distribution, around 24 Mt/yr of material is delivered to the network from the watershed.

The simulation are run for 3 years, from 1995 to 1998, with the first year used for initialization. To reduce computational time, we assumed sediment mobilization and transport to be nil in the whole network when the average daily discharge at the outlet is lower then the 20^{th} percentile of the average annual discharge in the reach, measured in the period 1995-2005. This hypothesis is considered reasonable as these timestep falls during the dry period, which correspond to very low water discharge, and therefore sediment transport, in the Lower Mekong river basin (Koehnken, 2014). The scenario whose outputs are most coherent with the previous knowledge of the system is then selected, and run for a second time for the entirety of the time horizon considered (1995-2005).

6.3.3 Reservoir impact assessment

Once sediment transport and delivery were assessed in the pristine, no-dams scenario, D-CASCADE was again applied on the 3S to predict the impacts on network sediment transport and delivery of series of reservoir on the main tributaries and their management strategies. The analysis in this chapter focuses on 5 dams on the lower 3S system, whose design features are reported in Table 6.1. One of these reservoir (LSS2) is already build and operative sine 2018, two (LSS3 and LSP3) are currently planned without bottom outlet. According to the preliminary sediment connectivity alteration assessment by Schmitt et al. (2018a), these dams would greatly contribute to the reduction of the network sediment yield to the outlet, due to their downstream position on the main

channels and their large impoundment volume and trapping efficiency. The other two reservoirs (LSS2-II and LSP2) were proposed by Annandale (2013) as an alternative to LSS2 to reduce sediment trapping and allow for feasible drawdown flushing. The original configuration by Annandale (2013) featured a third dam (Se San Upstream 1 - US1) which was located in close proximity to LSS3. As data on the actual design of the planned LSS3 and LSP3 dam are scarce and conflicting, we included the LSS3 dam with the design features of the proposed alternative US1. The LSP3 dams is defined using data from the Open Development Mekong database, which indicates a reservoir with relative low capacity compared to other databases. While Schmitt et al. (2018a) indicated the Lower Se Kong dam to be especially critical, references to the dam do not appear on the recent MRC reports (MRC (Mekong River Commission), 2019). Thus, in all the contemplated scenarios, the Se Kong river is devoided of any barrier.

To integrate the dynamic representation of reservoir features and dam operational strategies, we employ four novel add-ons components in the D-CASCADE modelling framework (More detail are available in Appendix B):

- *The dynamic reservoir storage modelling add-on* calculates the hydromorphological features, i.e. channel gradient, width, water velocity and depth, of the flooded or partially flooded reaches falling inside the reservoir impoundment, and traces their evolution thought time as the reservoir storage volume varies;

- *the reservoir management add-on* simulates reservoir release strategy which determines the reservoir release in each timestep. In this work, we implement the 4 parameter rule curve illustrated in Figure 6.2, which determines for each day of the year the target water level as a linear interpolation between the minimum and maximum target level, given their respective dates on which they should be reached . As the 3S basin hydrology is characterized by a clear distinction between wet and dry season, we set the minimum and maximum target level at respectively 50% and 90% of the FSL at the start of the simulation, and their dates to the start and end of the monsoon season (Mid-May and mid-October). In this way, the reservoir is at its minimum when we expect high inflow rate, and slowly fills up to store the flood volume as much as possible to use for energy production without resorting to the spillways to release excessive input flow (Piman et al., 2013; Wild and Loucks, 2014; Wild et al., 2016);

- *the reservoir sediment trapping add-on* estimates the sediment deposit inside each reservoir in each timestep, as well as the loss in reservoir storage capacity due to continuous sedimentation. In turn, this loss will influence the maximum reservoir volume at full supply level used in the reservoir management add-on to determine dam release;

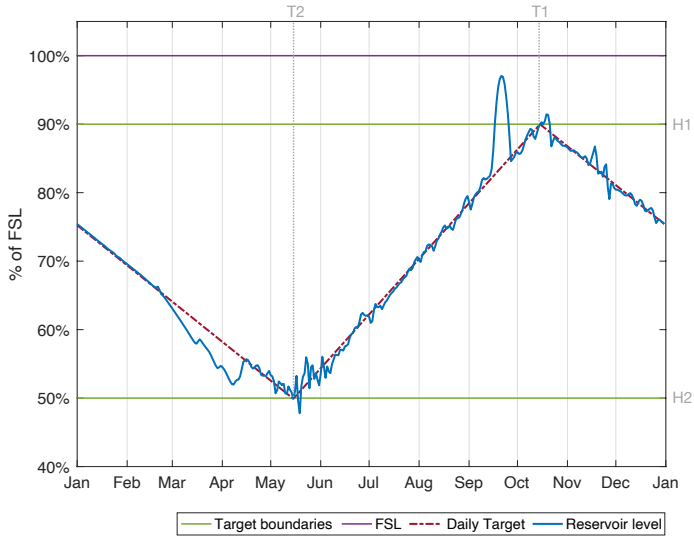

Figure 6.2: *4 parameters release rule curve implemented for the reservoirs in the case study. Each day the rule determines the target water level, based on linear interpolation between the maximum and minimum reservoir level (H1 and H2) and their respective dates (T1 and T2). The target level, in turn determines the target release for the timestep. Reservoir levels refer to the simulated LSS3 reservoir water height across year 1998.*

- *the downstream water discharge add-on*, finally, updates the daily discharge for all reaches downstream the reservoir according to the water release from the dam. In case of reservoir in series, the release of the upstream dam influence the discharge of all reaches until the downstream dam location. Thus, water input to the downstream dam is directly influenced by the release of the upstream dam in the same timestep.

The simulations with reservoirs are initialized as follows: first 1), we select the pristine network sediment transport scenario among the one defined in the previous section 6.3.2 which best mirrors the field knowledge of the sediment delivery from the 3S, and we run it for the entirety of the modelling timeframes (1995-2005), then 2) different scenario of dam development are defined, to explore alternative configurations of dam portfolios. 3) The reduced riven network is then extracted, which includes only the flooded reaches at FSL for all reservoirs in the scenario and all reaches downstream the dams, and the sediment input for each timestep is characterized. For each of the new source reaches of the reduced network, we extract the sediment yielded by their subbasin in each timestep, obtained by the full-network, pristine scenario selected; and characterize it as an additional sediment input to the reach. Finally 4), we

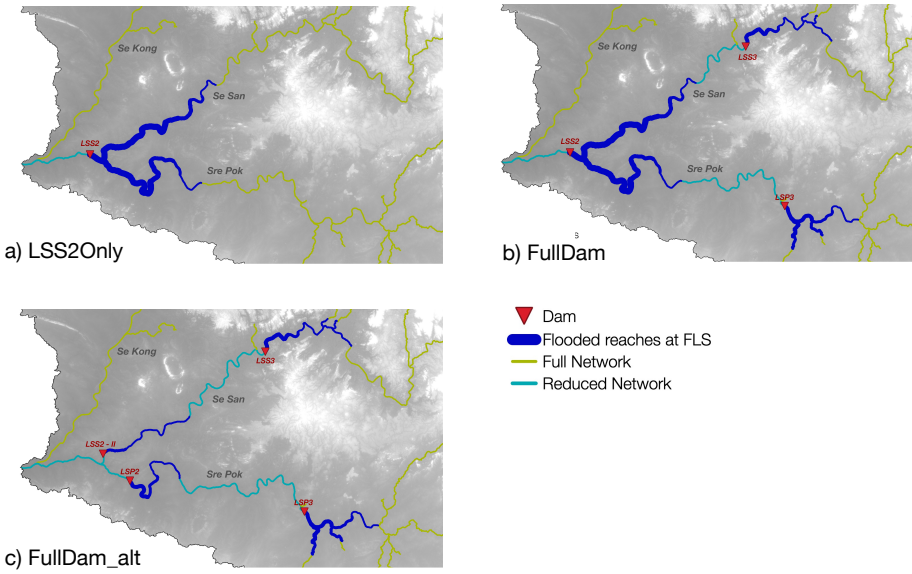

Figure 6.3: *Reduced network extension, dams location and flooded reaches at full supply level for the three dam development scenarios considered in the analysis.*

run D-CASCADE for the different dam portfolios scenarios, and collect distributed data on catchment sediment yields and GSDs, as well as reservoirs water and sediment volumes for each timestep.

In this work, we analyse three dam development scenarios for the 3S river system, focusing solely on the downstream dams listed in Table 6.1:

- **LSS2Only**: this portfolio only include the Lower Se San 2 reservoir, the largest and most downstream dam;
- **FullDam**: this portfolio features all reservoirs currently planned or present on the lower 3S system, i.e. the LSS2, LSS3 and LSP3 dams;
- **FullDam_Alt**: this scenario consider the alternative configuration for the LSS2 dam proposed by Annandale (2013) (LSS2_II, LSP2 and LSS3 reservoirs), as well as the LSP3 dam.

Figure 6.3 displays the reduced network and flooded reaches at full supply level for each of the selected scenarios.

6.3.4 Reservoir sediment management

Given its proven effectiveness in reducing sediment storage in reservoir (Atkinson, 1996; White, 2001; Kondolf et al., 2014a), this study focuses only on drawdown sediment flushing and its effects on reservoirs sediment storage and

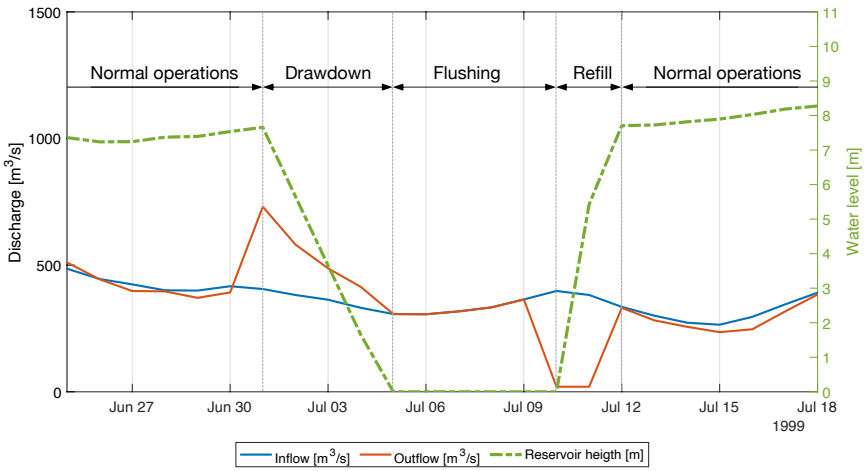

Figure 6.4: *Visualization of a successful drawdown flushing process as simulated in D-CASCADE by the drawdown flushing add-on. The figure refers to a 25-days period during a flushing operation in the LSS3 dam for the simulated year 1999.*

downstream sediment delivery. A standard drawdown flushing operation is composed by three phases:

1. *Drawdown*: the reservoir impoundment is completely emptied using the hydropower and bottom outlets.

2. *Flushing*: Once the basin drainage is completed, flushing operations continue for 5 days: river-like conditions through the reservoir are restored and the free-flow discharge is passed through the now-empty reservoir and out the bottom gates. The hydraulic force of the water flow is used to scourge materials from the reservoir sediment storage.

3. *Refill*: When flushing is completed, the bottom gates are closed and the reservoir level is raised up to the daily target level.

To include drawdown flushing in the modelling framework, a specific add-on have been designed. The component, when activated, modifies the release strategy of the reservoir to accomplish a complete cycle of drawdown flushing. To improve the effectiveness of the flushing operations, the add-ons component includes specific boundaries and parameters, reported. Figure 6.4 presents an example of simulated drawdown flushing operation for the LSS3 dam.

Drawdown is only attempted at specific periods of time in the year. In tropical climates characterized by a high hydrological variability caused by the monsoons, flushing operations during the dry season are not suggested, as the hydraulic forces of the reservoir inflow may be not sufficient to successfully mo-

bilize material in the impoundment and refill the reservoir quickly afterwards as not to lose hydropower production. A high sediment concentration downstream the reservoir during this time window may also disrupt natural biological cycles, as local species have adapted to low sediment delivery during the dry season (Baran and Nasielski, 2011). On the other hand, flushing during the main portion of the wet season would probably be ill advised, as water input may frequently exceeds the design discharge, preventing or slowing downs drawdown operations. Thus, the preferable timing for drawdown flushing is considered the beginning of the wet season (July-August), where incoming discharge should provide enough hydraulic force to erode part of the sediment storage without exceeding the discharge capacity of the bottom outlets (White, 2001; Wild et al., 2016) . To allow for synchronization between flushing operation in series of consecutive reservoirs, the flushing time window is kept the same for all dams. Moreover, drawdown is also facilitated in this period of time, as its corresponds to minimum storage levels in reservoirs, according to the release strategy described in Section 6.3.3.

During the set time window, flushing is initiated if the inflow rate to the reservoir fail into a user-defined range. This boundary is defined to avoid flushing operations during low-flow periods, to maximise sediment entrainment in the reservoir, while avoiding excessive inflow which could surpass the bottom outlet discharge rate. To avoid rapid water level decrease, which would increase the risk of bank failure and landslides in the reservoir (Wild et al., 2016), drawdown rate is limited to 2 m/day. This has the added benefit of ensuring released flow is comparable to standard early-wet season discharges. In case drawdown is not completed after a fixed amount of days, set to 15 days in the simulation, the operation is interrupted for 10 days and then attempted for a second time. This procedure is repeated until drawdown is achieved, or the annual time window for the flushing operations closes.

Once the reservoir is emptied and free-flow is achieved in the impoundment, flushing is continued for a maximum duration of five days. If the inflow exceeds the bottom outlet design discharge, the operation is interrupted and refill starts. In each timestep during drawdown and flushing phases, the morphological features of the once-flooded reaches are updated automatically by the dynamic reservoir storage modelling add-on. When empty, channels regain their original, pre-dam construction characteristics. The quantity of sediment removed in each of the former flooded reaches is determined via standard D-CASCADE operations. The restoration of free-flow hydromorphological conditions in the interested reaches is expected to raise sediment transport capacity and lead to the mobilization of material from the deposit layer.

In the D-CASCADE simulation, we tested the effectiveness of flushing operations with 1-year and 2-years frequency for the FullDam_alt scenarios, whose

Dam	LSS3	LSP3	LSS2-II	LSP2
MRV/MAI	0.016	0.008	0.010	0.010
Flushing time window	July-August	July-August	July-August	July-August
Flushing frequency [year]	1 / 2	1 / 2	1 / 2	1 / 2
Inflow rate range for flushing [m^3/s]	277 - 864	521 - 1,000	327 - 966	630 - 1,123
Maximum drawdown rate [m/day]	2	2	2	2
Flushing duration [days]	5	5	5	5
Maximum drawdown duration [days]	15	15	15	15

Table 6.2: *Flushing parameters for the reservoir in the FullDam_alt scenario (LSS3, LSP3, LSS2-II, LSP2). When available, flushing parameters are derived from Wild et al. (2016). MRV/MAI indicates the total reservoir capacity to mean annual inflow ratio, which according to Kondolf et al. (2014b) must not exceed 0.04 for drawdown flushing to be successful.*

portfolio includes all reservoirs with small enough ratio of reservoir capacity to mean annual flow to allow for successful flushing. As reported in 6.2, all select reservoir do not exceed the 0.04 ratio threshold set by Kondolf et al. (2014b). We assume all these dams to be equipped with bottom outlets, whose maximum discharge capacity is hypothesised as identical to the design discharge. Table 6.2 also reports the values of the flushing parameters for the simulations. The lower boundary of the inflow range to trigger flushing is set ot the mean annual inflow rate to the reservoir, while the upper boundary is the dam design discharge.

6.4 Results

6.4.1 3S system sediment budgets estimation

Figure 6.5 shows the average annual sediment yield and the average median grain size for the five simulation scenarios, as well as the GSD for the five grain classes considered. The simulations run from 1995 to 1998. Given the lag between catchment sediment delivery to the network and sediment transport to the outlet, the first year was employed for model initialization and, therefore, not considered for the results.

As expected, the results show an evident rise in network sediment yield as the input D50 decreases, as fine sediment sizes are transported faster and at higher rates, while coarser grain classes tend to be trapped in deposit zones where entrainment capacity is low. In the scenario with finer input D50 (0.01 mm), the sediment yield at the outlet (22.9 Mt/yr) approaches the total sediment input to the system (24 Mt/yr), meaning virtually the entirety of the river network reaches acts like transit zones, letting sediment pass through with minimal sediment retention in deposit zones (Figure 6.5 a).

All simulations show distinct sediment fining patterns along the network

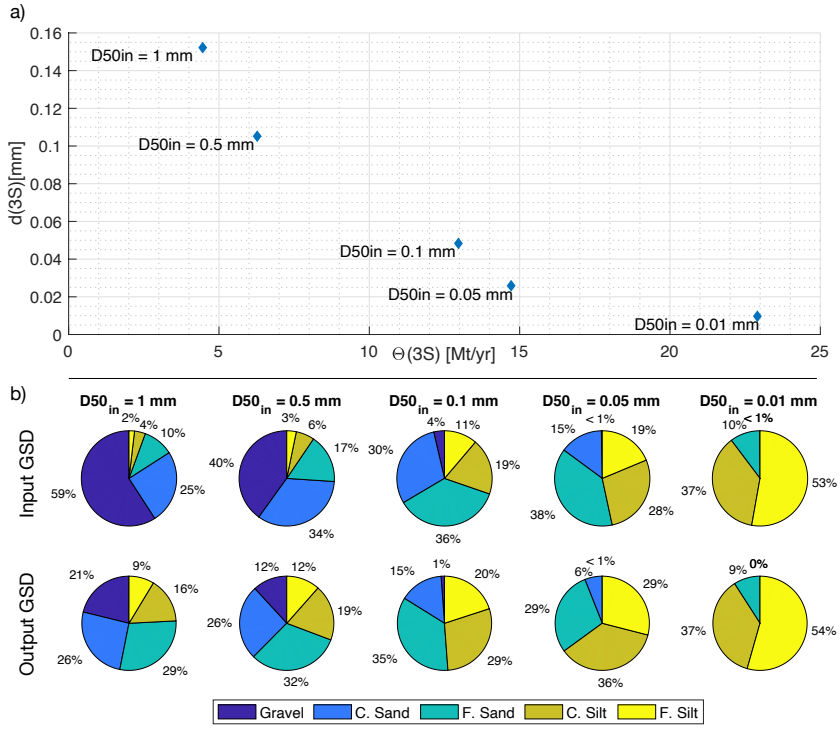

Figure 6.5: *D-CASCADE model outputs of the unimpeded river network, for five different scenario of input sediment median grain size. Figure a) shows the network sediment yield ($\Theta(3S)$ [Mt/yr]) and median grain size (d(3S) [mm]) for the five scenarios, labelled based on the input D50. Figure b) shows for all scenarios the input and output grain size frequency for each on the five sediment classes considered.*

course due to the preferential transport rate for fine grain classes measured by the Engelung & Hansen fractional sediment transport formula. For the simulation with coarse input D50, the difference between input and output GSD is stark, as the majority of the coarse material ends up trapped in low-transport reaches that act like choke-points, while the finer classes, initialized in lesser quantities, are transported more easily through the network. However, at finer input D50 scenarios, as the sediment yield approaches the cumulative sediment delivery from the watershed, a more significant fraction of the input material is delivered to the outlet, and thus the resemblance between input and output GSDs increases (Figure 6.5 b).

Given the results of the five sediment budget simulation alternatives, we selected the $D50_{input}$ = 0.05 mm scenario as the most likely to most closely representing sediment delivery from the 3S. This decision is due to the high total

sediment yield of the simulation (14.7 Mt/yr), which most closely resembles the estimates by Koehnken (2014) (16-18 Mt/yr), as well as the high sand fraction in the delivered material, which mirrors the high sand delivery from the 3S observed in literature (Bravard et al., 2014; Kondolf et al., 2014b; Piman et al., 2016).

Having selected a sediment yield scenario, we run it for the entirety of the time horizon considered (1995-2005). Figure 6.6 shows the distributed model outputs for the selected simulation. Sediment fining patterns are evident for all three of the main rivers, with median grain size decreasing as we proceed downstream and average sediment mobilization rates increases (Figure 6.6 a). By observing average sediment transport to the outlet, we notice how sediment transport raise by almost one order of magnitude during the wet season compared to the rest of the year (Figure 6.6 b). Moreover, sediment delivery during the monsoon season seems to contain a higher coarse fraction, as sand and gravel requires a higher discharge to be mobilized in considerable quantities (Figure 6.6 c) Without barriers on the river, the model indicates that the Se Kong river delivers the most material among the three rivers, followed by the Sre Pok and the Se San. The Se Kong river yield is also more rich in sand (43%) compared to the other rivers (32%-33%) (Figure 6.6).

6.4.2 Cumulative impact assessment of multiple reservoir operations

We ran D-CASCADE on the 3S network from 1995 to 2005 for the three dam development scenarios defined in section 6.3.3. Figures 6.7 and 6.8 show the daily variation in water storage for each of the reservoirs included in the simulations, together with the input discharge and the output release from both the standard outlets and the spillways, for the ten years model time horizon. The results show how dams tend to dampen the effects of floods on the downstream river network by storing excessive discharge in their reservoirs when possible, especially at the monsoon season when the stored volume is still low. The effect is especially evident for the LSS2 reservoir, which due to its large storage capacity, can absorb flood pulses in the impoundment without increasing the release. For all other reservoirs, the release is typically very similar to water input for most of the year. Occasional drought may lower the reservoir water level below the minimum target, as the release cannot fall below the lower boundary set by the design minimum release.

However, all reservoirs struggle to store the high discharges which characterize the wet season, having to consistently resort to the spillways to avoid overfilling and maintaining the reservoir at full supply level for large portions of the season. This eventuality is especially frequent for the LSS2-II and LSP2 dams, due to their relatively small impoundment volume and downstream po-

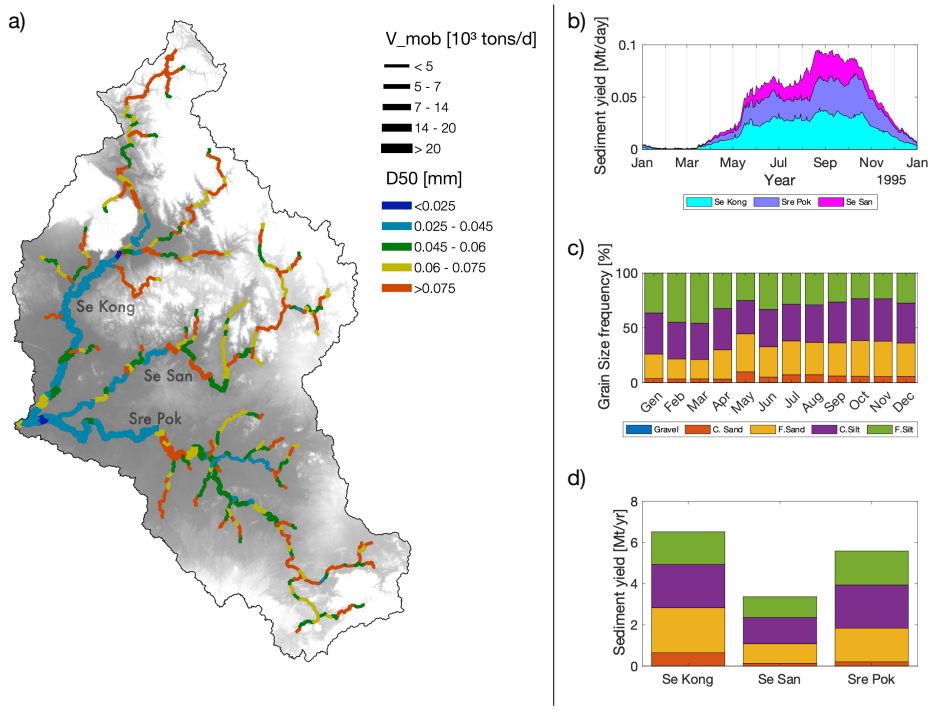

Figure 6.6: *Sediment transport characteristics across the 3S system for the entire simulation horizon (1995-2005), for the $D50_{input}$=0.05 mm catchment yield scenario. Figure a) shows the average median grain size (D50) of the total sediment content (deposited and mobilized) and the average daily mobilized material of each reach. b) displays the average daily sediment yield partitioned by tributary of provenance. c) shows the monthly average GSD of the network sediment delivery to the outlet, while d) divides the average annual sediment yield based on river system of provenance and grain class transported*

sition, which leads to increased input flows.

Moreover, all reservoir struggle to accommodate the discharge during the wet season, having to resort to the spillways in case of major floods. Spillway activation is persistent in downstream reservoirs, where it happens consistently and frequently thorough each year, to the point that the reservoirs are filled to full supply level for a large part of the monsoon season.

Figure 6.9 illustrates the modelled catchment sediment yield to the output under different dam development scenarios. All dam development scenarios lead to a decrease in sediment yield at the outlet, as expected. In both the LSS2Only and FullDam scenarios, the total sediment yield decreases by around 50%, while the combined delivery from the Se San and Sre Pok drops by 85%,

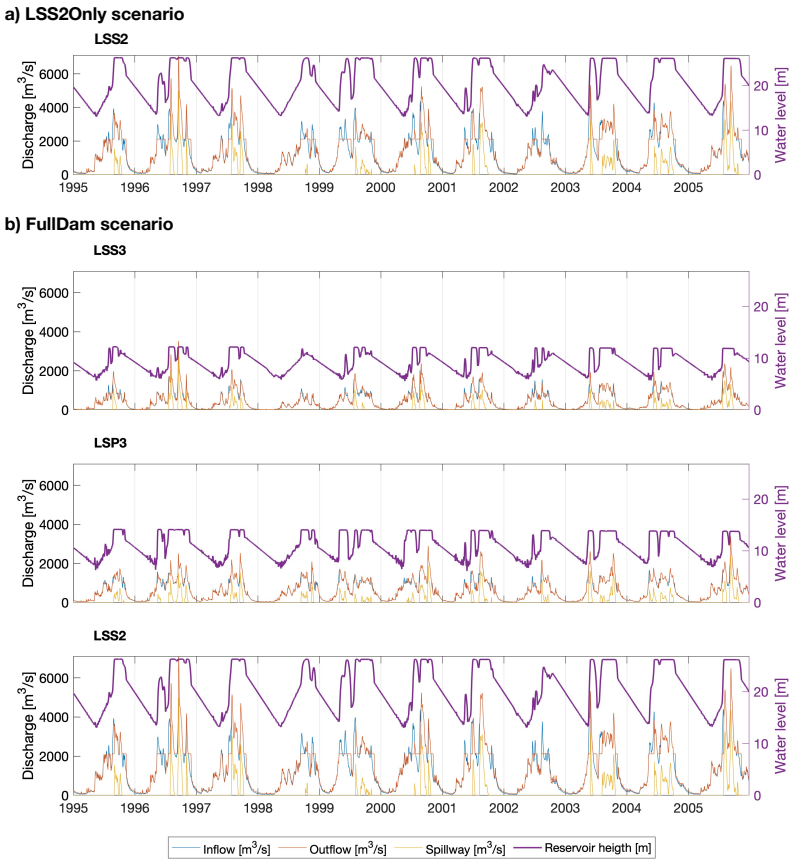

Figure 6.7: *Daily water level, input flow and reservoir discharge via standard outlets and spillways for the reservoirs in a) the LSS2Only and b) the FullDam scenarios, across the entire simulation horizon (1995-2005). Water level in the reservoir cannot exceed the Full Supply Level (FSL), which decreases according to the stored sediment volume*

averaging around 1.35 Mt/yr instead of the 9 Mt/yr in the pristine case. The sediment starvation is predominantly caused by the LSS2 dam, because of its massive impounded volume and high water residence time. The similarities between the two scenarios with LSS2 are probably due to the trapping effect of the downstream dam, which lets the same volume of sediment pass through the reservoirs irrespective of the amount of sediment delivered from upstream.

Instead, the proposed alternative dam configuration to the LSS2 has a significantly lower impact on sediment delivery. In this scenario, cumulative sediment yield from the Se San-Sre Pok system decreases by 47% (4.71 Mt/yr) . The more contained sediment retention is due to the smaller impounded volume and water residence time in the alternative reservoirs, which raises hydraulic

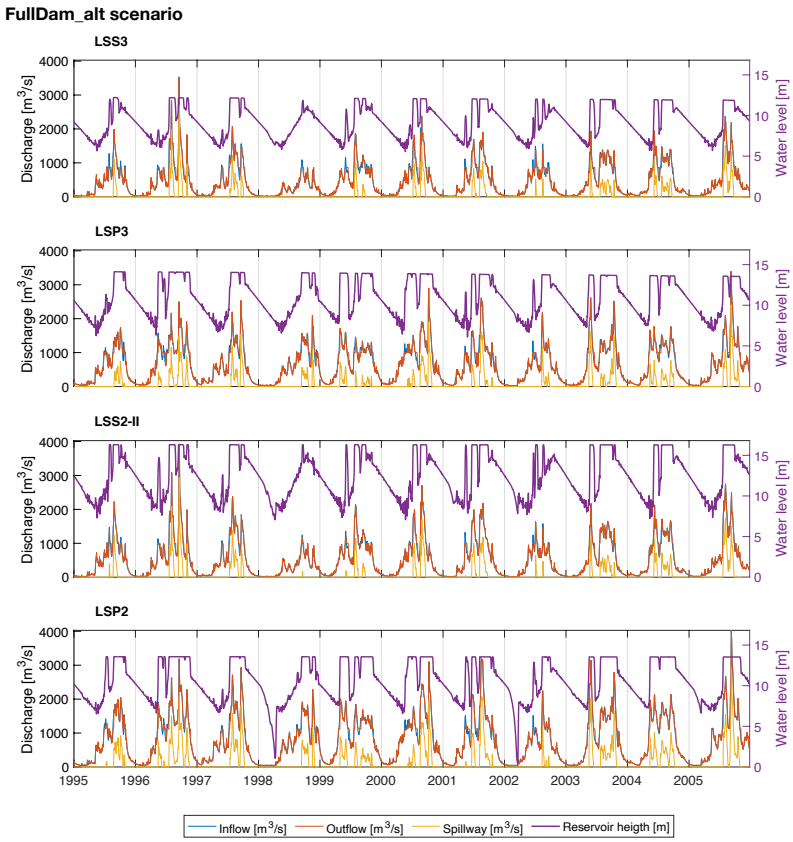

Figure 6.8: *Daily water level, input flow and reservoir discharge via standard outlets and spillways for the four reservoirs reservoirs in the FullDam_alt scenarios, across the entire simulation horizon (1995-2005).*

forces inside the impoundment, transport capacity, and ultimately sediment release.

Another significant effect of reservoir placement in the network is the preferential trapping of finer grain sizes. In all scenarios, the sediment mixture delivered to the outlet is significantly more dominated by silt than for the pristine scenario, as sand fractions are more easily detained inside the reservoir by low transport capacity in the flooded reaches. This reduction is particularly severe for the two LSS2 scenarios, where virtually no sand is delivered to the lower Mekong from the Se San and Sre Pok rivers (98 % reduction), but is also present in the FullDam_alt scenario (64 % reduction).

The effects on reservoir water storage of sediment trapping under different dam development scenarios are described in Table 6.3. As expected, in the case of multiple reservoirs in series, as in the two MultiDam scenarios, sediment

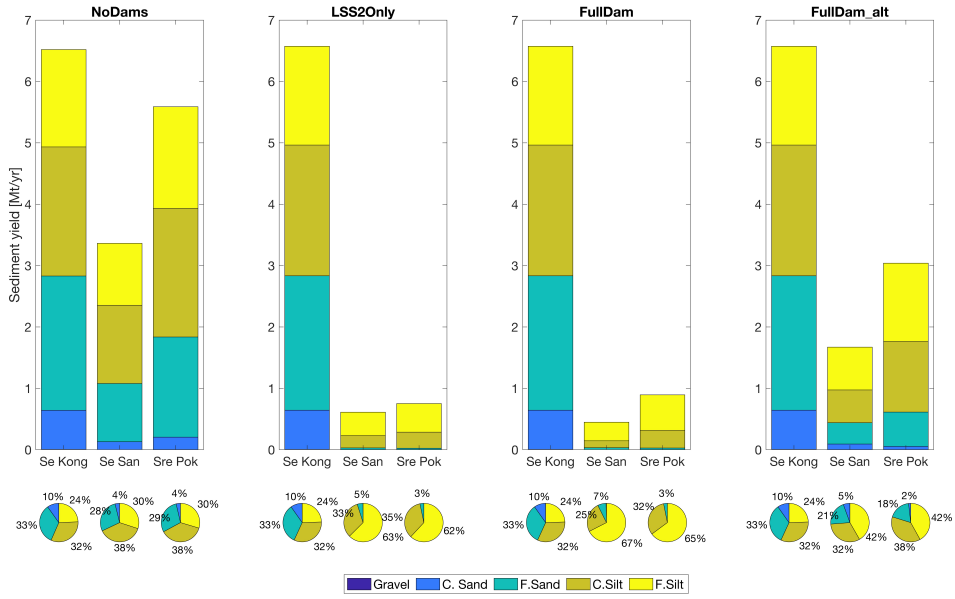

Figure 6.9: *Average annual catchment sediment yield to the Lower Mekong river under different dam development scenarios, partitioned by 3S main river systems and grain size classes. In all scenarios, the Se Kong river is not influenced by dam development and thus delivers the same sediment volumes.*

trapping and consequent storage capacity losses affect the upstream reservoir considerably more. On the other hand, dams situated downstream other barriers benefit from the lack of material in the input discharge due to the upstream sediment starvation.

6.4.3 Cumulative effects of drawdown flushing operations

Figure 6.10 shows the effects of simulated drawdown flushing operations both on the reservoirs storage capacity and the 3S cumulative sediment yield to the Mekong, for the annual and biannual frequency scenarios. Flushing implementation, as expected, provides positive results for sediment deposit removal, although the benefits are still insufficient to contrast runaway sediment retention (Figure 6.10 a). This is especially evident for the two upstream dams (LSS3 and LSP3), where the accretion rate of the sediment storage is only barely decreased by flushing. At the end of the simulation horizon, both LSP3 and LSS3 reported an absolute difference in storage loss of around 0.4 % (7.7% to 7.2% for LSP3, 5.5% to 4.9% for LSS3) for the annual frequency scenario, corresponding to a 7% to 11% reduction in the total sediment storage. Flushing seems to effectively contrast sediment trapping only on the LSS2-II reservoir, and to less extents,

Scenario	Dam	Avg. ann. sed. trapped [Mt/yr]	Avg. ann. lost impoundment [%]	10 yr impoundment loss [%]
LSS2Only	LSS2	7.50	0.16%	1.78%
FullDam	LSS3	3.00	0.50%	5.50%
	LSP3	3.79	1.00%	7.70%
	LSS2	4.70	0.10%	1.12%
FullDam_alt	LSS3	3.01	0.50%	5.50%
	LSP3	3.79	0.71%	7.70%
	LSS2-II	0.15	0.05%	0.55%
	LSP2	1.32	0.16%	1.77%

Table 6.3: *Sediment storage increase and subsequent water storage capacity loss for each reservoir in each dam development scenario. The relative impoundment loss is calculated based on the water volume at FSL at the beginning of the simulation. The average annual sediment trapped and the correlated average annual lost impoundment are calculated without the first year of simulation, used for model initialization.*

the LSP2. For the two downstream reservoirs, in fact, the absolute difference in storage loss falls around 0.4% (1.8% to 1.4% for the LSP2, 0.6% to 0.2% for the LSS2-II). However, given the limited sediment storage in the basins, these differences correspond to a decrease of 22% and 61% in the final sediment storage.

Flushing efficiency in the simulations appears highly variable, and strongly correlated with inflow rate. Operations may be 2 or 3 times more effective depending on the incoming discharge. Moreover, flushing seems to have a more erratic effect on sediment storages in the downstream dams, which oscillates less regularly than the other two reservoirs. This effect is most likely due to the influence of upstream flushing operations on downstream deposits. While flushing parameters (Table 6.2) are designed so that the time window for flushing operations synchronize for the four dams analyzed, differences in hydrology may dis-couple flushing timings in reservoirs in series. When this happens, the released material upstream ends up trapped in the downstream impoundment. An example of this effect is the flushing operation in 2001: where high inflow during flushing in the LSS3 reservoir resulted in massive deposit scourging upstream and subsequent deposition in the downstream LSS2-II reservoir.

Figure 6.10 b, instead, illustrated the benefits of drawdown flushing on the cumulative sediment yield of the 3S system. Total sediment delivery improves by 0.5 Mt/yr and 1.3 Mt/yr for the biannual and annual flushing scenario, respectively, corresponding to an 4% - 10% increase in network sediment yield. No discernable fluctuations in yield GSD are reported in the simulations.

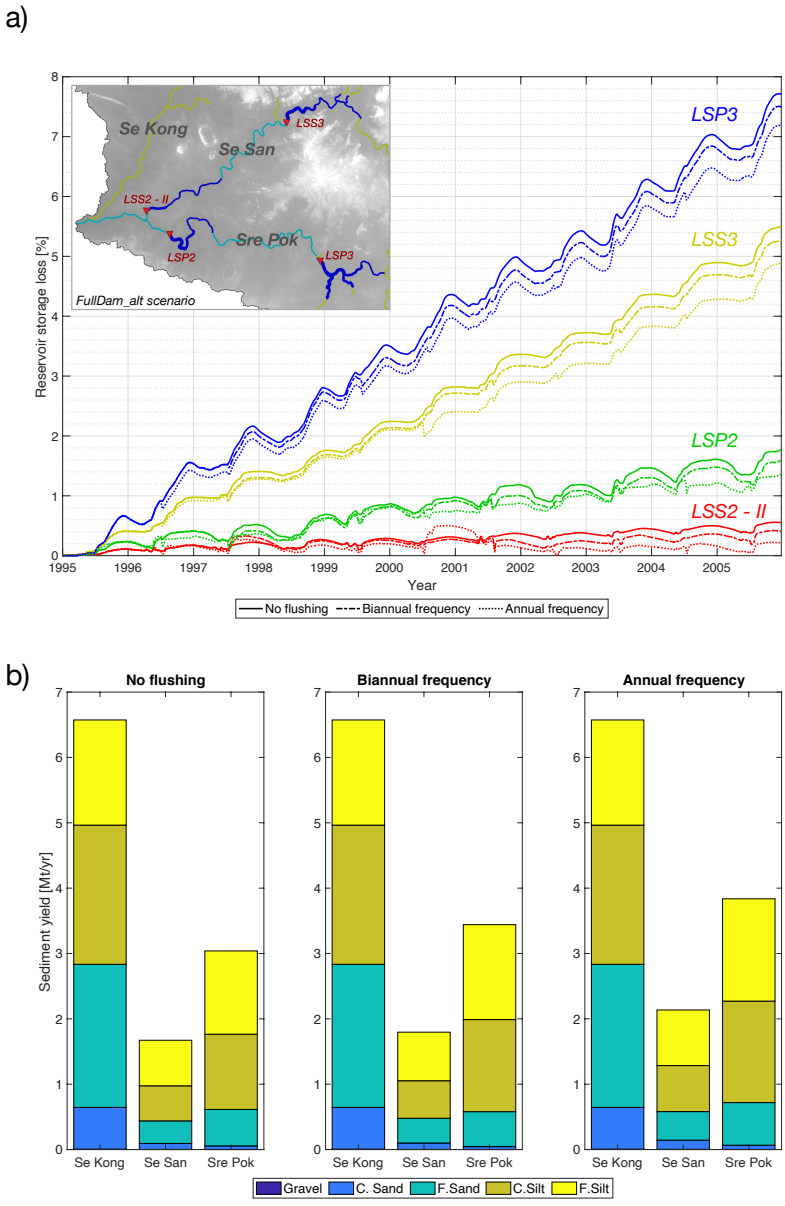

Figure 6.10: *D-CASCADE results for the simulated annual and biannual flushing, for the four reservoirs in the FullDam_alt scenario. Figure a) shows the effects of multiple flushing operations on the cumulative reservoir water storage losses, compared to the no flushing baseline (straight line). Figure b) compares average annual basin sediment yield for the baseline and the two flushing scenarios.*

6.5 Discussion

6.5.1 3S pristine sediment budgets reconstruction

By employing simple estimations of annual sediment yield as input to the system, D-CASCADE is able to generate complex and believable scenarios of sediment delivery and transport in the un-impounded 3S system. For all the five input sediment GSDs scenarios, the interactions between the multiple sediment transport processes across the whole network resulted in complex spatiotemporal sediment transport, deposition, and delivery patterns, which, however, share some common properties. In particular, all simulations resulted in coherent basin-scale sediment fining, which is frequently observed of large sand-bed river systems (Morris and Williams, 1999; Frings, 2008). Sediment fining is accompanied by a general increase in sediment load as we proceed downstream. Sediment transport, in particular for the coarse fractions, is concentrated during the wet season.

The system's overall efficiency for sediment delivery is highly dependent on the type of material initialized as input. For finer grain sizes, the river network conveys material with greater efficiency, to the point that in the finer input scenario ($D50_{input}$ = 0.01 mm) 91% of the catchment sediment yield is delivered to the outlet. On the other hand, coarser sediments tend to be detained at higher rates as they travel downstream: in the coarser scenario ($D50_{input}$ = 1 mm), where gravel constituted 59% of the catchment yield, the total trapping efficiency of the network rises to 81% of the cumulated input over the simulation horizon.

Ultimately, the scenario with input D50 equal to 0.05 mm appeared the most promising, as its network sediment yield most closely resembled other estimates from literature (Koehnken, 2014) while guaranteeing the consistent delivery of sand particles which characterized the 3S system (Bravard et al., 2014; Kondolf et al., 2014b; Piman et al., 2016).

6.5.2 Dynamic reservoirs operations impact assessment

The model results on sediment yield and type are coherent with literature on reservoir impacts on river system morphology. In all the scenarios considered, the inclusion of dams results in a remarkable decrease in sediment delivery to the outlet. Dam trapping efficiency varies according to their flooded area and the impounded volume, as well as their location. Furthermore, reservoir sediment trapping affects different sediment classes at varying degrees, with fine sediments carried in suspension escaping the impounded area at higher frequencies due to preferential transport.

The LSS2 reservoir, with its massive flooded surface, has by far the biggest

impact on river sediment delivery. Its position on the Se San - Stre Pok's confluence means materials from both rivers end up stored in the basin, while its massive flooded area means cascades must cross several flooded reaches with low transport capacity to escape the reservoir. The current planned configuration of dams (LSS2, LSS3, and LSP3) would significantly reduce the sand sediment yield to the Lower Mekong. As sand delivery plays a crucial role in conserving the morphological stability of the Mekong delta, the decrease in sand yield would contribute to the risk of coastal land loss and delta subsidence below sea level. Sediment retention could be even higher given many other reservoirs located or planned upstream of the barriers considered.

On the other hand, while sharing the almost exact location of LSS2, the alternative dams LSS2-II and LSP2 trap considerable less material due to their small impoundment and subsequent low average residence time of the water in the reservoir, which means hydraulic forces in the reservoir are enough to entrain and transport part of the incoming material out of the impoundment.

The model results also indicate that the LSS2 dam acts like a chokepoint for sediment delivery, effectively fixing a very low upper boundary to the volume of sediment able to escape from the reservoirs. As long as the sediment delivery to the LSS2 dam stays above this boundary, the sediment release downstream LSS2 will be virtually unchanged. This effect causes the yields from the LSS2Only and FullDam scenarios to be similar despite the additional presence of upstream reservoirs in the second scenario (Figure 6.9). Thus, the model indicates that building reservoirs above the LSS2 dam may have little to no effect on the overall sediment yield to the outlet.

Finally, the results for the sediment trapping show that, given the large sediment yield of the 3S system, reservoirs with relatively contained water storage capacity are especially susceptible to impoundment filling from sediment trapping. After ten years, losses in the LSP3 reservoir amount to almost 8%, meaning that, if no sediment management strategies are devised, the structure's service life may be considerably shorter than planned.

Annual and biannual flushing operations are simulated across the 11-year time horizon. The results showcase how flushing is effective in removing deposited material from the dam's impoundment. However, the impacts of drawdown flushing operations seem insufficient to contrast cumulative sediment retention in upstream reservoirs. The sediment removal rate from flushing is considerably lower than the deposition rate caused by the trapping of sediment-rich inflow discharge.

Flushing appears to be more effective in downstream reservoirs, where upstream sediment retention leads to less material delivery to the impoundment. Annual flushing operations in the LSS2-II lead to a removal of more than half of the sediment storage at the end of the simulation horizon. Another noticeable

benefit of these sediment management options seems to be an increase in the cumulative sediment delivery to the Mekong river, although far from sufficient to restore the pristine sediment yield. While changes in the flushing parameter, e.g., an longer operation time window, may improve the overall effectiveness, these results suggest that on the 3S river seduction flushing alone may not be enough to contrast reservoir sedimentation and sediment starvation. However, it undoubtedly provides moderate benefits contrasted to the scenario where no sediment management strategy is performed. The high sediment concentration in the inflow during the wet period also reduces flushing efficiency, as it effectively decreases the fraction of water flow transport capacity available to mobilized deposited volumes during free-flow conditions.

The results on the 3S also demonstrate how vital coordination between reservoirs is to guarantees the efficacy of sediment management operations. If no or limited communication is present, the research suggests the possible risk of flushing operations in upstream dams leading to adverse effects in downstream reservoirs. At the same time, coordinated operations may decrease flushing efficiency in downstream reservoirs, as more of the discharge transport capacity would be used to carry sediment flushed from upstream and less to entrain material in the deposits.

6.5.3 Opportunities and limitations for further research

Sediment budget

The results of the sediment budget estimations demonstrate the potential of the D-CASCADE model to reconstruct sediment connectivity patterns across time and space, even in data-scarce environments such as the 3S system, where the lack of consistent and distributed information on river morphology and sediment transport limits the application of more traditional models with high data requirement. With only large-scale datasets on river hydromorphology and catchment sediment yield, D-CASCADE generated coherent scenarios of sediment delivery which return reasonable results when validated with the limited data available in the literature.

However, these simulations are based on several strong assumptions. First, the hypothesis of uniform and constant sediment delivery rates through the year most likely clashes with real-world conditions. We assume the rate and composition of soil erosion and detachment to be influenced by local meteorological conditions, land use, and lithology. On the 3S, we expect catchment sediment yield to increase during the wet season and be influenced by agricultural practices. Further study could integrate distributed erosion models like RUSLE (Renard, 1997; Ranzi et al., 2012) to derive dynamic sediment yields for the entirety of the river basin. Alternatively, by abandoning the hypothesis of

uniform basin-wide grain-size distribution and catchment yield and generating heterogeneous patterns of sediment delivery differentiated by magnitude and GSDs, the D-CASCADE model could explore a vaster range of sediment delivery scenarios.

Hypotheses on transport capacity and sediment velocity are also necessary to compute transport rates and sediment delivery. Future studies would benefit from sensitivity analysis on the most crucial parameters in the formulas employed, e.g. the active layer thickness d_a (Eq 4.1) and characteristic vertical length of sediment transport $H_{a,c}$ (Eq 4.6 and eq 4.7). Moreover, the effectiveness of Engelund & Hansen and especially the use of the Bed Material Fraction (BMF) approach to obtain fractional transport rates could be tested versus other formulas, as they do not explicitly how interactions between particles of different sizes may influence particle motion, e.g., via a "hiding factor" (Wilcock and Crowe, 2003).

The model's only sediment sources are the catchment sediment yields defined by Kondolf et al. (2014b). However, sediment delivery may not be limited to this one process: solid materials could be entrained by previously available sediment stores and sinks on the floodplains, along the river path (sediment bars and banks), and stored on the river bed. Sediment delivery could also increase due to anthropic activities like sand mining on the channel, which employs heavy equipment, mobilizes a large amount of material, and changes the morphological features on the worksite and beyond. This factor may have a profound influence in this case study, as large-scale sand mining activities have been observed across the entirety of the Lower Mekong (Hackney et al., 2020).

Reservoir management

D-CASCADE successfully integrated reservoir management in the modelling framework by including multiple add-ons components that explore the dynamic evolution of the sediment storage in three dimensions and update the hydromorphological conditions of both the flooded and downstream reaches accordingly. The four parameters rule curve implemented in the model, while simple, allows for the simulation of the effects of time-varying release strategies on the system. Future research may improve the complexity of the representation of the operating strategy, e.g., by including piecewise linear function (Dang et al., 2020) or more complex functions, or by defining optimal release according to the daily market energy price in case of hydropower dams, or other objectives like flood protection or water supply.

Our study also did not consider the effects of dead storage in reservoirs, which is present in virtually all large reservoirs and designed to provide space below the intakes to safely store the incoming sediment volume without lowering the reservoir hydraulic jump and energy production. Moreover, we assumed

dams to be designed with bottom outlets necessary for drawdown flushing. In reality, very few dams possess this kind of infrastructural adaptation, and so sediment flushing may not be feasible in the manner described in this analysis.

The evaluation the benefits and limitations of sediment management strategy like drawdown flushing operations represents a novelty in the application of large-scale conceptual sediment models, and demonstrates the usefulness of including the representation of the temporal dimension in CASCADE. The timing and synchronization of flushing operations in multiple reservoirs, in fact, can only be accomplished via the spatiotemporal tracing of the material movement throughout the network. Our analysis on the feasibility of drawdown did not consider the uncertainties brought by the variation of flushing parameters listen in Table 6.2, with the sole exception of flushing frequency. This is due to limited knowledge on the actual feasibility and possible designs of flushing facilities on the proposed reservoirs, which would require a more in-depth, structural analysis.

Other variables intrinsic to the model may also influence the reservoir impact assessment. For example, sediment porosity ϕ increases the actual volume occupied by the sediment storage compared to the dry volume carried by cascades. While in our simulation this parameter is considered constant, future analysis may necessitate a dynamic representation of its evolution through time, as progressive sediment consolidation, type of material composing the deposit and the frequency of sediment reworking, e.g., caused by drawdown flushing, may all influence its value and the subsequent loss of sediment storage.

In this research, the mobilized sediment volume during flushing is determined by the reservoir reaches transport capacity in free-flow conditions. By all accounts, the now-empty reaches are treated by the model as conventional river channels, and erosion is measured according to standard D-CASCADE operations. However, sediment mobilization in channels and material remobilization during flushing may be better represented as two distinct processes, thus simulated with different formulas to describe transport and erosion rate. For example, Wild et al. (2016) and Atkinson (1996) assume sediment volume removed by flushing as a function of the geometry of the cross-sectional area of the reservoir sediment before flushing and the design of the bottom outlets. Their analysis, however, ignores the potential reduction is sediment transport due to sediment-rich flushing inflows. However, bottom outlet discharge capacity may indeed increase sediment scourging at the mouth of the dam. At the same time, the channel width and depth of flushed reaches may profoundly differ from their original, pre-dam construction values used in the simulation when the reservoir is empty.

The parameters for the release rule curve and the flushing frequency, duration, and timing were defined a-priori based on literature knowledge on stan-

dard reservoir water and sediment management strategies for reservoirs located in wet tropical climates. However, the chosen parameter selection is most likely not optimal to maximize energy production from hydropower, i.e., reducing spillway use while maintaining a high hydraulic jump and preserving network sediment connectivity and delivery.

Model outputs suggest that flushing efficiency is tightly correlated with inflow discharge. Integrating forecast in the decision-making process may therefore allow for better timing of drawdown flushing initiatives. For example, the El Niño Southern Oscillation (ENSO) has profound effects on the hydroclimatic conditions of the Mekong (Räsänen and Kummu, 2013; Chowdhury et al., 2021). Thus, flushing may even be timed to exploit the increase in precipitation and flushing discharge brought by La Niña events.

To search for more efficient strategies for dam water and sediment management, D-CASCADE could be integrated into optimization-based frameworks, as was the case for the original CASCADE model in Schmitt et al. (2018a, 2019) for respectively the 3S basin and the entire Mekong fluvial system. The structure of the D-CASCADE model may allow the analysis to include sediment connectivity conservation among the competing optimization objectives. A more thorough analysis could include the entire ensemble of existing and planned reservoirs in the 3S basin to address even more risk factors and provide further combinations of sustainable dam development and management portfolios.

For flushing operations, parameters optimization may yield insight into optimal flushing timing and duration for multiple dams to guarantee improved operational performance. Optimization may also indicate better timing and synchronization for flushing operations in multi-dam schemes, to synergize multiple sediment management efforts at the network scale and avoid deposition of flushed sediment in downstream reservoirs storages. While this analysis focuses on the effects of reservoir management on sediment connectivity and deposition, the model structure would also allow the quantification of energy production. Therefore multi-objective optimization with algorithms like BORG (Hadka and Reed, 2013), coupled with D-CASCADE would return Pareto-optimal management portfolios, which indicate interesting trade-offs between sediment connectivity conservation and economic gains.

The distributed and time-dependent outputs of the D-CASCADE model allow for the definition of multiple indicators of sediment (dis)connectivity to be employed in multi-objective analysis. This research described sediment transport disruption mostly in terms of changes in magnitude and type of sediment delivery to the Mekong and reservoirs sedimentation. However, further analysis may require more specialized morphological indicators to evaluate sediment transport in multiple strategic spots on the river to map better the basin-wide distributed alterations or monitor disturbances in ecological hotspots.

6.6 Conclusion

The study presented in this chapter marks the first application of a dynamic sediment connectivity modelling framework on a basin-wide scale with the explicit objective of characterizing the cumulative effect of dam management strategies of series of dams on the reservoir storage capacity and the sediment connectivity of the downstream network.

The D-CASCADE model provided reasonable sediment budget estimates for the 3S river system employing only large-scale datasets, demonstrating the potential of these types of conceptual models for the extraction of morphological information in data-scarce environments already seen in other works (Schmitt et al., 2018b; Czuba, 2018; **?**).

The integration of reservoirs in the modelling structure, possible via specific add-ons components, allows for daily simulation of dam operational strategies and their cumulative effects on network sediment transport and sediment trapping and storage in the dam basin. We explored different dams configurations scenarios on the 3S system, focusing on the downstream structures both planned and already existing, as they are regarded as the most impacting on the network sediment connectivity (Schmitt et al., 2018a). D-CASCADE quantified the reduction of sediment yield to the Lower Mekong river given by these dam portfolios. The current planned configuration would results in a net yield reduction of around 50%, as sediment contribution from the Se San and Sre Pok decreases to 15% of the original value. The alternative scenario proposed by Annandale (2013) would present a viable alternative to conserve at least partially sediment delivery, as the reduction to the catchment yield would be limited to 26%. The model also estimates impoundment storage losses due to sediment trapping to be especially worrying for the smaller reservoir due to the high sediment load carried by the 3S system. The planned LSS3 and LSP3 reservoir would experience a loss of 5.5% and 7.7% of their total water storage capacity after 11 years of simulation.

Frequent drawdown flushing would help mitigate the effects of reservoirs on sediment transport, although just to a moderate degree, as the high sediment concentration in the water discharge of the 3S system would still lead to noticeable sedimentation in the impoundment and sediment starvation downstream. With annual flushing, for the alternative dam development scenario outlet sediment delivery would decrease by 21%, although reservoirs sedimentation would not experience much slowdown, especially in upstream reservoirs.

Appendix B

In this appendix, we provide more detailed information on the add-ons components used in the D-CASCADE modelling framework in chapter 6 to integrate reservoirs in the model structure, as well as simulate different release strategies and their effects on the hydrology of the network downstream the dam, as well as the water and sediment storage in the reservoir. These components are then used on the 3S river system, as described in chapter 6

B.1 Dynamic reservoir storage modelling add-on

A specific D-CASCADE add-on component was added to the model to integrate a dynamic representation of reservoirs on the graph-like network structure employed by D-CASCADE (Figure B.1 a). The process representation includes modelling the impoundment characteristics, i.e., stored water and sediment volumes, reservoir height and area, and their response to changing hydrological conditions and different operational strategies.

First, each dam is placed on the network node closer to its real location, and its reservoir volume is initialized. Using topological information derived from the DEM employed for network extraction, we obtained reservoir height (H_r) and total surface area (A_r) for different values of stored volume (V_r) , uniformly extracted between zero and the reservoir full supply level (FLS) (m). In this way, it is possible to obtain height and surface area for each possible value of reservoir volume by linearly interpolating between two tabulated values (functions $f_{H,r}(V_r)$ and $f_{A,r}(V_r)$)

In each timestep, we derive reservoir area and water level at the dam from the storage volume; then we determine the partially or fully inundated reaches upstream each dam based on node elevation data from the DEM and the reservoir impounded volume for the timestep, following the procedure used in Schmitt et al. (2018a). In this way, reservoirs are represented as composed of multiple longitudinal compartments, each constituted by a single flooded reach (Figure B.1 b). In each of these compartments, the channel features used to determine fractional transport rates are altered to reflect the new conditions of the river

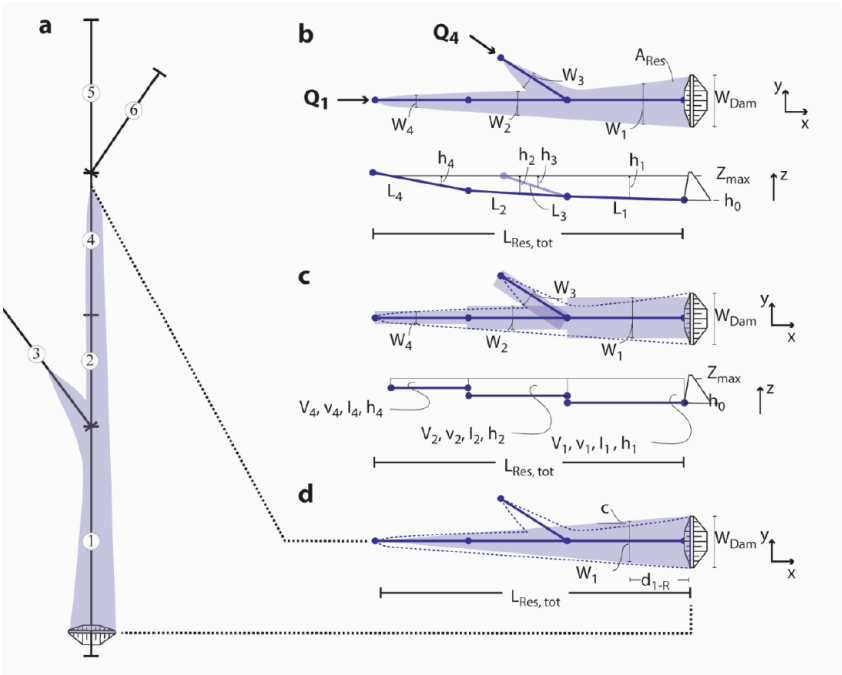

Figure B.1: *Estimation of hydraulic parameters for multiple compartments of a reservoir impoundment (Volume, velocity, and depth) relative to the reservoir volume in a single timestep. (a, superimposition of reservoir flooded area on a 6-reaches river network. Plan-view and cross-sectional parameters for a reservoir with 4 inundated edges and two tributaries (b) as extracted from the DEM. c): Representation of reservoir dimensions as set of rectangular compartments and definition of certain geometric parameters, especially width, for each edge by assuming a simplified, triangular geometry of the reservoir (d). Figure from Schmitt et al. (2018a), supplementary material.*

reach. In particular, water level ($h_{i,t}$), compartment width ($W_{i,t}$), water velocity ($v_{i,t}$) and channel gradient ($S_{i,t}$) are all changed accordingly.

The original reservoir geometry is adapted to suit the new compartments' representation: each flooded reach is modelled as a rectangular compartment with constant width. The water level of the compartment is derived as an average of the water level in each reach node, given by the dam level in the timestep, derived from the stored volume and the nodes elevation (Figure B.1 c). To derive the compartment width, we assumed the reservoir impoundment to be shaped like an isosceles triangle, whose base corresponds to the dam width and the height to the total reservoir length so that the width at the headwater is zero (Figure B.1 d). Thus, the width in each flooded node is given as a function of the dam width and the distance from the node to the dam. The reach width is

then derived as the mean of the downstream and upstream node width (or zero if the reach is only partially flooded). Therefore, the total volume stored in the compartment is determined through:

$$V_{i,t} = h_{i,t} * W_{i,t} * L_i \tag{B.1}$$

Where L_i is the reach length.

The energy slope of the compartment is derived according to the formula:

$$S_{i,t} = \frac{v_{i,t}^2}{2g} \tag{B.2}$$

where $v_{i,t}$ is the average flow velocity in reach i at time t:

$$v_{i,t} = \frac{L_i}{V_{i,avg}/Q_{i,avg}} \tag{B.3}$$

where $V_{i,avg}/Q_{i,avg}$ is the average residence time of the water in the reservoir (Ward, 1980). As these reservoirs are operated for hydropower production and therefore tend to maximize hydraulic jump when possible, we assumed $V_{i,avg}$ to be equal to $V_{i,FSL}$, i.e. the compartment volume at FSL.

B.2 Reservoir management add-on

This additional component, which works in tandem with the dynamic reservoir storage modelling add-on, is designed to determine the daily water release for the timestep $R_{r,t}$ according to the reservoir release strategy, and therefore the total volume of the reservoir in the next timestep $V_{r,t+1}$ via the formula:

$$V_{r,t+1} = V_{r,t} - R_{r,t} + Q_{r,t}^{in} \tag{B.4}$$

Where $Q_{r,t}^{in}$ is the water input to the reservoir at time t, corresponding to the discharge relative to the reach directly upstream the dam node.

In our study, we apply a simple operating rule curve to determine the optimal reservoir volume in each timestep $V_{r,t}^{target}$, which depends on four parameters, i.e. the the minimum and maximum impoundment storage that each reservoir should reach within a year ($V_{r,min}^{target}$ and $V_{r,max}^{target}$) and the date at which the two values should be reached ($T_{r,min}^{target}$ and $T_{r,max}^{target}$) (Dang et al., 2020). The target volume in each timestep $V_{r,t}^{target}$ is determined by linearly interpolating between these two extremes according to the date relative to the current timestep. The target release $R_{r,t}^{target}$ for each reservoir is then determined as:

$$R_{r,t}^{target} = max(V_{r,t} + \widehat{Q}_{r,t,day}^{in} - V_{r,t}^{target}, 0) \tag{B.5}$$

where $\widehat{Q}^{in}_{r,t,day}$ is the estimated daily water input in the reservoir at time t (m^3), derived from the estimated instantaneous water input $\widehat{Q}^{in}_{r,t}$. In an ideal scenario, the dam operator would know exactly the water input to the reservoir in each timestep $Q^{in}_{r,t}$ ($\widehat{Q}^{in}_{r,t} = Q^{in}_{r,t}$), and could therefore plan the water release to precisely meet the reservoir volume target. However, as this information cannot be precisely acquired at the beginning of each timestep, the dam operating rule requires an estimated daily discharge to determine the target release. This information can be acquired via daily discharge forecasts or autoregressive, data-driven models (Soncini-Sessa et al., 2007). In our case study, we designed the release strategy to assume water discharge equal to the value of the previous timestep ($\widehat{Q}^{in}_{r,t} = Q^{in}_{r,t-1}$).

The actual release of the dam $R_{r,t}$ used in eq.B.4 is equal to $R^{target}_{r,t}$, unless:

- $R^{target}_{r,t} < R^{min}_{r,t}$, where $R^{min}_{r,t}$ is the minimum allowed discharge from the reservoir, in which case $R_{r,t} = R^{min}_{r,t}$. In this work, we assume $R^{min}_{r,t}$ to be the first percentile of the water discharge (1995-2005) in the first reach downstream the dam;
- $V_{r,t} + Q^{in}_{r,t,day} - R^{target}_{r,t} > V^{FSD}_{r,t}$, where $V^{FSD}_{r,t}$ is the reservoir volume at full supply level at time t. In this case, target release is not enough to avoid the activation of the reservoir spillways. Thus, release is increased accordingly until R^{design}_{r}, i.e. the design discharge for the reservoir;
- $V_{r,t} + Q^{in}_{r,t,day} - R^{design}_{r} > V^{FSD}_{r,t}$. If the reservoir full supply level is topped even when the reservoir release matches the design discharge, the excessive volume is released via spillways until $V_{r,t+1} = V^{FSD}_{r,t}$. Thus, in this case $R_{r,t} = R^{design}_{r} + R^{spillway}_{r,t}$, where

$$R^{spillway}_{r,t} = V_{r,t} + Q^{in}_{r,t,day} - R^{design}_{r} - V^{FSD}_{r,t} \tag{B.6}$$

B.3 Reservoir sediment trapping add-on

This add-on component records the total volume stored in each reservoir in each timestep and decreases the reservoir full supply level (FLS) accordingly to mirror impoundment storage losses due to sediment trapping. In each timestep, the total sediment storage in each reservoir $V_{r,t}$ is defined as

$$V_{r,t} = \sum_{j=fl\_FLS} V_{d,j,t} + V_{i,j,t} \tag{B.7}$$

Where $V_{d,j,t}$ and $V_{i,j,t}$ are the total volumes carried by individual cascades located respectively in the deposit and incoming layers of reach j at time t, and fl_FLS contains all the reaches flooded by reservoir r at FSL.

The reservoir volume corresponding to full supply level $V_{r,t}^{FSD}$ at time t in reservoir r is therefore:

$$V_{r,t}^{FSD} = V_{r,1}^{FSD} - V_{r,t}/(1-\phi) \tag{B.8}$$

Where ϕ is the sediment porosity in the deposit layer.

B.4 Downstream water discharge add-on

Reservoir release alters the natural hydrological conditions of all the reaches downstream a reservoir, which affects the sediment transport capacity, reach sediment budget, and ultimately the system-wide spatiotemporal patterns of sediment delivery. To account for this in our framework, we assume water release from a dam instantaneously affects all downstream reaches, changing the hydrology according to the reservoir output discharge. We first measure the incremental discharge in a downstream reach j $\Delta Q_{j,t}$ as:

$$\Delta Q_{j,t} = Q_{j,t}^{nores} - Q_{r,t}^{nores} \tag{B.9}$$

$Q_{j,t}^{nores}$ is the water discharge for reach j downstream the reservoir and $Q_{j\_r,t}^{nores}$ is the discharge of the reach j_r where the dam is located in the pristine scenario, obtained by the VIC hydrological model. The new discharge for the reach $Q_{j,t}$ is given as:

$$Q_{j,t} = \Delta Q_{j,t} + R_{r,t} \tag{B.10}$$

In the case of multiple reservoirs located in series on the same river, the upstream dam only affects the reaches between the node where it is located and the upstream the downstream dam. Thus, the new discharge, influenced by the upstream release strategy, will influence the input discharge $Q_{r,t}$ to the downstream reservoir, thus affecting the stored volume and dam release at time t.

B.5 Drawdown flushing add-on

The drawdown flushing add-on regulates the reservoir release during flushing operations, replacing the Reservoir management add-on (Section B.2) for the duration of the drawdown and flushing phases. The add-on is activated for a specific reservoir r once all the necessary triggers are reaches, those being:

- A sufficient time has passed from the previous flushing operation;
- the current timestep falls into the time window for flushing;

- the reservoir input discharge surpasses the lower boundary set by the minimum inflow rate, but does not exceed the reservoir design discharge.

The threshold values for these parameters are listed in Table 6.2.

During drawdown, the reservoir release target is set so that the daily drawdown rate $\Delta L_{r,t}$ for reservoir r in the timestep t does not exceeds the maximum rate $max(\Delta L_r)$, where :

$$\Delta L_{r,t} = f_{H,r}(V_{r,t+1}) - f_{H,r}(V_{r,t}) \tag{6.1}$$

Where $f_{H,r}(V_r)$ is the height-volume function for reservoir r, defined in section B.1, and $V_{r,t}$ and $V_{r,t+1}$ the reservoir volume in the current and future timesteps. While $V_{r,t}$ is known in each timestep, $V_{r,t+1}$ is given by Eq. B.4. As $V_{r,t+1}$ depends also on the input discharge, the drawdown strategy assumes water $Q^{in}_{r,t}$ input equal to the value of the previous timestep $Q^{in}_{r,t-1}$, similarly to the release strategy seen in Section B.2. Therefore the daily release $R_{r,t}$ during drawdown is the maximum possible release which guarantees:

$$\Delta L_{r,t}(R_{r,t}) \leqslant max(\Delta L_r) \tag{6.2}$$

The drawdown is continued until the reservoir volume reaches zero or the maximum drawdown duration is reached. If complete drawdown is not achieved, a new attempt is performed after a fixed pause (Table 6.2). Once the reservoir volume reaches zero, the flushing phase begins, during which $R_{r,t} = Q^{in}_{r,t}$. In the simulation, we assume bottom outlets to have a design discharge equal to the standard hydropower outlets. Thus, if $Q^{in}_{r,t}$ exceeds this threshold, flushing is interrupted and refill commences.

The modelization of the refill phase does not require a specific component; instead, reservoir release is determined by the standard reservoir operation defined in Section B.2.

7

Conclusion

Modelling basin-scale river sediment (dis)connectivity presents numerous challenges. Its interconnected nature requires a basin-scale perspective and extended temporal frames to capture the multiple hydromorphological and biological processes responsible for sediment delivery, transport, and deposition and their dynamic interactions across channels, hillslopes, and floodplains. However, this complex nature is also why the development of reliable basin-scale modelling tools represents such a necessity, as anthropic disturbances on the natural fluvial connectivity patterns may result in otherwise unforeseeable impacts on the river ecosystem goods and services. Planning and managing multiple alterations or infrastructures on large river systems comes with the significant risk of damaging fluvial ecosystems integrity and functionality, if the implications on sediment (dis)connectivity are not considered. These impacts, in turn, may lead to long-term economic costs and river livelihood degradation.

The purpose of this research is to contribute two exploratory modelling frameworks for large-scale sediment connectivity, designed to quantify, characterize and disaggregate sediment delivery and transport patterns. These tools rely on large-scale distributed datasets made available by advances in remote sensing and image processing technology. Therefore, they apply to large-scale, data-scarce river systems. Their flexible and data parsimonious structure also supports detail sensitivity analysis and parameter calibrations which benefits the robustness of the results.

In this chapter, we synthesize the key findings, opportunities, and limitations reported in the thesis, with a particular focus on the potentials and needs for future expansions of the modelling frameworks and integrations in water resource management and planning approaches.

7.1 Main findings

Modelling approaches

This thesis contributes two novel modelling frameworks for network-scale sediment transport, the new CASCADE toolbox and the Dynamic CASCADE model (D-CASCADE). Both these approaches are based on Schmitt (2016) model CASCADE (CAtchment Sediment Connectivity And DElivery). However, they expand upon the original approach to include a more comprehensive representation of hydromorphological processes to open opportunities to tackle different objectives that require greater details in (dis)connectivity representation.

The multi-class CASCADE model, reported in Chapter 2 and incorporated in the CASCADE toolbox (Tangi et al., 2019), characterize cascades not by single grain size, but as a combination of multiple heterogeneous sediment classes, each one associated with a specific frequency inside the cascade. Hence, the individual transport process is defined by the volume carried and the grain size distribution, which are prone to fluctuations as cascades move downstream. Combining the GSDs of the cascades in each reach also defines the GSD of the cumulative sediment load in that specific location, an essential metric for initializations and output validations. GSDs sampling is often performed in the field using basket samplers for bedload and suspended sediment samples for finer grains and is one of the most common measurements available in the literature for reach morphological characterization. The representation of fractional transport rates, facilitated by the definition of a-priori grain classes and the sub-cascade partitioning of individual cascades, guarantees a more robust representation of sediment transport, employing well-known empirical formulas. This formulation, in turn, replaces the implementation of grain size competition strategies which were among the most significant sources of uncertainties in previous CASCADE applications (Schmitt et al., 2016).

The dynamic CASCADE model (D-CASCADE), described in Chapter 4, introduces a dynamic sediment transport representation that offers many advantages. The original, static framework described sediment movement as a steady-state, establishing connectivity between multiple sources and sinks. However, the model struggles with changes whose time scales are briefer than those correlated with the definition of this type of connectivity. Besides, CASCADE simulates sediment connectivity in a stationary state under a single hydrological scenario, which is especially unlikely for high discharges, characterized by limited duration, and responsible for most sediment delivery. Delineating cascades movement across time and space allows for exploring the dynamic evolution of the river network and its hydromorphological properties. D-CASCADE can explore the effects of singular events on the river network, like major floods or

on-time sediment delivery events, or the cumulative effects of a sequence of specific events happening at different locations and with distinct chronological sequences. For example, similar floods on the same fluvial system may deliver different sediment yields and types according to the sequence of other hydromorphological ar anthropic events that happened beforehand, which contributed, for example, to the armouring or disarmouring of the river bed (Wilcock and DeTemple, 2005; Tabarestani and Zarrati, 2015), the availability and type of materials ready for transport (Heckmann and Schwanghart, 2013; Czuba et al., 2017; Sklar et al., 2017) and the alteration of the morphological features of the river (Fryirs and Brierley, 1999; Gregory, 2019). D-CASCADE can reproduce all these processes and more, making it an effective tool to explore morphodynamic evolutions in river networks. Furthermore, sediment in rivers typically spends more time stationed in deposit zones than transported by the current (Otto et al., 2009). Thus, proper modelling of the evolution of sediment deposits and sediment sinks is necessary for dynamic modelling of river (dis)connectivity. The representation of the sediment deposit as composed of layers of cascades stacked on top of each other guarantees a detailed tracing of the evolution of sediment storages, its composition, and the provenance of the material stored, and allows for the simulations of different processes like sediment deposits growth and erosion, bed armouring and GSDs alterations. Channel morphodynamic response to sediment delivery, deposition and entrainment are modelled at the reach scale via add-ons components, including more traditional, reach-scale 2-D and 3-D approaches, conceptual, graph-based methodologies, or empirical relations based on previous studies knowledge of the system. The ambition behind the development of the D-CASCADE model was to provide a tool to define indicators of sediment connectivity alterations and their impacts on river morphology, ecology, and productivity caused by large-scale planning and management tasks. The model was designed to be flexible, data parsimonious, and computationally effective. It is intended for integrated, basin-scale water management efforts, which requires multiple screening of the many different combinations of decision variables, planning options, and management strategies for hydromorphological impact assessments. While the original CASCADE model saw applications on cumulative sediment trapping estimation for multi-dam development schemes on the 3S system (Schmitt et al., 2018a) and the Mekong river (Schmitt et al., 2019), the lack of dynamic modelling of sediment transport processes meant the cumulative repercussion of continuous water management strategies could not be properly evaluated. D-CASCADE, however, is designed to simulate all these processes. Consequently, the model can evaluate the effects of reservoir operations, both routine decisions like daily release and exceptional like dam flushing and sluicing. Besides dams, the dynamic structure allows for impact assessment of land-use change

like deforestation and urbanization, and restoration initiatives like barrier removal, banks, hillslopes re-vegetation, and fluvial ecosystem rehabilitation.

Case study specific findings

This thesis presents large-scale sediment transport modelling applications of three different river networks, characterized by widely dissimilar scales, geographic locations, hydromorphological history, and research objectives.

The Vjosa river network, one of the last "wild" large European rivers, is characterized by an almost unimpeded river course and a wide variety of different fluvial forms, including large braided stretches, which constitutes a rarity among European fluvial systems (Schiemer et al., 2018; Belletti et al., 2020). Human disturbances are mostly concentrated on the hillslopes, as land-use change for agriculture and limited urbanization. On-the-river infrastructures are few and concentrated upstream and on the tributaries. However, large-scale dam development plans threaten to disrupt the morphological balance of the system, and in particular, to endangers the braided sections of the river, which are especially vulnerable to sediment connectivity disruptions (Peters et al., 2021). The pristine conditions of the Vjosa river mean this system is especially suited for static CASCADE applications, as we can reasonably assume the natural morphodynamic evolution of the river to bed irrelevant given the research objectives and the time-scales of these processes. The relative stability of the system also supports the application of the hypothesis of morphodynamic equilibrium of the river reaches (Ferguson et al., 2015) for the identification of the reaches GSDs via optimization. In the research, we generated reasonable estimates of grain size composition for the river reaches, which shows clear fining patterns, validated by field observations with satisfactory consistency. Results are reinforced by a global sensitivity analysis on different sources of uncertainty in the initialization parameters. We then included simulated sediment transport fluxes and GSDs in published braiding thresholds to identify channel resilience to sediment delivery alterations. Thus, with this study, we demonstrated how distributed output for sediment connectivity models, supported by extensive validations and sensitivity analysis, can be used in morphological analysis where field data are not available, a results exceptionally useful for studies in data-scarce environments where consisted and distributed information of hydromorphological features is not available.

The primary objective of applying D-CASCADE on the Bega river network was to validate the novel modelling framework's ability to capture relevant morphological processes with the correct timing and magnitude. The Bega river network offered an excellent case study to achieve this task, given the wealth of information and data available on the evolution of the hydromorphological features of the river system and its response to anthropic alterations in

the last 170 years. The model reproduced the major morphological changes in the river network in line with the field observations and historical reconstructions. Sediment delivery patterns and morphological features changes are identified, and their sources are disaggregated in time and space. Uncertainties in the reconstruction of the historic discharge dataset are accounted for by designing different hydrological scenarios. The knowledge of the system gained by historical simulations is used to predict future evolutions of river system sediment (dis)connectivity under different land-use scenarios. With this application, we showcase the D-CASCADE sediment (dis)connectivity model's effectiveness in quantifying basin scale sediment transport, delivery, and deposition through time and space. The integration of add-ons component for simulation of local morphological dynamics constitutes an important step to integrate modelling of large-scale connectivity processes with reconstructions of reach-scale alterations in a single, flexible framework and demonstrate how the firsts drive the others, and vice versa.

The application of the D-CASCADE model on the 3S system represents the first time a dynamic, basin-scale connectivity model explicitly accounts for reservoir water and sediment management when measuring estimates of catchment sediment yield. The estimation of the 3S total basin delivery demonstrates the potential of the new modelling framework to provide reasonable estimates of morphological parameters in data-scarce environments. Limited available estimates of sediment load from literature are used to narrow down the range of uncertainties on catchment sediment yield and identify a reasonable scenario based on the model output data. Specific add-ons components are devised and included in the framework to integrate the dynamic modelling of reservoir water and sediment storage. Other tools, instead, define the dam operational strategies and their impacts on the downstream hydrology, which will influence sediment transport in the main model loop. The model results demonstrate that even in the less impacting dam development scenarios analyzed, the sediment reduction from the tributaries influenced by the construction is reduced substantially (47%-85%). Coarse grain sizes are particularly affected by this reduction: sand delivery lowers by a minimum of 64% up to 97%. Repeated drawdown flushing on the 3S system are simulated for the most sustainable of the dam development scenario analysed. While flushing is effective in removing stored material in the reservoirs, the high sediment content of water inflow to the reservoirs means deposition rate greatly exceeds flushing removal rate. Nevertheless, annual sediment flushing in all reservoirs would results in a 8% increase in sediment yield to the outlet compared to the scenario without sediment management. The model output also highlight the necessity of careful synchronization between dams in series, as uncoordinated flushing initiatives may results increased sedimentation in the downstream reservoirs due to de-

position of upstream flushed materials.

7.2 Limitations and future research

The CASCADE toolbox and the D-CASCADE constitute useful modelling tools to tackle the "sediment delivery problem" at the basin scale. However, some key challenges remain, which may be addressed in future studies.

It is imperative to clarify that while D-CASCADE may be perceived as a direct upgrade of the original CASCADE and CASCADE toolbox, the two approaches vary in terms of sediment transport modelling structure, computational efforts, and data requirements which makes them more or less suited for applications in different case studies or for distinctive research objectives. The CASCADE toolbox approach returns a representation of sediment connectivity in a stationary state which is intended for preliminary screening of sediment transport and deposition in river network, and to identify interesting properties derived by interactions between network topology, morphology, hydrology, and sediment delivery, like sediment deposits, sinks, and choke-points. Moreover, its light computational load means multiple model runs can be performed in short timeframes, allowing for extensive sensitivity analysis to integrate uncertainties (Schmitt et al., 2018b; **?**), and perform multiple screening of different alterations portfolios (Schmitt et al., 2019, 2018a). D-CASCADE, instead, presents a heavier computation and memory load due to its daily time representation and deposit layer modelling. On a personal computer, for the same river network, a single CASCADE run typically takes less than a second, while running D-CASCADE for a single year may require minutes of computation. D-CASCADE is thus more suited for applications that focus on morphodynamic response to rapid alterations, typically caused by anthropic interventions on fluvial systems. D-CASCADE more complex structure means more parameters must be characterized, leading to a broader range of uncertainties and the need for extensive parameter characterization, validation, and sensitivity analyses.

In future applications, the two model could both be applied to the same case study. The CASCADE toolbox could be use its lighter computational time and data requirements to identify and quantify sediment transport patters at larger scales while incorporating uncertainties via Montecarlo simulations and sensitivity analysis. Afterwards, the D-CASCADE model could use the information extrapolated from the outputs of the CASCADE runs to reproduce dynamic sediment (dis)connectivity on a smaller section of the river network and explore competing strategies of water and sediment management for fluvial infrastructures.

Model structure and formulas

One of the design objectives of the CASCADE model, in all its iterations, is to guarantee computational efficiency and restricted data requirements to allow for repeated simulations, needed for detailed parameter sensitivity analysis and exploration of portfolios of decisions in strategic impact assessment studies. However, particularly for the D-CASCADE framework, the necessity for repeated loops on both the river reach and simulation timestep means that the computational time may grow substantially for large river networks and long time horizons, hindering the capacity for repeated model runs. As seen on the Bega and 3S river systems applications, a strategy for reducing computational time would be to skip simulation of timesteps characterized by low discharge, assuming sediment transport to be negligible in these instances. Alternatively, computation of reaches where sediment delivery is risible or that are out of the scope of the research objective may be discarded.

Another relevant problem for the D-CASCADE model is the memory requirement. In particular, deposit layer modelling as laid out in section 4.4.1 requires the storage of layer data for each timestep and each reach. Given that each layer is composed by a single cascade, large networks with hundreds of reaches the memory requirement may pose a significant problem. For example, for the 3S river system, the raw D-CASCADE output file for a single scenario of the unimpeded river network for 11 years of simulation (section 6.4.1) weight 5 GB. Changing the ID of the cascades from the single source reach to a cluster of neighboring reaches may reduce the memory requirement for representing sediment deposits.

All the applications of CASCADE and D-CASCADE presented in this thesis base their calculation of sediment budget on empirical sediment transport capacity equations, which are chosen according to the type of sediment considered, the knowledge of the system morphological properties and to maintain consistency with previous studies on the system. Thus, the output obtained assumes that these equations are appropriate to supply reasonable fractional transport rates for each sediment class. However, to be correct, this hypothesis should hold under the broad set of hydromorphological conditions observed in the network, including extreme hydrological events; and given the interaction between grains of different sizes and types. Evaluating the sensitivity of the model results on the empirical formulas of transport used may be necessary for forecasting or impact assessment studies, where the quantification of the sediment delivery is required to aid in informed decision-making on river management.

With its dynamic representation of sediment processes, D-CASCADE introduces more hypotheses on the parameters and formulas selected to calculate sediment budget and delivery. The formulation of sediment velocity is particu-

larly vulnerable to uncertainties due to its simple formulation and its reliance on parameters such as the vertical scale for sediment transport (eq 4.6) and active layer thickness (eq 4.3), which are themselves difficult to both characterized and reliably collect on the field on the scales needed for model use. Further studies on these parameters and their impacts on the model outputs are needed.

Finally, measurements of hydrological parameters, i.e., flow depth and mean flow velocity, in each reach are obtained by mean of the Manning-Strickler equation (Manning, 1891) for uniform, open channel flow, which is prone to errors in case of channel conditions differing from steady, deep flows (Ferguson, 2010). An alternative methodology to increase accuracy is to use the numerical step-methods employing the Strickler equation, like the hydrodynamic solver used in Schmitt et al. (2016). However, the iterative procedure would increase the computational time as data on depth and velocity are required for computation for each reach and each timestep.

Representation of hydromorphological processes

The inclusion of novel hydromorphological processes in the modelling framework of the CASCADE model is one of the critical tasks of the researches presented in this thesis. Future studies may expand on this objective by including new processes and increasing the representation accuracy of the one already present in the model.

Sediment supply to the network is among the most important and contentious parts of defining the modeling effort's boundary conditions. In this thesis, we presented three different methodologies to initialize sediment delivery and budget at the start of the simulation, all of which presents specific advantages and limitations. In the Vjosa case study, we assumed a balance in the source reach between sediment supply and transport capacity, meaning sediment flux carried by cascades in the source reaches were initialized as equal to the transport capacity of the channel. This hypothesis, also used in Schmitt et al. (2018b,a), is based on the general assumption that sources are in morphological equilibrium, which may not always be true in the case of sediment sinks where supply exceeds transport, or supply-limited reaches where the availability of material is the limiting factor for sediment transport. In the Bega river case study, we initialized all the material available for transport in the first timestep of the simulation as sediment storage in specific reaches. This method is coherent with the knowledge of the system, which showed that most of the sediment delivery processes were composed of material previously trapped in-channel and on the banks. Therefore, hillslopes delivery was considered negligible. Of course, this approach is only possible at the network scale in small and well-studied systems like the Bega river, where field studies have been conducted to reconstruct the extent of the sediment volumes release by channel incision

and bank expansion. On the 3S system, we employed basin-wide estimation of annual sediment yield from the hillslopes, based on lithological evidence, to initialize daily sediment delivery for each network reach according to direct drainage area and location (Kondolf et al., 2014b). This technique is based on large-scale estimations and does not require deep knowledge of the system, and therefore is bound to ignore local morphological features that may impact the sediment yield estimation. Moreover, the uniform partitioning of the annual yield to accommodate the daily model timestep does not consider the correlation between sediment detachment and delivery and the daily weather conditions, e.g., presence and intensity of precipitations and wind. The integration of empirical soil loss equations like USLE and RUSLE may help characterize daily hillslopes sediment detachment rate. Finally, a further step in consideration of hillslopes processes would be to integrate singular events of sediment delivery like rockfall and landslide, which could be represented as individual cascades entering a specific reach in a single timestep. The heterogeneous and intermittent delivery of material from these processes may be represented as a random process. For example, Czuba et al. (2017) modelled heterogeneous sediment delivery from bluff and ravines as a random Poisson process.

In the thesis, we also explore the morphological response of river channels to processes of sediment delivery, deposition, and entraining via specific add-ons components integrated into the modelling framework and operating at the reach level. These include the channel gradient add-on described in section 4.4.2 and the channel expansion and incision and overbank flooding add-ons presented for the Bega river network in section 5.3.3. The catalog of add-ons available for CASCADE can be expanded in future studies to further the representation of channel morphodynamic. For example, channel incision and expansion modelling in the Bega river is based on previous knowledge of the river system, thus specific to the case study. Alternatively, a specific add-on component could be defined to simulate bank erosion and subsequent mass failure brought by progressive removal of material from the bank toe, as seen in Lammers and Bledsoe (2018). Such a component would be based on empirical equations and, therefore, widely applicable. Other processes that could be represented are channel meandering, which would impact reach length and slope via lateral movement Lammers and Bledsoe (2018), and knickpoints migration, which would mobilize material in the channel bed and banks and change reach slope as the headcuts moves upstream.

Another critical dynamic with a profound impact on sediment (dis)connectivity is the interaction between channel and floodplains. The Bega case study focused only on the dampening effect on hydraulic forces during flood events and its impact on in-channel storages erosion. However, the extent of lateral interactions between floodplains and rivers is not limited

to this process. Floodplains typically behave like sediment sinks, sequestering material from the channels and storing it for a long extent of time. Thus, the interactions between these components may be further expanded by modelling floodplains as external sediment deposits linked to a specific river reach. These floodplains stores would be represented with the layered structure delineated in section 4.4, and would only connect to the main stream, and therefore exchange cascades with the network, during overbank flooding events, similarly to the modelization seen in (Gilbert and Wilcox, 2020).

Anthropic alterations impact assessment

In this thesis, we explored how river network (dis)connectivity may be impacted by the introduction of anthropic disturbances, in the form of sediment delivery reduction on the Vjosa river network, land use change in the Bega system and reservoirs inclusion and management in the 3S. Further studies may explore the effects of other alterations that affect sediment transport, e.g. gravel mining on the river banks and bed.

The original purpose of the D-CASCADE model is to provide a dynamic tool for sustainable sediment management in regulated rivers. The exploration of the effects of different sediment management strategies in series of reservoirs was performed in the 3S case study. However, the research results are based on assumptions and simplifications that may not hold in most real cases. For example, reservoir release schedules are based on simplistic strategies like rule curves or piecewise operating rules, which do not account, for example, for the energy demand and price or other secondary objectives like water supply for agricultural use or flood protection.

In any case, the results showcased so far demonstrated the effectiveness of D-CASCADE to explore the impact on sediment (dis)connectivity of different portfolios of basin-wide water resource management strategies. Hence, the next natural step will consists in the integration of D-CASCADE into optimization-based frameworks for strategic management of water resources, as it was the case for the original CASCADE model (Schmitt et al., 2018b, 2019). This time, however, the dynamic framework may allow the analysis to broader its scope from the simple reservoir siting to the full range of alternative water and sediment management strategies in reservoirs. Multiobjective evolutionary algorithms like BORG (Hadka and Reed, 2013) could be employed to derive optimal management portfolios from minimizing tradeoffs between multiple objectives. When considering, for example, hydropower generation along sediment transport, these optimization frameworks integrated with D-CASCADE would allow to identify and explore different scenarios of sustainable hydropower production for sediment connectivity conservation. Although this integration is outside the scopes of the thesis, it would, however be feasi-

ble employing well-known techniques that have successfully been applied for multi-objective optimal decision-making, without the need for further adaptations in both the D-CASCADE model and the optimization tools. The analysis may be further expanded to include other competing objectives, e.g. flood protection, agricultural demand, ecosystem protection, and more.

The 3S case study focused mostly on the cumulative network yield to the Mekong as an indicator of the sediment connectivity alterations. Future studies may instead employ more complex parameters, to consider not only sediment starvation at the outlet, but the distributed effects on the river network, with a particular focus on key reaches, like ecosystem hotspots or fragile morphological forms (Heckmann et al., 2018).

Finally, sediment management approaches in reservoir in D-CASCADE could be expanded by including other relevant strategies. These may include operations on the reservoir other than drawdown flushing, like pressure flushing, sluicing, dredging and dry excavation, or planning of support infrastructure for sediment management like sediment bypasses and off-channel storages.

7.3 Closing remarks

The study of network-scale river sediment (dis)connectivity and its impact on geomorphology, hydrology, biology and human livelihood have seen a small revolution in recent years thanks to the appearance of conceptual, numerical model which are able to characterize sediment routing in river network at large scale, thanks to increased availability in large-scale hydromorphological datasets. In this study, we contribute two modelling tools, the CASCADE toolbox and the D-CASCADE model, which conceptualize sediment delivery as a combination of individual sediment processes moving along a grid-like network. This modelling structure guarantees disaggregated informations on sediment flow in each section of the river, together with data on sediment provenance, type and behaviour. These framework are used to reconstruct and quantify alterations in sediment (dis)connectivity brought by anthropic alteration, as well as its impact on the network morphological features. Indicators of sediment regime alterations may be derived from these data, and included in integrated, multi-objective water resource planning and management to support sustainable decision making in complex and poorly understood river systems.

Bibliography

Abell, R., Thieme, M.L., Revenga, C., Bryer, M., Kottelat, M., Bogutskaya, N., Coad, B., Mandrak, N., Balderas, S.C., Bussing, W., et al., 2008. Freshwater ecoregions of the world: a new map of biogeographic units for freshwater biodiversity conservation. BioScience 58, 403–414.

Ackers, P., White, W.R., 1973. Sediment transport: new approach and analysis. Journal of the Hydraulics Division 99, 2041–2060.

Acreman, M., Arthington, A.H., Colloff, M.J., Couch, C., Crossman, N.D., Dyer, F., Overton, I., Pollino, C.A., Stewardson, M.J., Young, W., 2014. Environmental flows for natural, hybrid, and novel riverine ecosystems in a changing world. Frontiers in Ecology and the Environment 12, 466–473.

Almeida, R.M., Shi, Q., Gomes-Selman, J.M., Wu, X., Xue, Y., Angarita, H., Barros, N., Forsberg, B.R., García-Villacorta, R., Hamilton, S.K., et al., 2019. Reducing greenhouse gas emissions of amazon hydropower with strategic dam planning. Nature Communications 10, 1–9.

Ancey, C., 2020a. Bedload transport: a walk between randomness and determinism. part 1. the state of the art. Journal of Hydraulic Research 58, 1–17.

Ancey, C., 2020b. Bedload transport: a walk between randomness and determinism. part 2. challenges and prospects. Journal of Hydraulic Research 58, 18–33.

Andrews, E., Antweiler, R.C., 2012. Sediment fluxes from california coastal rivers: The influences of climate, geology, and topography. The Journal of Geology 120, 349–366.

Andrews, E.D., 1991. Sediment transport in the colorado river basin, in: Colorado River Ecology and Dam Management: Proceedings of a Symposium, May 24–25, 1990, Santa Fe, New Mexico, pp. 54–74.

Annandale, G., 2013. Climate resilient mekong: Sediment pass-through at lower se san 2. Tech. rep.,NHI, San Francisco. .

Ansar, A., Flyvbjerg, B., Budzier, A., Lunn, D., 2014. Should we build more large dams? the actual costs of hydropower megaproject development. Energy policy 69, 43–56.

Arias, M.E., Farinosi, F., Lee, E., Livino, A., Briscoe, J., Moorcroft, P.R., 2020. Impacts of climate change and deforestation on hydropower planning in the brazilian amazon. Nature Sustainability 3, 430–436.

Atkinson, E., 1996. The feasibility of flushing sediment from reservoirs .

Baran, E., Nasielski, J., 2011. Reservoir sediment flushing and fish resources. Report submitted by World Fish Center, Phnom Penh, Cambodia to Natural Heritage Institute, San Francisco, CA .

Belletti, B., de Leaniz, C.G., Jones, J., Bizzi, S., Börger, L., Segura, G., Castelletti, A., Van de Bund, W., Aarestrup, K., Barry, J., et al., 2020. More than one million barriers fragment europe's rivers. Nature 588, 436–441.

Benda, L., Dunne, T., 1997a. Stochastic forcing of sediment routing and storage in channel networks. Water Resources Research 33, 2865–2880.

Benda, L., Dunne, T., 1997b. Stochastic forcing of sediment supply to channel networks from landsliding and debris flow. Water Resources Research 33, 2849–2863.

Betrie, G.D., Mohamed, Y.A., van Griensven, A., Srinivasan, R., 2011. Sediment management modelling in the blue nile basin using swat model. Hydrology and Earth System Sciences 15, 807.

Beveridge, C., Istanbulluoglu, E., Bandaragoda, C., Pfeiffer, A.M., 2020. A channel network model for sediment dynamics over watershed management time scales. Journal of Advances in Modeling Earth Systems 12, e2019MS001852.

Bizzi, S., Dinh, Q., Bernardi, D., Denaro, S., Schippa, L., Soncini-Sessa, R., 2015. On the control of riverbed incision induced by run-of-river power plant. Water Resources Research 51, 5023–5040.

Bizzi, S., Pianosi, F., Soncini-Sessa, R., 2012. Valuing hydrological alteration in multi-objective water resources management. Journal of hydrology 472, 277–286.

Bizzi, S., Piégay, H., Demarchi, L., Van de Bund, W., Weissteiner, C., Gob, F., 2019. Lidar-based fluvial remote sensing to assess 50–100-year human-driven channel changes at a regional level: The case of the piedmont region, italy. Earth Surface Processes and Landforms 44, 471–489.

Bizzi, S., Tangi, M., Schmitt, R.J., Pitlick, J., Piégay, H., Castelletti, A.F., 2021. Sediment transport at the network scale and its link to channel morphology in the braided vjosa river system. Earth Surface Processes and Landforms 46, 2946–2962. doi:https://doi.org/10.1002/esp.5225.

Boix-Fayos, C., de Vente, J., Martínez-Mena, M., Barberá, G.G., Castillo, V., 2008. The impact of land use change and check-dams on catchment sediment yield. Hydrological Processes: An International Journal 22, 4922–4935.

Bracken, L.J., Turnbull, L., Wainwright, J., Bogaart, P., 2015. Sediment connectivity: a framework for understanding sediment transfer at multiple scales. Earth Surface Processes and Landforms 40, 177–188.

Bravard, J.P., Goichot, M., Tronchère, H., 2014. An assessment of sediment-transport processes in the lower mekong river based on deposit grain sizes, the cm technique and flow-energy data. Geomorphology 207, 174–189.

Briere, C., Giardino, A., van der Werf, J., 2011. Morphological modeling of bar dynamics with delft3d: the quest for optimal free parameter settings using an automatic calibration technique. Coastal Engineering Proceedings: sediment 1, 1–12.

Brierley, G.J., Cohen, T., Fryirs, K., Brooks, A., 1999. Post-European changes to the fluvial geomorphology of Bega catchment, Australia: implications for river ecology. Freshwater Biology 41, 839–848. URL: https://onlinelibrary.wiley.com/doi/abs/10.1046/j.1365-2427.1999.00397.x, doi:https://doi.org/10.1046/j.1365-2427.1999.00397.x. _eprint: https://onlinelibrary.wiley.com/doi/pdf/10.1046/j.1365-2427.1999.00397.x.

Brierley, G.J., Fryirs, K., 1998. A fluvial sediment budget for upper Wolumla Creek, south coast, New South Wales, Australia. Australian Geographer 29, 107–124. doi:10.1080/00049189808703206.

Brierley, G.J., Fryirs, K., 2000. River styles, a geomorphic approach to catchment characterization: Implications for river rehabilitation in Bega catchment, New South Wales, Australia. Environmental Management 25, 661–679. ISBN: 0364-152X Publisher: Springer.

Brierley, G.J., Fryirs, K.A., 2005. Geomorphology and river management: applications of the river styles framework. John Wiley & Sons.

Brierley, G.J., Fryirs, K.A., 2013. Geomorphology and river management: applications of the river styles framework. John Wiley & Sons.

Brismar, A., 2002. River systems as providers of goods and services: a basis for comparing desired and undesired effects of large dam projects. Environmental Management 29, 598–609.

Brooks, A.P., Brierley, G.J., 1997. Geomorphic responses of lower bega river to catchment disturbance, 1851–1926. Geomorphology 18, 291–304.

Buffington, J., Montgomery, D., 2013. Geomorphic classification of rivers. In: Shroder, J.; Wohl, E., ed. Treatise on Geomorphology; Fluvial Geomorphology, Vol. 9. San Diego, CA: Academic Press. p. 730-767. , 730–767.

Burnhill, T., 2009. Modelling the cumulative barrier and passage effects of mainstream hydropower dams on migratory fish populations in the Lower Mekong Basin. Mekong River Commission.

Candel, J., Kleinhans, M., Makaske, B., Wallinga, J., 2021. Predicting river channel pattern based on stream power, bed material and bank strength. Progress in Physical Geography: Earth and Environment 45, 253–278.

Carcaillet, J., Mugnier, J.L., Koçi, R., Jouanne, F., 2009. Uplift and active tectonics of southern albania inferred from incision of alluvial terraces. Quaternary Research 71, 465–476.

Cardno, 2018. Floodplain Risk Management Study - Bega River. Bega Valley Shire Council , 214doi:https://begavalley.nsw.gov.au/cp_content/resources/bega_brogo_rivers_final_FRMS(1).pdf.

Carling, P., 2009. Bdp scenario assessment specialist report: Geomorphology and sediment. Discharge and Sediment Monitoring Project 2009-2010, Information and Knowledge Management Programme .

Castelletti, A., Pianosi, F., Soncini-Sessa, R., 2008. Integration, participation and optimal control in water resources planning and management. Applied Mathematics and Computation 206, 21–33.

Castelletti, A., Yajima, H., Giuliani, M., Soncini-Sessa, R., Weber, E., 2014. Planning the optimal operation of a multioutlet water reservoir with water quality and quantity targets. Journal of Water Resources Planning and Management 140, 496–510.

Cavalli, M., Trevisani, S., Comiti, F., Marchi, L., 2013. Geomorphometric assessment of spatial sediment connectivity in small alpine catchments. Geomorphology 188, 31–41.

Cheung, A.K.L., O'sullivan, D., Brierley, G., 2015. Graph-assisted landscape monitoring. International Journal of Geographical Information Science 29, 580–605.

Chow, J., Kopp, R.J., Portney, P.R., 2003. Energy resources and global development. Science 302, 1528–1531.

Chowdhury, A.K., Dang, T.D., Nguyen, H.T., Koh, R., Galelli, S., 2021. The greater mekong's climate-water-energy nexus: How enso-triggered regional droughts affect power supply and co2 emissions. Earth's Future 9, e2020EF001814.

Church, M., 2006. Bed material transport and the morphology of alluvial river channels. Annu. Rev. Earth Planet. Sci. 34, 325–354.

Church, M., Ferguson, R., 2015. Morphodynamics: Rivers beyond steady state. Water Resources Research 51, 1883–1897.

Ciavola, P., 1999. Relation between river dynamics and coastal changes in albania: an assessment integrating satellite imagery with historical data. International Journal of Remote Sensing 20, 561–584.

Clément, M.P., Piégay, M.H., 2003. Les rivières torrentielles des montagnes drômoises: évolution contemporaine et fonctionnement géomorphologique actuel (massifs du diois et des baronnies) .

Consultative Group on International Agricultural Research, 2008. Srtm 90m digital elevation database v4.1 | cgiar-csi.

Coulthard, T.J., Van De Wiel, M.J., 2017. Modelling long term basin scale sediment connectivity, driven by spatial land use changes. Geomorphology 277, 265–281.

Covault, J.A., Craddock, W.H., Romans, B.W., Fildani, A., Gosai, M., 2013. Spatial and temporal variations in landscape evolution: Historic and longer-term sediment flux through global catchments. The Journal of Geology 121, 000–000.

Czuba, J.A., 2018. A lagrangian framework for exploring complexities of mixed-size sediment transport in gravel-bedded river networks. Geomorphology 321, 146–152.

Czuba, J.A., Foufoula-Georgiou, E., 2014. A network-based framework for identifying potential synchronizations and amplifications of sediment delivery in river basins. Water Resources Research 50, 3826–3851.

Czuba, J.A., Foufoula-Georgiou, E., 2015. Dynamic connectivity in a fluvial network for identifying hotspots of geomorphic change. Water Resources Research 51, 1401–1421.

Czuba, J.A., Foufoula-Georgiou, E., Gran, K.B., Belmont, P., Wilcock, P.R., 2017. Interplay between spatially explicit sediment sourcing, hierarchical river-network structure, and in-channel bed material sediment transport and storage dynamics. Journal of Geophysical Research: Earth Surface 122, 1090–1120.

Dang, T.D., Chowdhury, A., Galelli, S., 2020. On the representation of water reservoir storage and operations in large-scale hydrological models: implications on model parameterization and climate change impact assessments. Hydrology and Earth System Sciences 24, 397–416.

Demarchi, L., Bizzi, S., Piégay, H., 2017. Regional hydromorphological characterization with continuous and automated remote sensing analysis based on vhr imagery and low-resolution lidar data. Earth Surface Processes and Landforms 42, 531–551.

Demarty, M., Bastien, J., 2011. Ghg emissions from hydroelectric reservoirs in tropical and equatorial regions: Review of 20 years of ch4 emission measurements. Energy Policy 39, 4197–4206.

Detert, M., Weitbrecht, V., 2013. User guide to gravelometric image analysis by basegrain. Advances in Science and Research; Fukuoka, S., Nakagawa, H., Sumi, T., Zhang, H., Eds , 1789–1795.

Dufour, S., Rinaldi, M., Piégay, H., Michalon, A., 2015. How do river dynamics and human influences affect the landscape pattern of fluvial corridors? lessons from the magra river, central–northern italy. Landscape and Urban Planning 134, 107–118.

Dyson, M., Bergkamp, G., Scanlon, J., 2003. Flow: the essentials of environmental flows. IUCN, Gland, Switzerland and Cambridge, UK , 20–87.

Eaton, B., Millar, R.G., Davidson, S., 2010. Channel patterns: Braided, anabranching, and single-thread. Geomorphology 120, 353–364.

Engelund, F., Hansen, E., 1967. A monograph on sediment transport in alluvial streams. Technical University of Denmark 0stervoldgade 10, Copenhagen K. .

Fehr, R., 1987. Einfache bestimmung der korngrössenverteilung von geschiebematerial mit hilfe der linienzahlanalyse. Tec21 105, 1104–1109.

Ferguson, R., 1981. Channel form and channel changes. British rivers 90, 125.

Ferguson, R., 2010. Time to abandon the manning equation? Earth Surface Processes and Landforms 35, 1873–1876.

Ferguson, R., Church, M., Rennie, C., Venditti, J., 2015. Reconstructing a sediment pulse: Modeling the effect of placer mining on fraser river, canada. Journal of Geophysical Research: Earth Surface 120, 1436–1454.

Forzieri, G., Feyen, L., Rojas, R., Flörke, M., Wimmer, F., Bianchi, A., 2014. Ensemble projections of future streamflow droughts in europe. Hydrology and Earth System Sciences 18, 85–108.

Fouache, E., Gruda, G., Mucaj, S., Nikolli, P., 2001. Recent geomorphological evolution of the deltas of the rivers seman and vjosa, albania. Earth Surface Processes and Landforms: The Journal of the British Geomorphological Research Group 26, 793–802.

Frasson, R.P.d.M., Pavelsky, T.M., Fonstad, M.A., Durand, M.T., Allen, G.H., Schumann, G., Lion, C., Beighley, R.E., Yang, X., 2019. Global relationships between river width, slope, catchment area, meander wavelength, sinuosity, and discharge. Geophysical Research Letters 46, 3252–3262.

Frings, R.M., 2008. Downstream fining in large sand-bed rivers. Earth-Science Reviews 87, 39–60.

Fryirs, K., 2013. (Dis)Connectivity in catchment sediment cascades: a fresh look at the sediment delivery problem. Earth Surface Processes and Landforms 38, 30–46. doi:10.1002/esp.3242.

Fryirs, K., Brierley, G.J., 1998. The character and age structure of valley fills in upper Wolumla Creek catchment, south coast, New South Wales, Australia. Earth Surface Processes and Landforms 23, 271–287. URL: https://onlinelibrary.wiley.com/doi/abs/10.1002/%28SICI%291096-9837%28199803%2923%3A3%3C271%3A%3AAID-ESP867%3E3.0.CO%3B2-5, doi:https://doi.org/10.1002/(SICI)1096-9837(199803)23:3<271::AID-ESP867>3.0.CO;2-5.

Fryirs, K., Brierley, G.J., 1999. Slope–channel decoupling in Wolumla catchment, New South Wales, Australia: the changing nature of sediment sources following European settlement. CATENA 35, 41–63. doi:10.1016/S0341-8162(98)00119-2.

Fryirs, K., Brierley, G.J., 2001. Variability in sediment delivery and storage along river courses in Bega catchment, NSW, Australia: implications for geomorphic river recovery. Geomorphology 38, 237–265. doi:10.1016/S0169-555X(00)00093-3.

Fryirs, K.A., 2017. River sensitivity: A lost foundation concept in fluvial geomorphology. Earth Surface Processes and Landforms 42, 55–70.

Fryirs, K.A., Brierley, G.J., Hancock, F., Cohen, T.J., Brooks, A.P., Reinfelds, I., Cook, N., Raine, A., 2018. Tracking geomorphic recovery in process-based river management. Land Degrad Dev 29, 3221–3244. URL: http://doi.wiley.com/10.1002/ldr.2984, doi:10.1002/ldr.2984.

Fryirs, K.A., Brierley, G.J., Preston, N.J., Kasai, M., 2007. Buffers, barriers and blankets: the (dis) connectivity of catchment-scale sediment cascades. Catena 70, 49–67. ISBN: 0341-8162 Publisher: Elsevier.

Fryirs, K.A., Wheaton, J.M., Bizzi, S., Williams, R., Brierley, G.J., 2019. To plug-in or not to plug-in? geomorphic analysis of rivers using the river styles framework in an era of big data acquisition and automation. Wiley Interdisciplinary Reviews: Water 6, e1372.

Gallup, J.L., Sachs, J.D., Mellinger, A.D., 1999. Geography and economic development. International regional science review 22, 179–232.

Gilbert, J.T., Wilcox, A.C., 2020. Sediment routing and floodplain exchange (serfe): A spatially explicit model of sediment balance and connectivity through river networks. Journal of Advances in Modeling Earth Systems 12, e2020MS002048.

Gilvear, D.J., Spray, C.J., Casas-Mulet, R., 2013. River rehabilitation for the delivery of multiple ecosystem services at the river network scale. Journal of environmental management 126, 30–43.

Giuliani, M., Herman, J.D., Castelletti, A., Reed, P., 2014. Many-objective reservoir policy identification and refinement to reduce policy inertia and myopia in water management. Water resources research 50, 3355–3377.

Gran, K.B., Czuba, J.A., 2017. Sediment pulse evolution and the role of network structure. Geomorphology 277, 17–30.

Gregory, K.J., 2019. Human influence on the morphological adjustment of river channels: The evolution of pertinent concepts in river science. River Research and Applications 35, 1097–1106.

Grill, G., Lehner, B., Lumsdon, A.E., MacDonald, G.K., Zarfl, C., Liermann, C.R., 2015. An index-based framework for assessing patterns and trends in river fragmentation and flow regulation by global dams at multiple scales. Environmental Research Letters 10, 015001.

Gurnell, A., Rinaldi, M., Belletti, B., Bizzi, S., Blamauer, B., Braca, G., Buijse, A., Bussettini, M., Camenen, B., Comiti, F., et al., 2016. A multi-scale hierarchical framework for developing understanding of river behaviour to support river management. Aquatic sciences 78, 1–16.

Hackney, C.R., Darby, S.E., Parsons, D.R., Leyland, J., Best, J.L., Aalto, R., Nicholas, A.P., Houseago, R.C., 2020. River bank instability from unsustainable sand mining in the lower mekong river. Nature Sustainability 3, 217–225.

Hadka, D., Reed, P., 2013. Borg: An auto-adaptive many-objective evolutionary computing framework. Evolutionary computation 21, 231–259.

Hadka, D., Reed, P., 2015. Large-scale parallelization of the Borg multiobjective evolutionary algorithm to enhance the management of complex environmental systems. Environmental Modelling & Software 69, 353–369.

Hassan, M.A., Church, M., Schick, A.P., 1991. Distance of movement of coarse particles in gravel bed streams. Water Resources Research 27, 503–511.

Heckmann, T., Cavalli, M., Cerdan, O., Foerster, S., Javaux, M., Lode, E., Smetanová, A., Vericat, D., Brardinoni, F., 2018. Indices of sediment connectivity: opportunities, challenges and limitations. Earth-Science Reviews 187, 77–108.

Heckmann, T., Schwanghart, W., 2013. Geomorphic coupling and sediment connectivity in an alpine catchment—exploring sediment cascades using graph theory. Geomorphology 182, 89–103.

Heckmann, T., Schwanghart, W., Phillips, J.D., 2015. Graph theory—recent developments of its application in geomorphology. Geomorphology 243, 130–146.

Hohensinner, S., Egger, G., Muhar, S., Vaudor, L., Piégay, H., 2021. What remains today of pre-industrial alpine rivers? census of historical and current channel patterns in the alps. River Research and Applications 37, 128–149.

Horner, G.J., Baker, P.J., Mac Nally, R., Cunningham, S.C., Thomson, J.R., Hamilton, F., 2010. Forest structure, habitat and carbon benefits from thinning floodplain forests: managing early stand density makes a difference. Forest ecology and management 259, 286–293.

Hortle, K.G., 2009. Fisheries of the mekong river basin, in: The Mekong. Elsevier, pp. 197–249.

Hsu, S.M., Holly Jr, F.M., 1992. Conceptual bed-load transport model and verification for sediment mixtures. Journal of Hydraulic Engineering 118, 1135–1152.

Imhof, A., Lanza, G.R., 2012. World rivers review. World Watch 28.

International Energy Agency, 2015. World energy outlook special report on southeast asia. France International Energy Agency (IEA) .

Jager, H.I., Efroymson, R.A., Opperman, J.J., Kelly, M.R., 2015. Spatial design principles for sustainable hydropower development in river basins. Renewable and Sustainable Energy Reviews 45, 808–816.

Jager, H.I., Smith, B.T., 2008. Sustainable reservoir operation: can we generate hydropower and preserve ecosystem values? River research and Applications 24, 340–352.

James, L.D., 2015. Man and Water: The Social Sciences in Management of Water Resources. University Press of Kentucky.

Jansen, R.B., 2012. Advanced dam engineering for design, construction, and rehabilitation. Springer Science & Business Media.

Jansson, M.B., Erlingsson, U., 2000. Measurement and quantification of a sedimentation budget for a reservoir with regular flushing. Regulated Rivers: Research & Management: An International Journal Devoted to River Research and Management 16, 279–306.

Kantoush, S., Sumi, T., 2010. River morphology and sediment management strategies for sustainable reservoir in japan and switzerland. Annuals of Disaster Prevention Research Institute .

Keesstra, S., Nunes, J.P., Saco, P., Parsons, T., Poeppl, R., Masselink, R., Cerdà, A., 2018. The way forward: can connectivity be useful to design better measuring and modelling schemes for water and sediment dynamics? Science of the Total Environment 644, 1557–1572.

Khan, S., Fryirs, K., Bizzi, S., 2021. Modelling sediment (dis) connectivity across a river network to understand locational-transmission-filter sensitivity for identifying hotspots of potential geomorphic adjustment. Earth Surface Processes and Landforms .

Knighton, D., 1998. Fluvial forms and processes: A new perspective, arnold, london. Kolb, EJ, and KL Tanaka (2001), Geologic history of the polar regions of Mars based .

Koehnken, L., 2012. Discharge and sediment monitoring program—program review & data analysis. part 1: Program review & recommendations. Vientiane, Laos PDR: Mekong River Commission .

Koehnken, L., 2014. Discharge sediment monitoring project (dsmp) 2009–2013 summary and analysis of results. Final Report .

Kokubo, T., 1997. Predicting methods and actual result on flushing of accumulated deposits from dasidaira reservoir. ICOLD 19th 74.

Kondolf, G.M., 1994. Geomorphic and environmental effects of instream gravel mining. Landscape and Urban Planning 28, 225–243.

Kondolf, G.M., 1997. Hungry water: effects of dams and gravel mining on river channels. Environmental management 21, 533–551.

Kondolf, G.M., 2000. Assessing salmonid spawning gravel quality. Transactions of the American fisheries Society 129, 262–281.

Kondolf, G.M., Gao, Y., Annandale, G.W., Morris, G.L., Jiang, E., Zhang, J., Cao, Y., Carling, P., Fu, K., Guo, Q., et al., 2014a. Sustainable sediment management in reservoirs and regulated rivers: Experiences from five continents. Earth's Future 2, 256–280.

Kondolf, G.M., Lisle, T.E., Wolman, G.M., 2003. Bed sediment measurement. Tools in fluvial geomorphology 347, 395.

Kondolf, G.M., Rubin, Z.K., Minear, J., 2014b. Dams on the mekong: Cumulative sediment starvation. Water Resources Research 50, 5158–5169.

Kondolf, G.M., Schmitt, R.J., Carling, P., Darby, S., Arias, M., Bizzi, S., Castelletti, A., Cochrane, T.A., Gibson, S., Kummu, M., et al., 2018. Changing sediment budget of the mekong: Cumulative threats and management strategies for a large river basin. Science of the total environment 625, 114–134.

Krumbein, W.C., Aberdeen, E., 1937. The sediments of barataria bay. Journal of Sedimentary Research 7.

Kuby, M.J., Fagan, W.F., ReVelle, C.S., Graf, W.L., 2005. A multiobjective optimization model for dam removal: an example trading off salmon passage with hydropower and water storage in the willamette basin. Advances in Water Resources 28, 845–855.

Kummu, M., Lu, X.X., Wang, J.J., Varis, O., 2010. Basin-wide sediment trapping efficiency of emerging reservoirs along the mekong. Geomorphology 119, 181–197.

Lamb, M.P., Dietrich, W.E., Venditti, J.G., 2008. Is the critical shields stress for incipient sediment motion dependent on channel-bed slope? Journal of Geophysical Research: Earth Surface 113.

Lammers, R.W., Bledsoe, B.P., 2018. A network scale, intermediate complexity model for simulating channel evolution over years to decades. Journal of Hydrology 566, 886–900.

Larinier, M., 2000. Dams and fish migration. World Commission on Dams, Toulouse, France .

Larinier, M., 2001. Environmental issues, dams and fish migration. FAO fisheries technical paper 419, 45–89.

Latrubesse, E.M., Arima, E.Y., Dunne, T., Park, E., Baker, V.R., d'Horta, F.M., Wight, C., Wittmann, F., Zuanon, J., Baker, P.A., et al., 2017. Damming the rivers of the amazon basin. Nature 546, 363–369.

Lauer, J.W., Viparelli, E., Piégay, H., 2016. Morphodynamics and sediment tracers in 1-d (mast-1d): 1-d sediment transport that includes exchange with an off-channel sediment reservoir. Advances in Water Resources 93, 135–149.

Lauri, H., Moel, H.d., Ward, P.J., Räsänen, T.A., Keskinen, M., Kummu, M., 2012. Future changes in mekong river hydrology: impact of climate change and reservoir operation on discharge. Hydrology and Earth System Sciences 16, 4603–4619.

Lee, C., Foster, G., 2013. Assessing the potential of reservoir outflow management to reduce sedimentation using continuous turbidity monitoring and reservoir modelling. Hydrological Processes 27, 1426–1439.

Lehner, B., Liermann, C.R., Revenga, C., Vörösmarty, C., Fekete, B., Crouzet, P., Döll, P., Endejan, M., Frenken, K., Magome, J., et al., 2011. High-resolution mapping of the world's reservoirs and dams for sustainable river-flow management. Frontiers in Ecology and the Environment 9, 494–502.

Liébault, F., Piégay, H., 2001. Assessment of channel changes due to long-term bedload supply decrease, roubion river, france. Geomorphology 36, 167–186.

Liermann, C.R., Nilsson, C., Robertson, J., Ng, R.Y., 2012. Implications of dam obstruction for global freshwater fish diversity. BioScience 62, 539–548.

Ligon, F.K., Dietrich, W.E., Trush, W.J., 1995. Downstream ecological effects of dams. BioScience 45, 183–192.

Liu, J., Mason, P., Clerici, N., Chen, S., Davis, A., Miao, F., Deng, H., Liang, L., 2004. Landslide hazard assessment in the three gorges area of the yangtze river using aster imagery: Zigui–badong. Geomorphology 61, 171–187.

Lu, D., Li, G., Valladares, G.S., Batistella, M., 2004. Mapping soil erosion risk in rondonia, brazilian amazonia: using rusle, remote sensing and gis. Land degradation & development 15, 499–512.

Lugo, G., Bertoldi, W., Henshaw, A., Gurnell, A., 2015. The effect of lateral confinement on gravel bed river morphology. Water Resources Research 51, 7145–7158.

Magilligan, F.J., Nislow, K.H., 2005. Changes in hydrologic regime by dams. Geomorphology 71, 61–78.

Manning, R., 1891. On the flow of water in open channels and pipes: Institute of civil engineers of ireland transactions, v. 20 .

Mendoza, G.A., Martins, H., 2006. Multi-criteria decision analysis in natural resource management: A critical review of methods and new modelling paradigms. Forest ecology and management 230, 1–22.

Merritt, W.S., Letcher, R.A., Jakeman, A.J., 2003. A review of erosion and sediment transport models. Environmental Modelling & Software 18, 761–799.

Meybeck, M., Vörösmarty, C., 2005. Fluvial filtering of land-to-ocean fluxes: from natural holocene variations to anthropocene. Comptes Rendus Geoscience 337, 107–123.

Meyer-Peter, E., Müller, R., 1948. Formulas for bed-load transport, in: IAHSR 2nd meeting, Stockholm, appendix 2, IAHR.

Millar, R.G., 2005. Theoretical regime equations for mobile gravel-bed rivers with stable banks. Geomorphology 64, 207–220.

Millennium Ecosystem Assessment, 2005. Ecosystem and human well-being: biodiversity synthesis.

Milliman, J.D., Farnsworth, K.L., 2011. Runoff, erosion, and delivery to the coastal ocean. River discharge to the coastal ocean: a global synthesis, Cambridge University Press, Cambridge, UK , 13–69.

Milliman, J.D., Meade, R.H., 1983. World-wide delivery of river sediment to the oceans. The Journal of Geology 91, 1–21.

Mizuyama, T., 2008. Structural countermeasures for debris flow disasters. International Journal of Erosion Control Engineering 1, 38–43.

Molinas, A., Wu, B., 2000. Comparison of fractional bed-material load computation methods in sand-bed channels. Earth Surface Processes and Landforms: The Journal of the British Geomorphological Research Group 25, 1045–1068.

Molinas, A., Yang, C.T., 1986. Computer program user's manual for GSTARS (generalized stream tube model for alluvial river simulation). US Department of Interior, Bureau of Reclamation, Engineering and Research ….

Morris, P., Williams, D., 1999. A worldwide correlation for exponential bed particle size variation in subaerial aqueous flows. Earth Surface Processes and Landforms: The Journal of the British Geomorphological Research Group 24, 835–847.

MRC (Mekong River Commission), 2014a. Hydropower project database. Basin Development Plan Programme .

MRC (Mekong River Commission), 2014b. Hydropower project database. Basin Development Plan Programme .

MRC (Mekong River Commission), 2019. Basin-wide assessment of climate change impacts on hydropower production. Basin Development Plan Programme .

Mueller, E.R., Pitlick, J., 2013. Sediment supply and channel morphology in mountain river systems: 1. relative importance of lithology, topography, and climate. Journal of Geophysical Research: Earth Surface 118, 2325–2342.

Mueller, E.R., Pitlick, J., 2014. Sediment supply and channel morphology in mountain river systems: 2. single thread to braided transitions. Journal of Geophysical Research: Earth Surface 119, 1516–1541.

Mueller, E.R., Pitlick, J., Nelson, J.M., 2005. Variation in the reference shields stress for bed load transport in gravel-bed streams and rivers. Water Resources Research 41.

Mueller, E.R., Smith, M.E., Pitlick, J., 2016. Lithology-controlled evolution of stream bed sediment and basin-scale sediment yields in adjacent mountain watersheds, idaho, usa. Earth Surface Processes and Landforms 41, 1869–1883.

Murphy, B.P., Czuba, J.A., Belmont, P., 2019. Post-wildfire sediment cascades: A modeling framework linking debris flow generation and network-scale sediment routing. Earth Surface Processes and Landforms 44, 2126–2140.

Næsje, T., Jonssons, B., Skurdal, J., 1995. Spring flood: a primary cue for hatching of river spawning coregoninae. Canadian Journal of Fisheries and Aquatic Sciences 52, 2190–2196.

Naiman, R.J., Bilby, R.E., Bisson, P.A., 2000. Riparian ecology and management in the pacific coastal rain forest. BioScience 50, 996–1011.

Nicholas, A., Ashworth, P., Kirkby, M., Macklin, M., Murray, T., 1995. Sediment slugs: large-scale fluctuations in fluvial sediment transport rates and storage volumes. Progress in physical geography 19, 500–519.

Nittrouer, J.A., Viparelli, E., 2014. Sand as a stable and sustainable resource for nourishing the mississippi river delta. Nature Geoscience 7, 350–354.

Opperman, J., Grill, G., Hartmann, J., 2017. The power of rivers: Finding balance between energy and conservation in hydropower development. .

Orr, S., Pittock, J., Chapagain, A., Dumaresq, D., 2012. Dams on the mekong river: Lost fish protein and the implications for land and water resources. Global Environmental Change 22, 925–932.

Otto, J.C., Schrott, L., Jaboyedoff, M., Dikau, R., 2009. Quantifying sediment storage in a high alpine valley (turtmanntal, switzerland). Earth Surface Processes and Landforms: The Journal of the British Geomorphological Research Group 34, 1726–1742.

Palmieri, A., Shah, F., Annandale, G., Dinar, A., 2003. Reservoir conservation volume i: the rescon approach. Washington, DC: World Bank .

Palmieri, A., Shah, F., Dinar, A., 2001. Economics of reservoir sedimentation and sustainable management of dams. Journal of environmental management 61, 149–163.

Parker, G., Klingeman, P.C., 1982. On why gravel bed streams are paved. Water Resources Research 18, 1409–1423.

Parsons, A.J., Bracken, L., Poeppl, R.E., Wainwright, J., Keesstra, S.D., 2015. Introduction to special issue on connectivity in water and sediment dynamics. Earth Surface Processes and Landforms 40, 1275–1277.

Paulsen, C.M., Wernstedt, K., 1995. Cost-effectiveness analysis for complex managed hydrosystems: an application to the columbia river basin. Journal of Environmental Economics and Management 28, 388–400.

Peters, R., Berlekamp, J., Lucía, A., Stefani, V., Tockner, K., Zarfl, C., 2021. Integrated impact assessment for sustainable hydropower planning in the vjosa catchment (greece, albania). Sustainability 13, 1514.

Pfeiffer, A.M., Barnhart, K.R., Czuba, J.A., et al., 2020. Networksedimenttransporter: A landlab component for bed material transport through river networks. Journal of Open Source Software 5, 2341.

Piegay, H., Alber, A., Slater, L., Bourdin, L., 2009. Census and typology of braided rivers in the french alps. Aquatic Sciences 71, 371.

Pilgrim, E., Institution of Engineers, A., Pilgrim, D., Canterford, R., 1987. Australian rainfall and runoff. Institution of Engineers, Australia.

Piman, T., Cochrane, T., Arias, M., Green, A., Dat, N., 2013. Assessment of flow changes from hydropower development and operations in sekong, sesan, and srepok rivers of the mekong basin. Journal of Water Resources Planning and Management 139, 723–732.

Piman, T., Cochrane, T.A., Arias, M.E., 2016. Effect of proposed large dams on water flows and hydropower production in the sekong, sesan and srepok rivers of the mekong basin. River Research and applications 32, 2095–2108.

Poeppl, R.E., Fryirs, K.A., Tunnicliffe, J., Brierley, G.J., 2020. Managing sediment (dis) connectivity in fluvial systems. Science of The Total Environment 736, 139627.

Poeppl, R.E., Keesstra, S.D., Maroulis, J., 2017. A conceptual connectivity framework for understanding geomorphic change in human-impacted fluvial systems. Geomorphology 277, 237–250.

Poole, G.C., 2002. Fluvial landscape ecology: addressing uniqueness within the river discontinuum. Freshwater biology 47, 641–660.

Rahuel, J., Holly, F., Chollet, J., Belleudy, P., Yang, G., 1989. Modeling of riverbed evolution for bedload sediment mixtures. Journal of Hydraulic Engineering 115, 1521–1542.

Ranzi, R., Le, T.H., Rulli, M.C., 2012. A rusle approach to model suspended sediment load in the lo river (vietnam): Effects of reservoirs and land use changes. Journal of Hydrology 422, 17–29.

Räsänen, T.A., Kummu, M., 2013. Spatiotemporal influences of enso on precipitation and flood pulse in the mekong river basin. Journal of Hydrology 476, 154–168.

Reid, H., Brierley, G., 2015. Assessing geomorphic sensitivity in relation to river capacity for adjustment. Geomorphology 251, 108–121.

Renard, K.G., 1997. Predicting soil erosion by water: a guide to conservation planning with the Revised Universal Soil Loss Equation (RUSLE). United States Government Printing.

Richter, B.D., Baumgartner, J.V., Powell, J., Braun, D.P., 1996. A method for assessing hydrologic alteration within ecosystems. Conservation biology 10, 1163–1174.

Richter, B.D., Postel, S., Revenga, C., Scudder, T., Lehner, B., Churchill, A., Chow, M., 2010. Lost in development's shadow: The downstream human consequences of dams. Water Alternatives 3, 14.

Rinaldi, M., Surian, N., Comiti, F., Bussettini, M., 2013. A method for the assessment and analysis of the hydromorphological condition of italian streams: The morphological quality index (mqi). Geomorphology 180, 96–108.

Rizzoli, P., Martone, M., Gonzalez, C., Wecklich, C., Tridon, D.B., Bräutigam, B., Bachmann, M., Schulze, D., Fritz, T., Huber, M., et al., 2017. Generation and performance assessment of the global tandem-x digital elevation model. ISPRS Journal of Photogrammetry and Remote Sensing 132, 119–139.

Rosenberg, D.M., Berkes, F., Bodaly, R., Hecky, R., Kelly, C., Rudd, J.W., 1997. Large-scale impacts of hydroelectric development. Environmental Reviews 5, 27–54.

Roux, C., Alber, A., Bertrand, M., Vaudor, L., Piégay, H., 2015. "fluvialcorridor": A new arcgis toolbox package for multiscale riverscape exploration. Geomorphology 242, 29–37.

Sarkkula, J., Koponen, J., Lauri, H., Virtanen, M., 2010a. Mekong river commission (mrc)/information and knowledge management program detailed modelling support (dms) project: Origin, fate and impacts of the mekong sediments. Mekong River Commission, Vientiane, Lao PDR 53.

Sarkkula, J., Koponen, J., Lauri, H., Virtanen, M., 2010b. Origin, fate and role of mekong sediments. DMS Work Package 02/2 .

Schiemer, F., Drescher, A., Hauer, C., Schwarz, U., 2018. The vjosa river corridor: a riverine ecosystem of european significance. Acta ZooBot Austria 155, 1–40.

Schmitt, R., Bizzi, S., Castelletti, A., 2014. Characterizing fluvial systems at basin scale by fuzzy signatures of hydromorphological drivers in data scarce environments. Geomorphology 214, 69–83.

Schmitt, R., Bizzi, S., Castelletti, A., Kondolf, G., 2018a. Improved trade-offs of hydropower and sand connectivity by strategic dam planning in the mekong. Nature Sustainability 1, 96.

Schmitt, R., Rubin, Z., Kondolf, G., 2017. Losing ground-scenarios of land loss as consequence of shifting sediment budgets in the mekong delta. Geomorphology 294, 58–69.

Schmitt, R.J., Bizzi, S., Castelletti, A., 2016. Tracking multiple sediment cascades at the river network scale identifies controls and emerging patterns of sediment connectivity. Water Resources Research 52, 3941–3965.

Schmitt, R.J., Bizzi, S., Castelletti, A., Opperman, J., Kondolf, G.M., 2019. Planning dam portfolios for low sediment trapping shows limits for sustainable hydropower in the mekong. Science advances 5, eaaw2175.

Schmitt, R.J., Bizzi, S., Castelletti, A.F., Kondolf, G., 2018b. Stochastic modeling of sediment connectivity for reconstructing sand fluxes and origins in the unmonitored se kong, se san, and sre pok tributaries of the mekong river. Journal of Geophysical Research: Earth Surface 123, 2–25.

Schmitt, R.J., Kittner, N., Kondolf, G.M., Kammen, D.M., 2021. Joint strategic energy and river basin planning to reduce dam impacts on rivers in myanmar. Environmental Research Letters 16, 054054.

Schmitt, R.J.P., 2016. CASCADE - A framework for modeling fluvial sediment connectivity and its application for designing low impact hydropower portfolios. Phd thesis. Politecnico di Milano, Dipartimento di Elettronica, Informazione e Bioingegneria (DEIB).

Schmitt, R.J.P., 2017. Cascade-a framework for modeling fluvial sediment connectivity and its application for designing low impact hydropower portfolios .

Schumm, S.A., 1985. Patterns of alluvial rivers. Annual Review of Earth and Planetary Sciences 13, 5–27.

Schwanghart, W., Kuhn, N.J., 2010. Topotoolbox: A set of matlab functions for topographic analysis. Environmental Modelling & Software 25, 770–781.

Schwanghart, W., Scherler, D., 2014. Topotoolbox 2–matlab-based software for topographic analysis and modeling in earth surface sciences. Earth Surface Dynamics 2, 1–7.

Shih, S.M., Komar, P.D., 1990. Differential bedload transport rates in a gravel-bed stream: A grain-size distribution approach. Earth Surface Processes and Landforms 15, 539–552.

Sholtes, J.S., Doyle, M.W., 2011. Effect of channel restoration on flood wave attenuation. Journal of Hydraulic Engineering 137, 196–208.

Shrestha, B., Cochrane, T.A., Caruso, B.S., Arias, M.E., Wild, T.B., 2021. Sediment management for reservoir sustainability and cost implications under land use/land cover change uncertainty. Water Resources Research 57, e2020WR028351.

Simon, A., Rinaldi, M., 2006. Disturbance, stream incision, and channel evolution: The roles of excess transport capacity and boundary materials in controlling channel response. Geomorphology 79, 361–383.

Sivapragasam, C., Vasudevan, G., Maran, J., Bose, C., Kaza, S., Ganesh, N., 2009. Modeling evaporation-seepage losses for reservoir water balance in semi-arid regions. Water resources management 23, 853.

Sklar, L.S., Riebe, C.S., Marshall, J.A., Genetti, J., Leclere, S., Lukens, C.L., Merces, V., 2017. The problem of predicting the size distribution of sediment supplied by hillslopes to rivers. Geomorphology 277, 31–49.

Snelder, T.H., Lamouroux, N., Pella, H., 2011. Empirical modelling of large scale patterns in river bed surface grain size. Geomorphology 127, 189–197.

Soncini-Sessa, R., Weber, E., Castelletti, A., 2007. Integrated and participatory water resources management-theory. Elsevier.

Stevens, M.A., 2000. Reservoir sedimentation handbook—design and management of dams, reservoirs, and watershed for sustainable use. Journal of Hydraulic Engineering 126, 481–482.

Stroffek, S., Amoros, C., Zylberblat, M., 1996. La logique de réhabilitation physique appliquée à un grand fleuve: le rhône/a methodology for physical restoration applied to a major river: the rhône. Géocarrefour 71, 287–296.

Sumi, T., 2008. Evalutation of efficiency of reservoir sediment flushing in kurobe river, in: Proceedings 4th International Conference on Scour and Erosion (ICSE-4). November 5-7, 2008, Tokyo, Japan, pp. 608–613.

Surian, N., Rinaldi, M., 2003. Morphological response to river engineering and management in alluvial channels in italy. Geomorphology 50, 307–326.

Syvitski, J.P., Kettner, A.J., Overeem, I., Hutton, E.W., Hannon, M.T., Brakenridge, G.R., Day, J., Vörösmarty, C., Saito, Y., Giosan, L., et al., 2009. Sinking deltas due to human activities. Nature Geoscience 2, 681–686.

Syvitski, J.P., Milliman, J.D., 2007. Geology, geography, and humans battle for dominance over the delivery of fluvial sediment to the coastal ocean. The Journal of Geology 115, 1–19.

Syvitski, J.P., Peckham, S.D., Hilberman, R., Mulder, T., 2003. Predicting the terrestrial flux of sediment to the global ocean: a planetary perspective. Sedimentary Geology 162, 5–24.

Tabarestani, M.K., Zarrati, A., 2015. Sediment transport during flood event: a review. International Journal of Environmental Science and Technology 12, 775–788.

Takahara, T., Matsumura, K., 2008. Experimental study of the sediment trap effect of steel grid-type sabo dams. International Journal of Erosion Control Engineering 1, 73–78.

Tangi, M., Bizzi, S., Fryirs, K., Castelletti, A., 2022. A dynamic, network scale sediment (dis)connectivity model to reconstruct historical sediment transfer and river reach sediment budgets. Water Resources Research 58, e2021WR030784. doi:https://doi.org/10.1029/2021WR030784.

Tangi, M., Schmitt, R., Bizzi, S., Castelletti, A., 2019. The cascade toolbox for analyzing river sediment connectivity and management. Environmental Modelling & Software 119, 400–406.

Thareau, L., Giuliani, Y., Jimenez, C., Doutriaux, E., 2006. Gestion sédimentaire du rhône suisse: Implications pour la retenue de genissiat. Congrès du Rhône «Du Léman à Fort l'Ecluse, quelle gestion pour le futur .

United Nations, 2019. Sustainable Development Goals Knowledge Platform. URL: https://sustainabledevelopment.un.org.

(US), H.E.C., 1993. HEC-6, Scour and Deposition in Rivers and Reservoirs: User's Manual. US Army Corps of Engineers, Hydrologic Engineering Center.

Van Der Knijff, J., Younis, J., De Roo, A., 2010. Lisflood: a gis-based distributed model for river basin scale water balance and flood simulation. International Journal of Geographical Information Science 24, 189–212.

Varis, O., Kummu, M., Härkönen, S., Huttunen, J.T., 2012. Greenhouse gas emissions from reservoirs, in: Impacts of large dams: a global assessment. Springer, pp. 69–94.

Vaughan, I.P., Diamond, M., Gurnell, A., Hall, K., Jenkins, A., Milner, N., Naylor, L., Sear, D., Woodward, G., Ormerod, S.J., 2009. Integrating ecology with hydromorphology: a priority for river science and management. Aquatic Conservation: Marine and Freshwater Ecosystems 19, 113–125.

Vischer, D., 1997. Bypass tunnels to prevent reservoir sedimentation, in: Proc. 19th ICOLD Congress, Florence, Italy, 1997.

Vogel, R.M., 2011. Hydromorphology. Journal of Water Resources Planning and Management 137.

Vörösmarty, C.J., Meybeck, M., Fekete, B., Sharma, K., Green, P., Syvitski, J.P., 2003. Anthropogenic sediment retention: major global impact from registered river impoundments. Global and planetary change 39, 169–190.

Walling, D.E., 1983. The sediment delivery problem. Journal of hydrology 65, 209–237.

Walter, R.C., Merritts, D.J., 2008. Natural streams and the legacy of water-powered mills. Science 319, 299–304.

Wang, H.W., Kondolf, M., Tullos, D., Kuo, W.C., 2018. Sediment management in taiwan's reservoirs and barriers to implementation. Water 10, 1034.

Ward, P.R., 1980. Sediment transport and a reservoir siltation formula for zimbabwe-rhodesia. Civil Engineer in South Africa 22, 9–15.

Wentworth, C.K., 1922. A scale of grade and class terms for clastic sediments. The journal of geology 30, 377–392.

Wessel, B., 2018. TanDEM-X Ground Segment – DEM Products Specification Document. Technical Report. Deutsches Zentrum für Luft- und Raumfahrt (DLR). URL: https://elib.dlr.de/120422/.

Whipple, K.X., Tucker, G.E., 2002. Implications of sediment-flux-dependent river incision models for landscape evolution. Journal of Geophysical Research: Solid Earth 107, ETG–3.

White, R., 2001. Evacuation of sediments from reservoirs. Thomas Telford Publishing. doi:http://dx.doi.org/10.1680/eosfr.29538.

Wilcock, P.R., 1998. Two-fraction model of initial sediment motion in gravel-bed rivers. Science 280, 410–412.

Wilcock, P.R., Crowe, J.C., 2003. Surface-based transport model for mixed-size sediment. Journal of Hydraulic Engineering 129, 120–128.

Wilcock, P.R., DeTemple, B.T., 2005. Persistence of armor layers in gravel-bed streams. Geophysical Research Letters 32.

Wild, T., Loucks, D., 2012a. Assessing the potential sediment-related impacts of hydropower development in the mekong river basin, in: World Environmental and Water Resources Congress 2012: Crossing Boundaries, pp. 2236–2246.

Wild, T., Loucks, D., 2012b. Sedsim model: a simulation model for the preliminary screening of sediment transport and management in river basins, version 3.0: documentation and users manual. Department of Civil and Environmental Engineering, Cornell University, Ithaca, NY USA .

Wild, T.B., Birnbaum, A.N., Reed, P.M., Loucks, D.P., 2021. An open source reservoir and sediment simulation framework for identifying and evaluating siting, design, and operation alternatives. Environmental Modelling & Software 136, 104947.

Wild, T.B., Loucks, D.P., 2014. Managing flow, sediment, and hydropower regimes in the sre pok, se san, and se kong rivers of the mekong basin. Water Resources Research 50, 5141–5157.

Wild, T.B., Loucks, D.P., Annandale, G.W., 2019. Sedsim: A river basin simulation screening model for reservoir management of sediment, water, and hydropower. Journal of Open Research Software 7.

Wild, T.B., Loucks, D.P., Annandale, G.W., Kaini, P., 2016. Maintaining sediment flows through hydropower dams in the mekong river basin. Journal of Water Resources Planning and Management 142, 05015004.

Wild, T.B., Reed, P.M., Loucks, D.P., Mallen-Cooper, M., Jensen, E.D., 2018. Balancing hydropower development and ecological impacts in the mekong: Tradeoffs for sambor mega dam. Journal of Water Resources Planning and Management 145, 05018019.

Wilkinson, S.N., Prosser, I.P., Hughes, A.O., 2006. Predicting the distribution of bed material accumulation using river network sediment budgets. Water Resources Research 42.

Wischmeier, W.H., Smith, D.D., 1978. Predicting rainfall erosion losses: a guide to conservation planning. 537, Department of Agriculture, Science and Education Administration.

Wisser, D., Frolking, S., Hagen, S., Bierkens, M.F., 2013. Beyond peak reservoir storage? a global estimate of declining water storage capacity in large reservoirs. Water Resources Research 49, 5732–5739.

Wohl, E., Brierley, G.J., Cadol, D., Coulthard, T.J., Covino, T., Fryirs, K.A., Grant, G., Hilton, R.G., Lane, S.N., Magilligan, F.J., Meitzen, K.M., Passalacqua, P., Poeppl, R.E., Rathburn, S.L., Sklar, L.S., 2019. Connectivity as an emergent property of geomorphic systems. Earth Surface Processes and Landforms 44, 4–26. URL: https://onlinelibrary.wiley.com/doi/abs/10.1002/esp.4434, doi:https://doi.org/10.1002/esp.4434. _eprint: https://onlinelibrary.wiley.com/doi/pdf/10.1002/esp.4434.

Wong, M., Parker, G., 2006. Reanalysis and correction of bed-load relation of meyer-peter and müller using their own database. Journal of Hydraulic Engineering 132, 1159–1168.

World Commission on Dams, 2000. Dams and Development: A New Framework for Decision-making: the Report of the World Commission on Dams. Earthscan.

Wu, W., Wang, S.S., 2006. Formulas for sediment porosity and settling velocity. Journal of Hydraulic Engineering 132, 858–862.

Wyżga, B., Zawiejska, J., Radecki-Pawlik, A., 2016. Impact of channel incision on the hydraulics of flood flows: examples from polish carpathian rivers. Geomorphology 272, 10–20.

Yamazaki, D., O'Loughlin, F., Trigg, M.A., Miller, Z.F., Pavelsky, T.M., Bates, P.D., 2014. Development of the global width database for large rivers. Water Resources Research 50, 3467–3480.

Yang, C.T., 1973. Incipient motion and sediment transport. Journal of the hydraulics division 99, 1679–1704.

Yang, C.T., 1984. Unit stream power equation for gravel. Journal of Hydraulic Engineering 110, 1783–1797.

Yang, S., Milliman, J., Li, P., Xu, K., 2011. 50,000 dams later: erosion of the yangtze river and its delta. Global and Planetary Change 75, 14–20.

Zarfl, C., Lumsdon, A.E., Berlekamp, J., Tydecks, L., Tockner, K., 2015. A global boom in hydropower dam construction. Aquatic Sciences 77, 161–170.

Zheng, P.Q., Hobbs, B.F., Koonce, J.F., 2009. Optimizing multiple dam removals under multiple objectives: linking tributary habitat and the lake erie ecosystem. Water Resources Research 45.

Zhou, Z., 2007. Reservoir sedimentation management in china, powerpoint presentation in the advanced training workshop on reservoir sedimentation management.

Ziv, G., Baran, E., Nam, S., Rodríguez-Iturbe, I., Levin, S.A., 2012. Trading-off fish biodiversity, food security, and hydropower in the mekong river basin. Proceedings of the National Academy of Sciences 109, 5609–5614.